KINETIC ENERGIES AND REACTIONS OF TRAPPED IONS IN A FOURIER TRANSFORM ION CYCLOTRON RESONANCE MASS SPECTROMETER

By

JAMES EDWARD BRUCE

A DISSERTATION PRESENTED TO THE GRADUATE SCHOOL
OF THE UNIVERSITY OF FLORIDA IN PARTIAL FULFILLMENT
OF THE REQUIREMENTS FOR THE DEGREE OF
DOCTOR OF PHILOSOPHY

UNIVERSITY OF FLORIDA

1992

ACKNOWLEDGEMENTS

I have endured the construction of the house that is the commencement of my education; however, I know that I have not been alone in my endeavor. I would like to thank those people who helped me find my way. The foundation of my house lies at Troy State, and I would like to thank those professors there, particularly Dr. E. Ward and Dr. H. Muller, for believing in me enough to encourage me to attend graduate school. The framework of my house was built at the University of Florida by the many excellent professors and support staff there. I would especially like to thank Dr. Weltner and Dr. Vala for showing me enough about physical chemistry that I decided to build my house there. The amount of material I have learned at the University of Florida has provided for a very sturdy structure that will withstand many future additions. The walls of my house are well insulated with the support of my family; they prevented the winds of change from blowing through when it seemed like graduate school might not be the place for me. I would like to thank Dr. John Eyler, my research advisor, for his endless patience, encouragement, and the financial support that put the roof overhead. I must also thank Dr. Eyler for teaching me the true value of scrutiny in the field of science. Finally, I would like to thank my

Mother and Father for providing me with the tools that allowed me to build this house.

TABLE OF CONTENTS

ACKNOWLEDGEMENTS ii

ABSTRACT vi

CHAPTER

1 INTRODUCTION 1

2 THEORY AND INSTRUMENTATION 8

3 PRESSURE MEASUREMENTS 32

Introduction 32
Experimental 35
Results and Discussion 41
Conclusions 54

4 TIME-OF FLIGHT KINETIC ENERGY MEASUREMENTS . . 56

Introduction 56
Experimental 58
Results and Discussion 69
Conclusions 83

5 TRAPPED ION ENERGIES VIA EQUILIBRIUM MEASUREMENTS 86

Introduction 86
Experimental 88
Results and Discussion 92
Conclusions 104

6 TRAPPED ION ENERGIES VIA ION-MOLECULE REACTION KINETICS 106

Introduction 106
Experimental 108
Results and Discussion 113
Conclusions 124

7 APPLICATION OF ION-MOLECULE REACTIONS TO THE STUDY OF CLUSTERS 126

Introduction 126
Experimental 129
Results and Discussion 133
Conclusions 155

8 CONCLUSIONS 156

BIBLIOGRAPHY 163

BIOGRAPHICAL SKETCH 167

Abstract of Dissertation Presented to the Graduate School of the University of Florida in Partial Fulfillment of the Requirements for the Degree of Doctor of Philosophy

KINETIC ENERGIES AND REACTIONS OF TRAPPED IONS IN A FOURIER TRANSFORM ION CYCLOTRON RESONANCE MASS SPECTROMETER

By

James Edward Bruce

August 1992

Chairperson: Dr. John R. Eyler
Major Department: Chemistry

Three independent investigations to ascertain the kinetic energies of trapped ions in a Fourier transform ion cyclotron resonance (FTICR) mass spectrometer were performed. Two of these studies were accomplished with the observation of ion-molecule reactions. The quantification of ion-molecule reaction rate constants as well as equilibrium constants was employed for ion kinetic energy determinations. The third inquiry relied on ion time-of-flight measurements for more direct ion kinetic energy assessments.

The results from all three kinetic energy probes showed that after collisional thermalization, ions trapped in an FTICR mass spectrometer possess kinetic energies that are only slightly above thermal, in the 300 to 500 K range. In addition, the ion time-of-flight technique showed that trapped ion kinetic energies do form a Maxwell-Boltzmann distribution

of energies after collisional relaxation.

Ion-molecule reactions were also used to study the properties of cluster ions formed by laser ablation and laser desorption techniques. In an extension of earlier work performed on cluster cations to determine cluster ionization potentials by charge transfer bracketing, cluster anions of carbon and silicon were investigated by electron transfer bracketing to determine cluster electron affinities. The electron affinities of C_n, for n = 4 to 8, 60, and 70 and Si_2 were bracketed. The results of the abstraction of hydrogen atoms from various compounds by the smaller carbon cluster anions are also reported. Hydrogen atom abstraction was observed to occur only for the even numbered cluster anions.

CHAPTER 1
INTRODUCTION

Fourier transform ion cyclotron resonance (FTICR) methods have become quite popular in mass spectrometry, primarily because of their ability to trap ions for relatively long times. FTICR mass spectrometers can trap ions at low pressures for many minutes. For comparison, the typical lifetime of an ion in a time-of-flight mass spectrometer is generally less than a microsecond and in a quadrupole mass spectrometer it is between 10 and 100 microseconds.

In the hands of chemists, the ion trapping ability of FTICR instruments has frequently been used to study the chemistry of ions either through photochemistry or ion-molecule reactions. Many physical quantities are abstracted from studies of ion-molecule reactions with FTICR mass spectrometers. In addition to ion-molecule reaction rate constants (Anicich et al., 1977; McElvany et al., 1987b), these physical quantities include collision complex lifetimes (Anicich, et al., 1991), equilibrium constants (Devlin, et al., 1976; Taft, 1974), electron affinities (Sharpe et al., 1990), and ionization potentials (Lias and Ausloos, 1978; Bach and Eyler, 1990; Zimmerman et al., 1991a; Zimmerman et al., 1991b).

Ion cyclotron resonance mass spectrometers differ from most other types of mass spectrometers with respect to the determination of ion-molecule reaction rate constants. Mass spectrometers that do not trap ions can also be used to measure ion-molecule reaction rate constants; this is usually done by observing the pressure dependence of the reactant ion intensity. Since the time with which the ions can react with the neutrals is relatively short, kinetics studies performed with non-trapping mass spectrometers must be done at significantly higher pressure than those of FTICR mass spectrometers. FTICR instruments, on the other hand, require low pressures for trapping and detection. Higher pressures lead to a higher collision frequency which, in turn, leads to an increase in the rate of random walk processes responsible for trapping loss and an increase in the rate of transient decay due to the loss of coherent cyclotron motion. However, the low pressure requirement of FTICR mass spectrometers does not usually create problems for the observation of ion-molecule reactions. At lower pressures, ion-molecule reactions are simply followed for longer times. In fact, the low pressure trapping ability has been shown to be a distinct advantage for the measurements performed on fast ion-molecule reactions, such as rapid radiative association reactions (Anicich et al., 1990; Beggs et al., 1990; Dunbar et al., 1990; Fisher et al., 1990; Sen et al., 1991). These reactions could not be observed in the pressure regime of the selected

ion flow tube (SIFT), a mass spectrometric instrument designed entirely for the study of ion-molecule reactions (Adams and Smith, 1976).

However, the low pressures typically used in FTICR mass spectrometers may indirectly create difficulties for the observation of some ion-molecule reactions that are kinetic energy-dependent. The low pressure environment and effects due to the trapping potentials of FTICR mass spectrometer have lead to uncertainties regarding the kinetic energy of ions produced in this instrument. Collisional cooling occurs at a slower rate at lower pressures and the extent to which ions are cooled before they react has been questioned. Since any of the above-mentioned physical quantities may strongly depend on ion kinetic energy, development and assessment of schemes to estimate ion kinetic energies in a FTICR mass spectrometer are of great importance.

There has been considerable interest in the kinetic energy of ions produced in FTICR mass spectrometers, and determinations of these energies are still the subject of much debate (Katritzky et al., 1990; Katritzky et al., 1989; McMahon and Willett, 1990; Hanson et al., 1989; Grosshans et al., 1990). As mentioned earlier, SIFT instruments are used to study ion-molecule reactions. With a SIFT instrument, in fact with the entire class of instruments based on the flow tube technique, ions are not stored and reactions are investigated by varying the pressure of the reactant neutral

in a relatively high pressure (ca. 0.5 Torr) buffer gas in the flow tube. Discrepancies between rate constants determined by FTICR and SIFT or other flow tube variants are often ascribed to translationally excited ions in the FTICR mass spectrometer. There exist at least 6 cases in which the difference between reported flow tube rate constants and FTICR rate constants has been reconciled by assigning an effective temperature of 500 to 1000 K to ions in the Fourier transform ion cyclotron resonance mass spectrometer (Henchman, 1987).

The problem of measuring ion kinetic energies in a FTICR mass spectrometer can be approached in several ways. One technique that has been used successfully is ICR kinetic energy spectroscopy or kinetic energy release (Rincon et al., 1988; Mauclair et al., 1979). This method measures the kinetic energy of the products of either exoergic ion-molecule reactions or ion photodissociation to infer electronic state information. However, the technique is not applicable for the measurement of near thermal kinetic energies due to inefficient ion trapping for cell potentials below 100 meV. A second approach for the measurement of kinetic energy of ions in an ICR cell has employed ion time-of-flight determinations (Dunbar and Weddle, 1988). Pulsing the trapping potential to zero for increasingly longer periods of time and measuring the resulting ion intensity decay curve allowed ion kinetic energies to be evaluated. Unfortunately, this technique can be susceptible to stray potentials on the

trapping plates as well as to incompletely shielded potentials from the filament assembly. Experiments have been performed to reduce or eliminate this problem so that this technique may be applicable to ions produced by sources other than electron ionization.

Several chemical methods for measuring ion kinetic energies were discussed at a NATO conference (Bartmess, 1987). The methods included proton transfer equilibria, a negative ion equilibrium, and the charge exchange reaction of Ar^+ with N_2. The latter reaction seemed most convenient for study because of the simplicity of the reaction and reactants. Furthermore, this reaction has been heavily studied and considerable data exist on its energy dependence. The reaction could be studied with relative ease in FTICR instruments as well as in quadrupole ion traps. The study of FTICR ion kinetic energy presented in this dissertation was done in conjunction with a parallel investigation to determine the kinetic energy of ions in a quadrupole ion trap. Rate constants measured on these instruments were compared to prior studies of the kinetic energy dependence to obtain ion temperature estimates. More importantly, however, investigations to determine the effect of common FTICR parameters such as pressure and trapping voltage on ion kinetic energy were also carried out. Measurements performed on the Ar^+ and N_2 system were augmented by measurements on several other chemical "thermometers." These ion-molecule

reactions measured using both the FTICR mass spectrometer and the ion trap mass spectrometer, included two proton transfer equilibria and one charge transfer equilibrium. Judicious choice of reactants for which the standard free energy of protonation (or ionization) was known and subsequent measurements of the equilibrium constants for proton transfer (or charge transfer) allowed an estimate of the temperature of the system to be made.

In this dissertation, Chapter 2 addresses fundamental FTICR theory with special relevance to the study of ion-molecule reactions. Precise pressure measurements are crucial to accurate determination of ion-molecule reaction rate constants. Chapter 3 presents the results of three independent determinations of a system factor which accounts for the difference in pressure that exists between the location of the pressure sensor and the location of the reaction cell. Chapters 4, 5, and 6 show data gathered to estimate FTICR ion kinetic energy. Chapter 4 details the studies done with the ion time-of-flight technique. Problems with ion "reflection" were encountered and solutions are demonstrated. Chapter 5 includes the thermodynamic data taken to estimate ion kinetic energy. The results of two proton transfer systems and one charge transfer system are given. Data from the $Ar^+ + N_2$ system are presented in Chapter 6. An overall ion kinetic energy estimate based on this technique is given as well as the effect on ion kinetic energy produced by

varying the trapping voltage, pressure, and other parameters. Also discussed in this chapter is the expected contribution to reactivity from each of the two spin states of Ar^+ (J=3/2 and J=1/2). A kinetic model of this system is given using the rate constants from the work of Hamdan et al. (1984), and an explanation for the lack of observance of any spin state effect on the reactivity of the ions in the FTICR instrument is given.

The 7th chapter of this dissertation provides data regarding the applications of ion-molecule reactions. This chapter demonstrates the application of ion-molecule reactions to measure to electron affinities of C_{60}, C_{70}, and a few smaller carbon clusters. The rates of reaction of the two fullerene anions with tetrafluoro-1,4-benzoquinone, one of the electron transfer reference compounds used to bracket the electron affinities, were also measured and are reported in this chapter. The electron affinities of smaller carbon clusters (C_n with n=2 to 8) and Si_2 were investigated by a similar technique and the results are also included in this chapter. Finally, Chapter 8 presents conclusions on FTICR ion kinetic energies and applications of ion-molecule reactions for the determination of physical properties of gas phase molecules in the FTICR mass spectrometer.

CHAPTER 2
THEORY AND INSTRUMENTATION

The instrument used for the work presented in this dissertation was a Fourier transform ion cyclotron resonance (FTICR) mass spectrometer. The ancestry of this instrument can be traced back as far as the 1930s to the cyclotron particle accelerator used by Ernest O. Lawrence. However, the first use of the cyclotron phenomenon to determine the mass of ions did not occur until 1949, when Hipple, Sommer, and Thomas developed the Omegatron (Hipple et al., 1949). The first ion cyclotron resonance mass spectrometer was developed in the early 1960s. ICR progressed through the addition of electromagnets, drift cells, and marginal oscillator detectors. Although early instruments were extensively used to monitor ion-molecule reactions, they lacked two innovations, among many others, that were to come later and prove to be important for the study of reactions. The first was the ability to trap ions, which came in 1970 (McIver, 1970). The next came in 1974 with the concept of simultaneous detection of all ions using Fourier transform methods (Comisarow and Marshall, 1974). As was mentioned in the introductory chapter, the modern instrument is suitable for the study of ion-molecule reactions because of the ion

trapping ability as well as rapid detection and high resolution that the Fourier transform has afforded. This chapter presents theory regarding the operation of an FTICR mass spectrometer with special attention applied to factors affecting the observation of ion-molecule reactions with this device. Following this is a brief description of the instrument used for all work presented in later chapters.

Theory. Many excellent books (Buchanan, 1987; Marshall and Verdun, 1990), papers (Baykut and Eyler, 1986; Wanczek, 1989), and review articles (Marshall and Grosshans, 1991; Wilkins et al., 1989) exist on the theory involved in Fourier transform ion cyclotron resonance mass spectrometry; therefore, only a brief description will be given here. The motion of an ion in a magnetic field is described by the Lorentz equation,

$$\vec{F}=m\frac{d\vec{v}}{dt}=q(\vec{E}+(\vec{v}\times\vec{B})) \qquad (2.1)$$

where the vector F is the force exerted on an ion of charge q with a velocity vector of v by a magnetic field vector, B, and an electric field, E. Considering first the force due to the magnetic field, it is readily apparent that, due to the cross product in this term, only ions with velocities (or components of velocities) perpendicular to the magnetic field vector will experience a Lorentz force in the absence of an electric field. For ions with velocity vectors parallel to the magnetic field vector, this term is zero. Furthermore, the

force resulting from the magnetic field operation on the ion motion, for velocities not parallel the magnetic field vector, is perpendicular to both the velocity vector and the magnetic field vector. This force vector has a magnitude which is equal to the product of the magnitudes of the velocity and magnetic field vectors multiplied by the sine of the angle between them. Typically, the magnetic field vector is defined as the z-axis of a three-dimensional Cartesian coordinate system. Therefore, any velocity component an ion may have along the x- or y-axis will lead to a Lorentz force along the y- or x-axis respectively. Any component of velocity along the z-axis will remain unaffected by the magnetic field. Thus, to completely contain ions in an FTICR mass spectrometer, trapping potentials are required along the z-axis. If an ion has a z-component of velocity that is less than the applied trapping voltage (typically 1 to 2 volts) and the components along the other two axes are not too large, ions can be successfully trapped in a FTICR mass spectrometer. The comprehension of the requirement for a trapping potential is essential to the work of this dissertation, particularly for Chapters 4 through 6, because it is believed that the major factor producing ions with excess kinetic energy in a FTICR mass spectrometer is their motion in the trapping potential well. A model of the typical trapping potential well of an FTICR cell calculated with the program SIMION (Dahl and Delmore, 1988) is illustrated in Figure 2.1. Ions formed

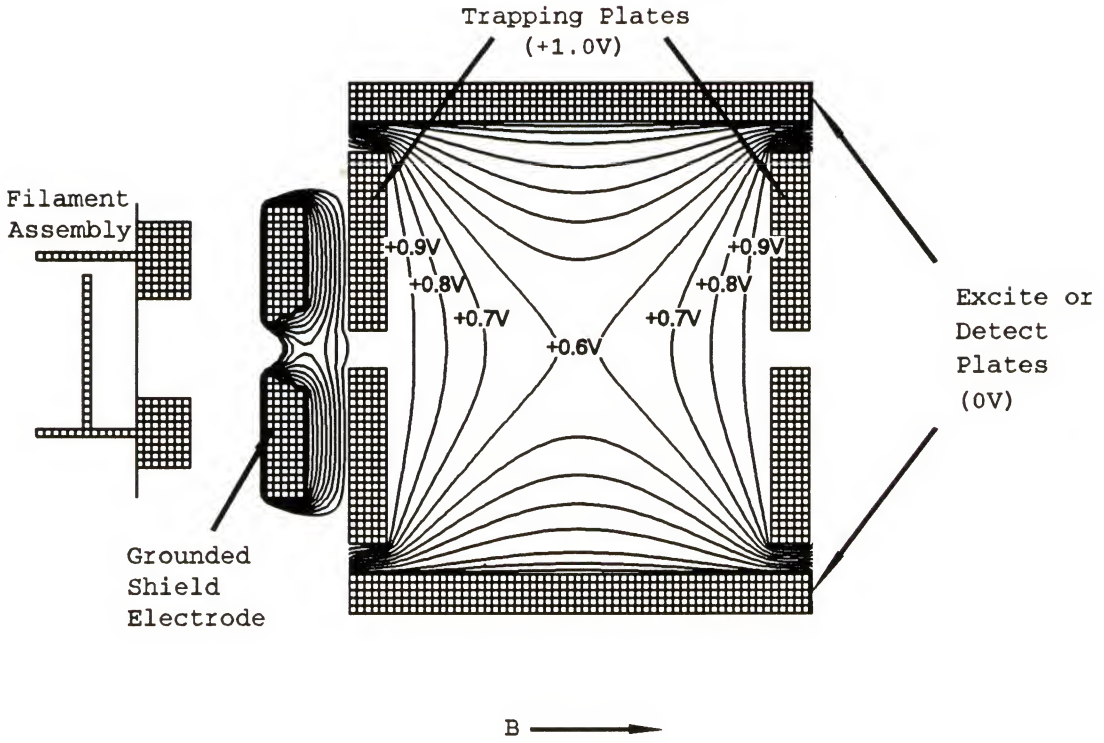

Figure 2.1. Equipotential lines in a standard cubic ion cyclotron resonance cell computed by SIMION. Trapping potential is 1.0 V, the potential applied to the filament assembly is 5.0 V. and all other electrodes are at 0 V.

by electron ionization close to the trapping plates will be translationally excited toward the center of the cell and will oscillate in the well with excess kinetic energy until they collide with neutral molecules and lose kinetic energy or are removed from the cell. Only those ions formed near the center of the cell will not be kinetically excited.

The previous paragraph described the conditions that lead to ion trapping in a FTICR mass spectrometer and provided a justification for the investigation of trapped ion energies in an FTICR mass spectrometer. This section deals with some fundamental aspects of ion detection and, for now, the problems associated with translational excitation by the trapping potential well are disregarded. Ions formed in an ICR cell usually have initial velocities that form a random distribution of angles with the magnetic field vector. From the Lorentz equation, Equation (2.1), the kinetic energy can be divided into two components. One component is along the z-axis and the other component is perpendicular to the z-axis (governed by the B term as discussed above). Because of the random distribution of angles the initial velocity vectors form with the magnetic field vector, the initial motion of the average ion will consist of both motion along the z-axis (sometimes called trapping oscillation) and perpendicular (cyclotron) motion, as illustrated in Figure 2.2. This figure is a model of ion motion created with the program SIMION and shows a vertical slice through the center of a 1 inch cubical

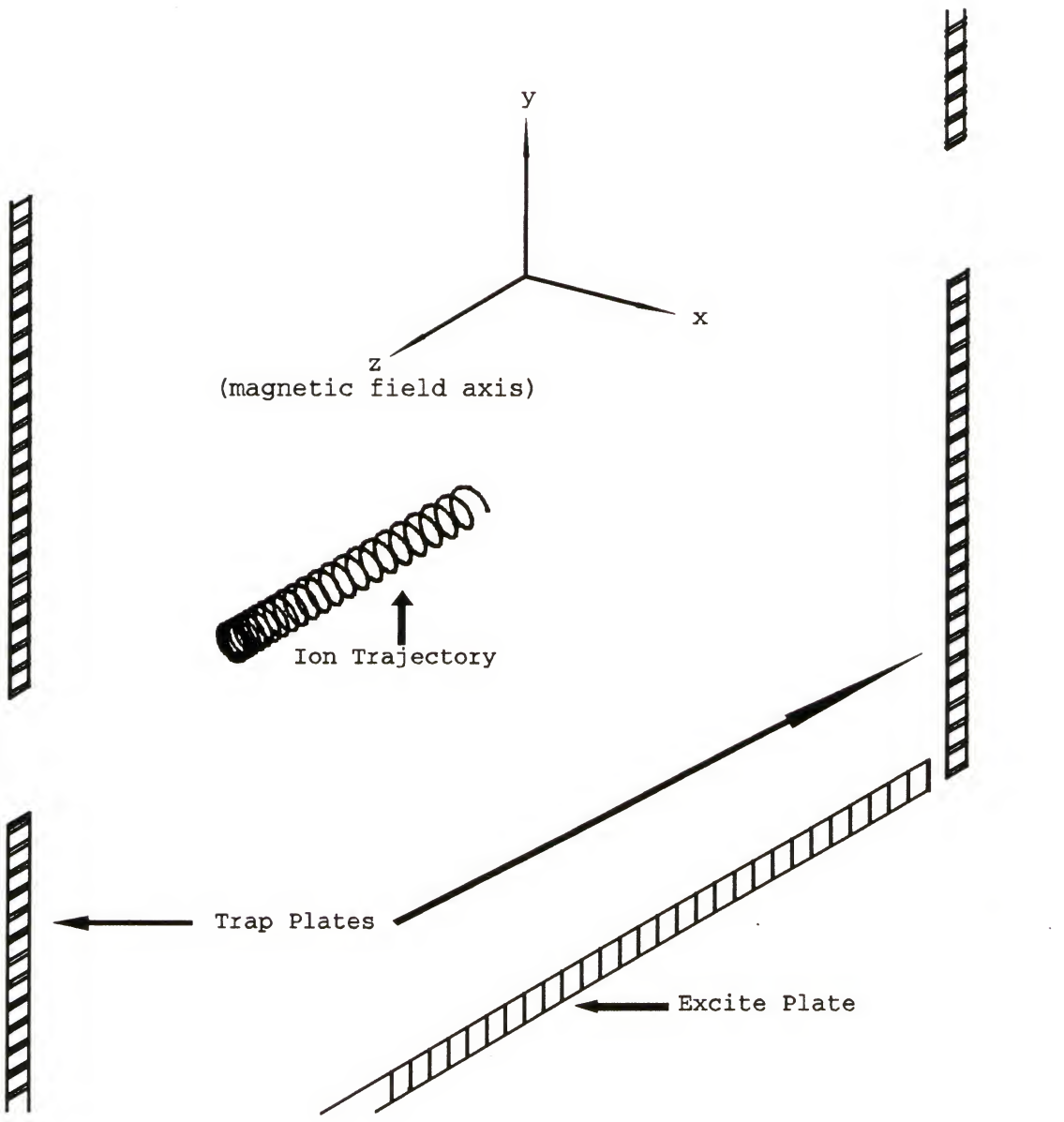

Figure 2.2. SIMION representation of ion motion in an FTICR mass spectrometer. The ion is formed at the center of the cell with a kinetic energy of 5 eV. The trapping electrodes are held at +1.0 Volts and all other electrodes are at ground potential.

ICR cell. The results were obtained with a m/z = 50 amu ion created at the center of the cell with 5 electron volts of kinetic energy. By varying the initial velocity vector angle with respect to the magnetic field vector, roughly 90% of the initial 5 eV kinetic energy resulted in cyclotron motion. The remaining 10% resulted in trapping oscillation. The relatively high energy of 5 eV was chosen so that the resulting cyclotron orbit was large enough to be viewed easily. Parameters for this model include a magnetic field of 3 T, a trapping potential of 1 Volt, and ground potential on all other electrodes. Although the equipotential lines are not drawn in this figure, evidence of the trapping potential well is apparent in the compression of the coil-like structure representing the ion trajectory, as the ion approaches the trapping plate. This compression along the z-axis is indicative of the gradually reducing z-velocity of the ion as the z-kinetic energy is transformed into potential energy. For a trapped ion, the motion along the z axis will momentarily stop and then the ion will begin to acquire velocity in the opposite direction along the magnetic field axis.

In the absence of collisions, the cyclotron motion will form a stable orbit. The orbit is stable because of the balance of the two forces, Lorentz and centrifugal. The Lorentz force, due to the magnetic field, exerts a force toward the center of the orbit. As was mentioned earlier, this force is perpendicular to both the magnetic field vector

and the velocity vector. The centrifugal force balances the Lorentz force and is given by mv^2/r, where m is the mass of the particle, v is the velocity of the particle, and r is the radius of the orbit. Equating the Lorentz and centrifugal forces, as does occur for stable cyclotron orbits, one obtains

$$\frac{mv^2}{r}=qvB \tag{2.2}$$

For demonstrative purposes, the situation where the initial velocity is completely perpendicular to the magnetic field vector is considered here and shown in Figure 2.3. Thus the Lorentz force is the product of the magnetic field vector magnitude and the velocity vector magnitude multiplied by the sine of 90°. Canceling a v from both sides gives

$$\frac{mv}{r}=qB \tag{2.3}$$

and dividing both sides by m, one obtains

$$\frac{v}{r}=\frac{qB}{m} \tag{2.4}$$

where v/r is the definition of angular frequency. It becomes clear that, due to the equation of these two forces, the angular frequency of cyclotron motion, ω_c, is dependent only upon the mass to charge ratio of a particle and the magnetic field with which it is confined.

$$\omega_c=\frac{qB}{m} \tag{2.5}$$

Furthermore, for a given ion in a constant magnetic field, the

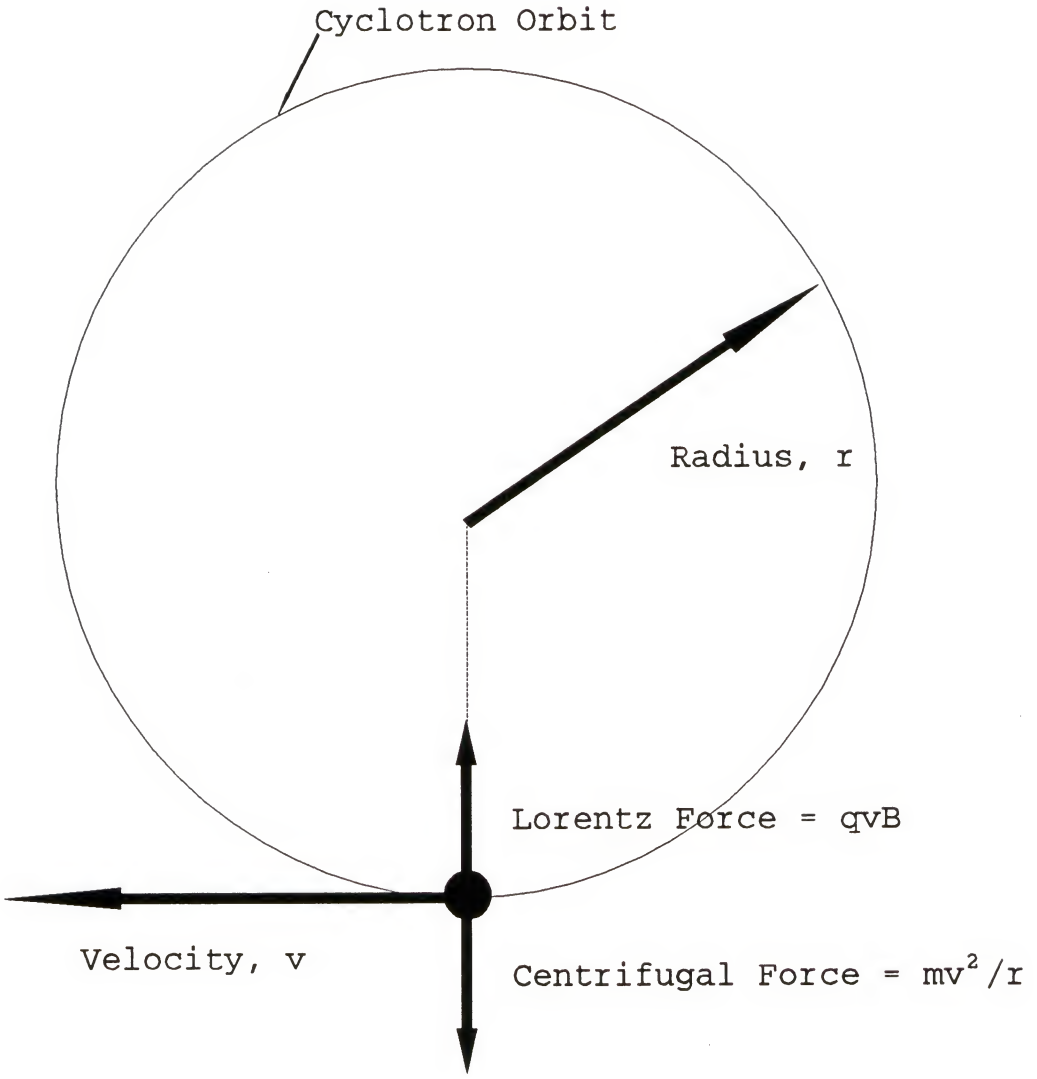

Figure 2.3. Schematic representation of the relationship between the Lorentz force and the centrifugal force for an ion with a stable cyclotron orbit and a velocity, v, that is perpendicular to the magnetic field vector, B.

quotient of v/r is also a constant and therefore an increase in velocity (in any direction perpendicular to the magnetic field) results in a linear increase in the radius of the cyclotron orbit; the cyclotron frequency remains constant. This discussion provides the basis for understanding ion motion within a Fourier transform ion cyclotron resonance mass spectrometer. However, in most cases the cyclotron frequency of the ion is not expressed in radians/second, but rather in hertz. This requires division on both sides of Equation (2.4) by a factor of 2π. Therefore, the cyclotron frequency of an ion in hertz is given by

$$f_c = \frac{v}{2\pi r} = \frac{qB}{2\pi m} \qquad (2.6)$$

Ion detection in a FTICR mass spectrometer is most commonly accomplished by measuring image currents induced by the ions on opposed plates called the "receive" plates. This image current signal is dependent upon several factors, such as the number of ions, how close to the receive plates the ions travel, and the coherence of the cyclotron motion of all ions of a given mass. As was mentioned earlier, the initial ion motion is a combination of trapping and cyclotron motion. However, the initial cyclotron radii are relatively small and the phase of the cyclotron orbits is random. These two factors force the initial induced image current to be zero. Excitation of the cyclotron motion is required for ion detection.

Cyclotron motion of the ions is excited and made coherent by the application of voltages to another pair of opposed plates known as the "excite" plates. Several techniques for ion excitation exist; however, only two are employed for the work presented in this dissertation. The two methods used here include the standard chirp excitation (Marshall and Roe, 1980) and a newer technique known as impulse excitation (McIver et al., 1988). They both perform essentially the same function and a description of the chirp mode follows.

The method of excitation known as the chirp is commonly used to excite a wide range of ions within a short time period. A radio frequency (RF) alternating voltage pulse is applied to two parallel excite plates as shown in Figure 2.4. The polarity of the pulse applied to one excite plate is opposite to that applied to the other plate. The typical peak to peak voltage of this pulse is 20 Volts for a standard cubic 1 inch cell. The frequency of the alternation is scanned within the pulse, beginning with low frequency and scanning to high frequency. An ion will receive net cyclotron excitation only when the frequency of the applied excitation equals the cyclotron frequency of the ion. Therefore, the frequency range over which the RF is scanned is determined by the mass range that is to be examined. Ions remain close to the center of the cell until the driving frequency equals their cyclotron frequency. Then the ions are excited and their cyclotron orbits become larger. Excitation continues until the applied

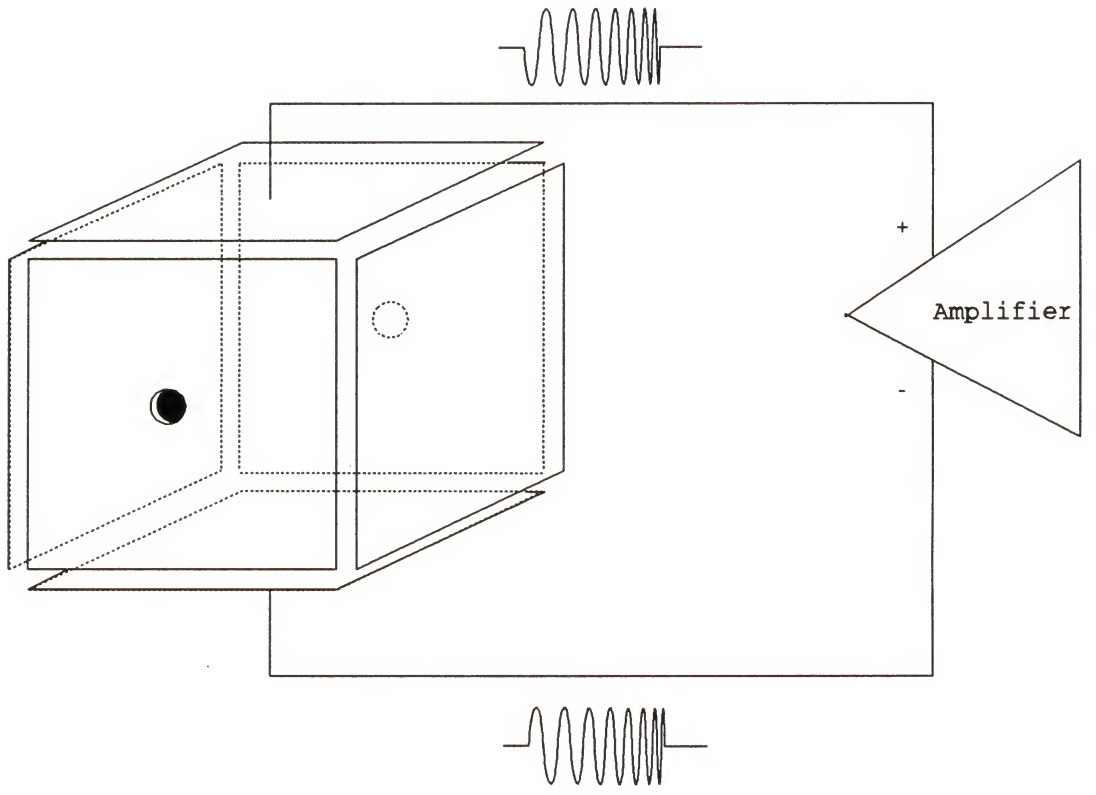

Figure 2.4. This schematic shows an ICR cell with an RF chirp excitation amplifier connected to the two excite plates. The signal input on one plate is 180° out of phase with that on the other.

RF shifts away from the ions' cyclotron frequency or the ion strikes one of the plates of the cell (is ejected). All ions of a given mass to charge ratio are excited coherently and after excitation this packet of ions will continue to orbit until a collision with a neutral molecule disrupts the motion or the ions are removed from the cell.

After the excitation pulse and before ions are removed from the cell, either by collisions or by a quench pulse (usually a voltage pulse of opposing polarity applied to both trap plates to remove all ions) the image currents induced by the ions on the receive plates are converted to voltages and amplified. For the case where all ions have the same mass to charge ratio, the resulting voltage signal oscillates at a frequency equal to the ions' cyclotron frequency. After another stage of amplification, the resulting digitized time domain signal, sometimes called a transient, appears as shown in Figure 2.5. This is the transient due to benzene cations in a benzene pressure 1.6×10^{-6} torr. The decay in signal is caused by the loss of ions from the cell (minor) and the loss of coherence of motion due to the collisions with neutral species (major). This signal is processed and Fourier transformed to produce a frequency domain spectrum as shown in Figure 2.6.

A newer method of excitation, known as impulse (McIver et al., 1988) excitation, also increases the size and produces more coherent cyclotron orbits of trapped ions. However, this

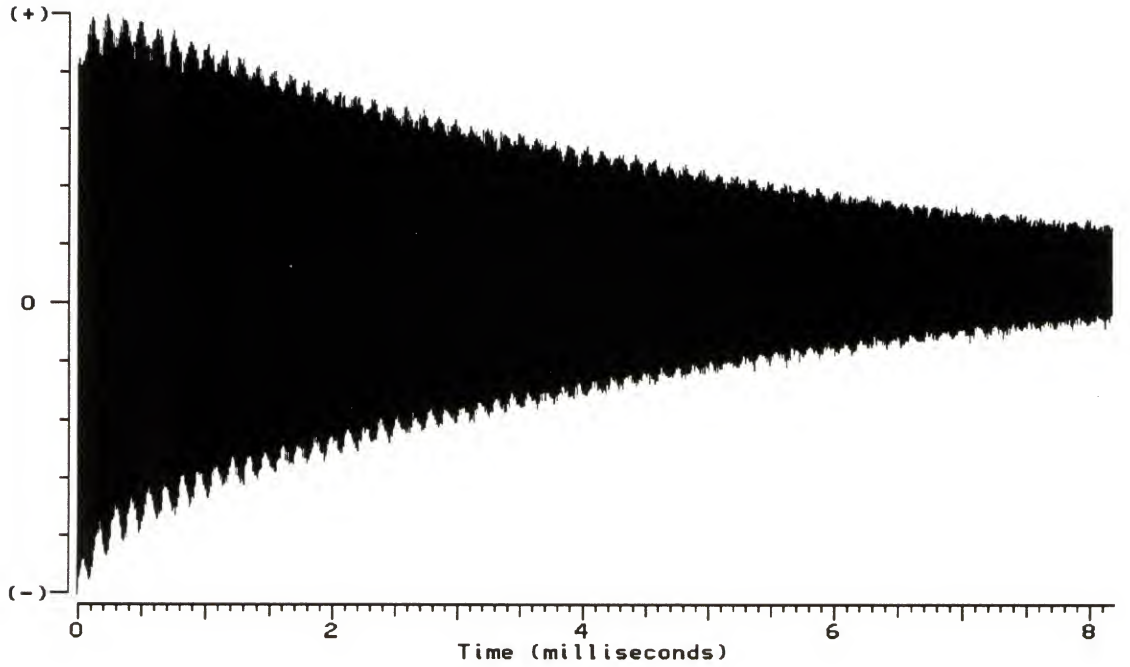

Figure 2.5. This is the digitized time domain signal (transient) for benzene cations produced by electron ionization in a benzene sample of pressure 1.6 x 10^{-6} torr.

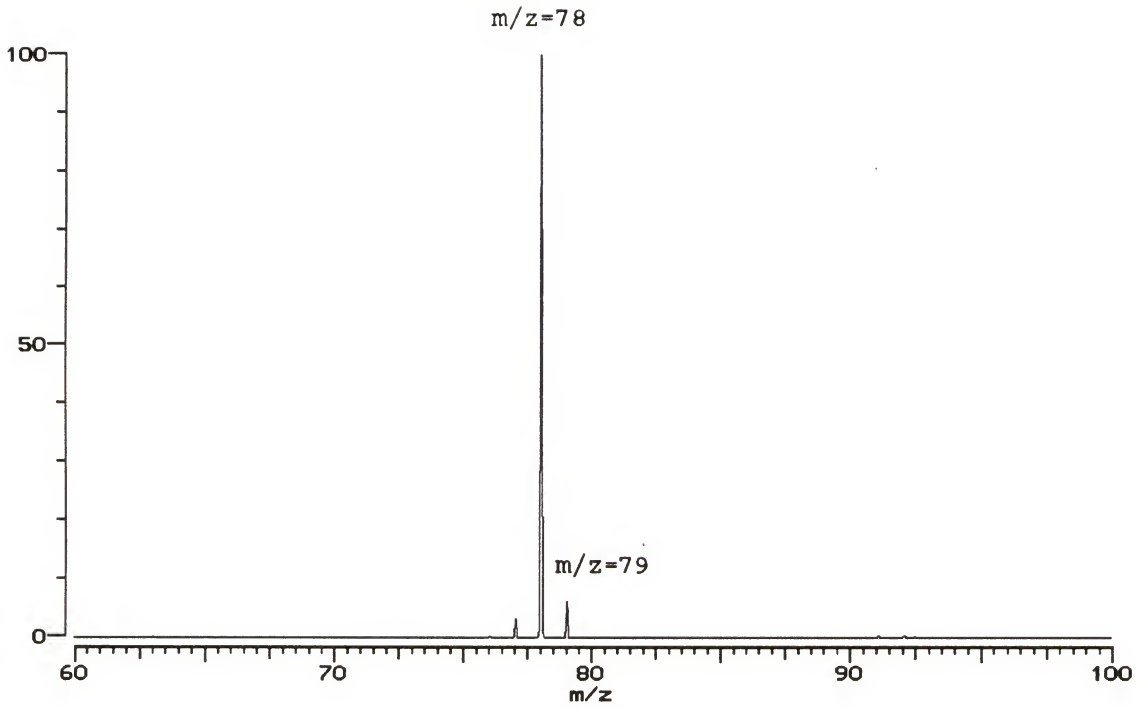

Figure 2.6. This is the Fourier transformed (frequency domain) spectrum of benzene cations resulting from the detection of the transient observed in Figure 2.6.

mode does not rely on resonant excitation, such as the chirp. Voltages are again applied with opposing signs to the excitation plates; however, in this case the voltages are much larger dc pulses of very short duration, approximately 1 microsecond. The typical voltage used here is near 1000 volts. This technique has many advantages over the chirp mode: it achieves simultaneous acceleration of all ions, it is easier to use, and in most cases, it can give better isotope ratios. However, due to the restraint of modern electronics on the shaping of high voltage pulses, this technique loses sensitivity at lower masses (below 100 amu for a 3 Tesla instrument). Consequently, this technique was only applied in limited studies presented in this dissertation. Studies were chosen for impulse excitation only if accurate relative peak heights were not a major concern, such as the electron affinity bracketing experiments on C_{60} and C_{70} reported in Chapter 7.

Instrumentation. The instrument used for this work was a Fourier transform ion cyclotron resonance mass spectrometer. A schematic drawing of the instrument, with the exception of the computer and electronics used for experiment control and signal analysis is shown in Figure 2.7. The magnet, vacuum chamber, pumps, inlet system, electronics, and computer were all original equipment obtained as a standard Nicolet FT/MS-1000 mass spectrometer. The magnet was an Oxford 3 Tesla horizontal bore superconducting magnet with a 6 inch inside

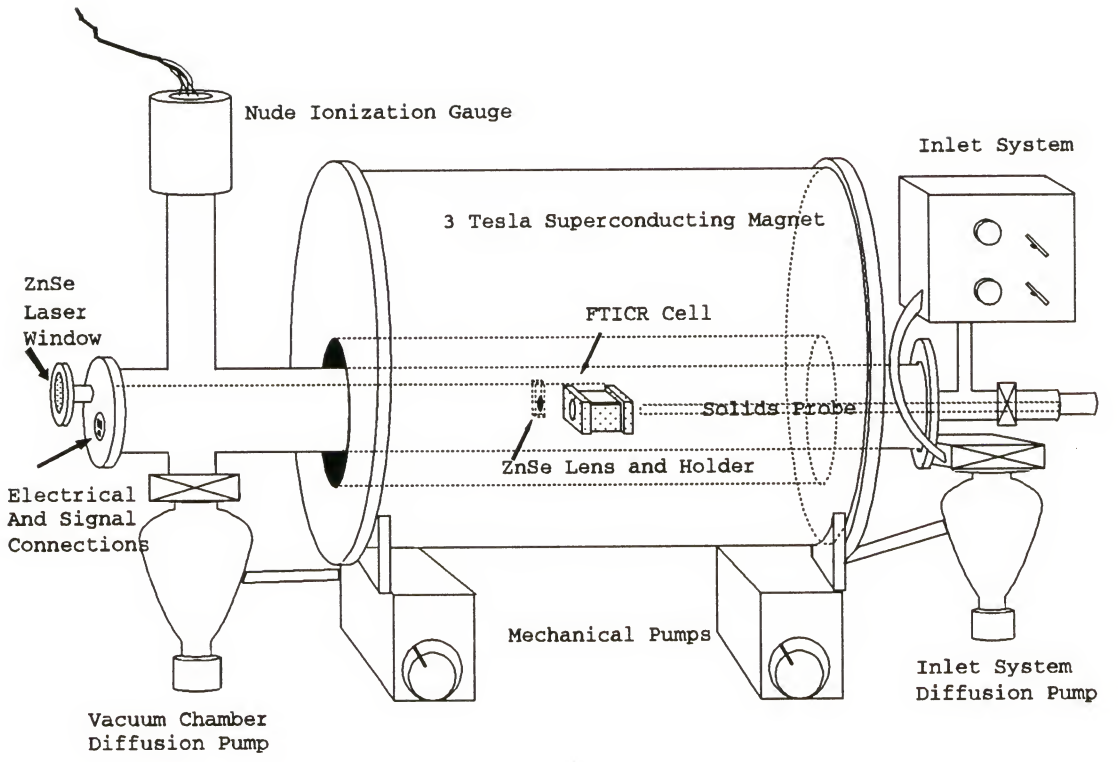

Figure 2.7. This is a drawing of the instrument used for all work presented here.

diameter. The system had a vacuum chamber with an inside diameter of 2.875 inches. Most experiments were done with a standard 1 inch cubic stainless steel cell. However, some experimentation was done to determine the effects of a longer cell and the effects of less magnetic material, such as rhodium-flashed, silver-plated copper. Also, minor modifications were made to the standard cell to allow the use of lasers. These modifications included drilling holes in trap plates and using coarse wire mesh for trap plates. The pumps on this system were Alcatel oil diffusion pumps backed by mechanical pumps. As is shown in Figure 2.7, there was one 300 L/s diffusion pump on the vacuum system and one 150 L/s diffusion pump that served as the inlet pump for sample preparation. Because of the high stray magnetic fields of the superconducting solenoid, the nude ionization gauge used for pressure measurement on the vacuum chamber was shielded with μ-metal and placed in a position somewhat removed from the FTICR cell. The possibility that this configuration leads to the development of a pressure difference between the cell and the ionization gauge was investigated quite thoroughly. The results of these investigations are presented in Chapter 3. The ionization gauge controller used for all studies was a Granville-Phillips (Model # 274 025) digital ionization gauge controller. Gas and liquid samples were introduced to the cell through the heated sample inlet. This inlet housed two Varian precision leak valves and roughing valves and was

continuously maintained at a temperature of 100°C. Solid samples with relatively high vapor pressures can also be used with this inlet. Also present, but not shown in Figure 2.7, was another leak valve and roughing valve. These valves were not routinely heated and were used primarily for gaseous samples. Lower vapor pressure solids were directed into the vacuum chamber through the solids probe inlet port. Solids deposited onto the stainless steel probe tip were laser-desorbed to produce both positive and negative ions.

Lasers used for the work presented in Chapter 7 were a Lumonics excimer laser, converted for CO_2 lasing and operating at an output wavelength of 10.6 μ for fullerene ion production and a Continuum Nd:YAG laser for silicon cluster anion production. Figure 2.8 shows the typical cell and lens arrangement employed for laser desorption experiments. The laser beam entered the vacuum chamber through the ZnSe window shown in Figure 2.7. The beam was focussed inside the vacuum chamber with a 3 inch focal length ZnSe lens and passed through a 5 mm hole on the trap plate closest to the lens. After passing through the cell, the beam exited through the other trap plate, which was constructed of coarse stainless steel mesh. The probe was positioned such that the focal point of the laser was directly on the probe tip surface. The spot size covered by the beam was about 1 mm for the CO_2 laser and 0.1 mm for the Nd:YAG laser. The CO_2 laser was controlled via its external trigger option with TTL pulses that came from

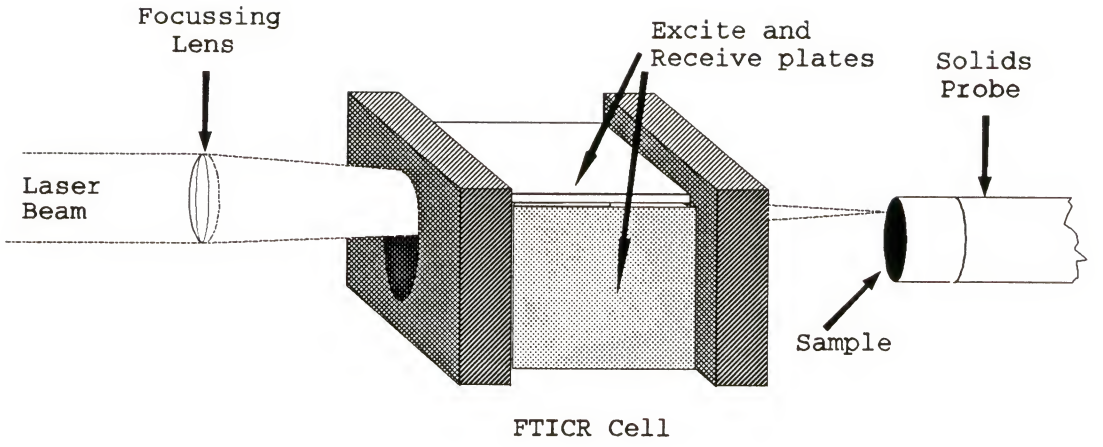

Figure 2.8. Arrangement of the ZnSe lens, FTICR cell, and solids probe used for laser desorption experiments.

the computer used to collect and analyze mass spectrometric data. The Nd:YAG laser had a similar option, but due to the typical requirements of Nd:YAG lasers, this interface was more complicated. To obtain reproducible, stable laser output, pulsed Nd:YAG lasers must be operated in a continuously pulsing manner. This means that the flashlamps must be continuously pulsing at a constant frequency (10 Hz). When a laser pulse is desired, a Q-switch is opened to allow the laser beam to exit the laser cavity. The Nd:YAG laser was synchronized to the mass spectrometer with the use of a photodiode and the external trigger option of the computer

used to control the mass spectrometer. A schematic representation of this interface is given in Figure 2.9.

The problems associated with the precise timing normally required for laser interface were avoided with this configuration. Exact synchronization of the laser with the mass spectrometer was achieved because the computer controlling the experiment was used in the external trigger mode (this mode was available on the newer IonSpec personal computer-based data station discussed below). In this mode, the computer waited for a pulse from the photodiode indicating that the laser had fired. It then began generating all the pulses and acquiring the data common to the FTICR experiment. However, after the transient was acquired a final pulse was produced by the computer that was directed to the laser electronics that controlled the Q-switch of the Nd:YAG laser. This caused the laser to fire again, and thus signal averaging over any number of experiments was performed, preserving the temporal relationship between the laser and the mass spectrometer. All that was required from the operator was the initial pulse to fire the laser for the first experiment.

Two different computers (and associated electronics) were used for experiment control and data acquisition for the work presented in this dissertation. The first computer was a Nicolet 1280 minicomputer. This system was somewhat limited in its capabilities, such as mass range and speed. This system was not equipped for impulse excitation and

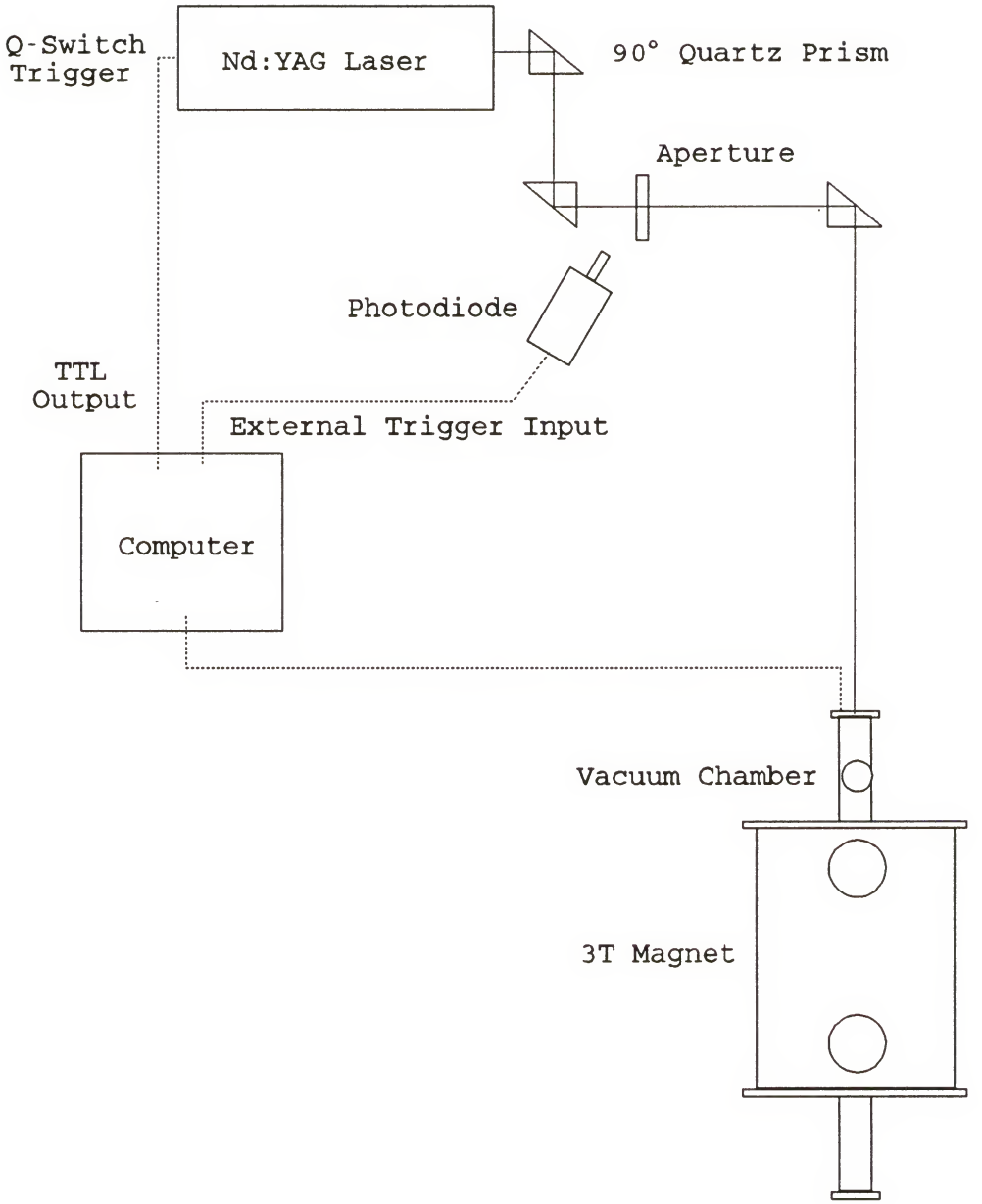

Figure 2.9. A schematic representation of the interface used to synchronize the mass spectrometer to the Nd:YAG laser.

consequently, only the chirp mode was used with it. This system was also restricted to 64 K or fewer data points per transient. Due to the slower analog to digital converter (5.32 MHz versus 16 MHz on the newer IonSpec system discussed below), the lower mass cutoff for this system was 17.3 amu. However, various techniques were employed that allowed this cutoff to be lowered and these methods are mentioned in Chapter 3. The software operating system for this computer, while eminently versatile, was cumbersome and slow. Even so, a direct comparison between this system and the newer one revealed that the Nicolet 1280 still held the advantage with respect to the signal to noise ratio by a factor of about 2. Furthermore, obtaining a simple mass spectrum was far easier on the Nicolet system because nearly all parameters are under computer control and as such, little parameter optimizing was required. This instrument was used for some of the pressure measurements presented in Chapter 3, for some of the equilibrium measurements presented in Chapter 5 and for all the kinetics experiments presented in Chapter 6.

The newer IonSpec data station was based on the Compaq 33 Mhz 386 personal computer, a 9 bit, 16 Mhz analog-to-digital converter, and a Vortex array processor. With this computer, this system was able to Fourier transform up to 512 K data points in a fraction of the time it took the Nicolet 1280 to transform even 8 K points. This instrument provided the ability to perform both chirp and impulse excitation with

only a software switch to change modes. This instrument also possessed the external trigger option that was necessary for the simple Nd:YAG laser interface that was discussed above. Probably the biggest advantage of this computer was the fact that it allowed data storage on much more modern media such as high density floppies, standard personal computer hard drives and Bernoulli boxes. This feature allowed the user to store time plot data, such as kinetics or equilibrium data, in ASCII form directly from the Omega operating software. This greatly assisted the subsequent data analysis with spreadsheet or kinetics fitting programs on the Compaq or virtually any other personal computer.

CHAPTER 3
PRESSURE MEASUREMENTS

Introduction

As was mentioned in the introductory chapter, FTICR mass spectrometers are frequently used to measure ion-molecule reaction rate constants. The more frequently employed method for reaction rate coefficient determination with an FTICR mass spectrometer involves the observation of ion intensities as a function of time. For the bimolecular reaction

$$A^+ + B \rightarrow C^+ + D \qquad (3.1)$$

the rate of change of the concentration (or intensity) of A^+ can be written as

$$\frac{d[A^+]}{dt} = -k[A^+][B] \qquad (3.1)$$

where [B] is the concentration (or pressure for gas phase) of reactant B. Multiplying both sides by $dt/[A^+]$ and integrating from time=0 to time=t, the equation

$$\int_0^t \frac{d[A^+]}{[A^+]} = \int_0^t -k[B]dt \qquad (3.2)$$

is obtained. For kinetics studies performed on an FTICR mass spectrometer, and many other instruments, the pressure of B,

[B] is always much greater than the intensity of A^+, $[A^+]$. Consequently, a pseudo-first order approximation is applied and the integrated rate equation can be written as

$$\ln[A^+]_t - \ln[A^+]_0 = -kt[B] \qquad (3.3)$$

Adding $\ln[A^+]_0$ to both sides and then clearing the natural log, one obtains the equation

$$[A^+]_t = [A^+]_0 e^{-k[B]t} \qquad (3.4)$$

Furthermore, since the pressure of B is much larger than $[A^+]$ and remains constant, Equation (3.4) may be written as

$$[A^+]_t = [A^+]_0 e^{-k't} \qquad (3.5)$$

where k' is the pseudo-first order rate constant.

The intent of this rudimentary derivation is to illustrate that the normal mode of operation for the determination of ion-molecule reaction rate constants with an FTICR mass spectrometer involves the pseudo-first order approximation. Kinetics experiments performed on an ICR instrument measure the pseudo-first order reaction rate constant. To report bimolecular reaction rate constants, one must divide k' by the pressure of the reactant B. Thus accurate bimolecular rate constants can only be obtained with precise pressure measurements.

Two correction factors must be considered for pressure measurements taken directly from an ionization gauge on an FTICR mass spectrometer. The first, and more common source of error of these measurements, is due to gauge sensitivity. The

ionization gauge sensitivity is dependent on the polarizability and ionization potential of the gas being measured and for this reason different gases at the same pressure can give different ionization gauge readings. This error is corrected with the implementation of an empirical sensitivity correction factor.

The second, and usually much larger, correction of the ionization gauge pressure readings is employed to account for the difference in pressure that exists between the ionization gauge and the ICR reaction cell. Because typical FTICR mass spectrometers use relatively high field superconducting magnets and ionization gauges that are affected by magnetic fields, instrument designs are constrained such that the ionization gauge is located external to the magnetic field and a significant distance away from the ICR cell, as is illustrated in Figure 2.7. The difference in pressure is also corrected with an empirical factor, called the system factor. The implementation of sensitivity correction factors is quite routine and they are determined by plotting the simultaneous pressure readings from an ionization gauge and a capacitance manometer on a sample of trapped gas. The inverse of the slope of such a plot (with the capacitance manometer readings on the abscissa) is the sensitivity correction factor for the particular gas that was used perform the measurements. The system factor is more difficult to quantify and the remainder of this chapter will present the results of three independent

attempts to determine the system factor for the FTICR instrument used throughout this dissertation.

Experimental

The instrument used for all the work presented in this chapter was the standard Nicolet FT/MS-1000 mass spectrometer with the Nicolet 1280 minicomputer described in Chapter 2. For some of the pressure measurements presented here and for the kinetics experiments described in Chapter 6, the actual pumping speed of this system as used was somewhat less than 300 L/s, because the main gate valve that isolates the vacuum chamber from the pump was partially closed (reproducibly to a 1/4 open position). Operation with a partially closed valve was beneficial because it greatly reduced pressure fluctuations and the system factor (defined below). Typical background pressures were in the low 10^{-9} torr region even with the valve in the 1/4th open position. Pressure measurements were made with two Granville-Phillips ionization gauge controllers (both were model number 274 025) and two Huntington Thoria coated nude ionization gauges and one Baratron Capacitance manometer (MKS Baratron 200 series, type 270A). Methane, argon and nitrogen gases used were ultra high purity grade and were used without further purification. Liquid samples were generally spectro grade and were subjected to several freeze pump thaw cycles before use. Solid samples included ferrocene and $Fe(acac)_3$. Both solids were pumped on

for several minutes at pressures near 10^{-3} Torr prior to use.

The system factor is defined by

$$f_{sys} = \frac{P_{cell}}{P_{ion\ gauge}} \qquad (3.6)$$

where P_{cell} and $P_{ion\ gauge}$ are the pressures at the cell and ion gauge respectively. The system factor was evaluated by performing three distinct experiments. The first measurement involved the kinetic energy-independent (Meot-ner, 1979) reaction

$$CH_4^+ + CH_4 \rightarrow CH_5^+ + CH_3 \qquad (3.2)$$

This most-studied ion-molecule reaction was used for calibration purposes in these studies. The time sequence used for this experiment is shown in Figure 3.1. CH_3^+ and CH_4^+ ions were formed during the beam event. All ions were then allowed a relaxation period, usually 100 ms. This relaxation delay was implemented to allow time for collisions to relax the ions to the center of the cell, where the detection efficiency has been shown to be the highest. More information regarding the relaxation delay and its effect on ion intensities is presented in Chapter 6. After the relaxation delay, a variable length delay was employed to measure the time dependence of the ion signals. At the end of the reaction period, ions were excited by the application of an radio frequency pulse to the excitation plates. Ion transient response signals, normally 16 K data points acquired in the broadband mode, were then detected, amplified, digitized, and

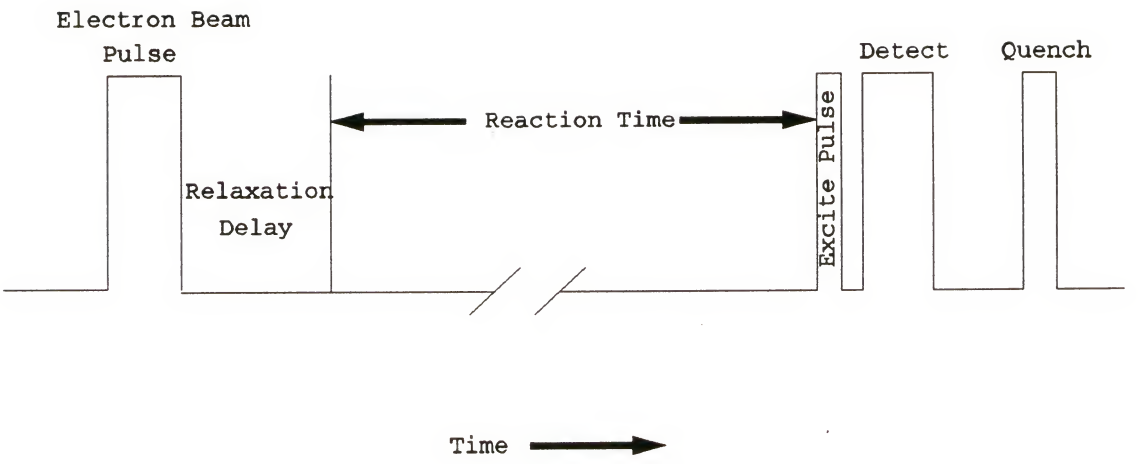

Figure 3.1. A schematic representation of the sequence of events used for kinetics measurements of the kinetic energy independent reaction, $CH_4^+ + CH_4 \rightarrow CH_5^+ + CH_3$.

signal averaged. The maximum digitizing frequency for this instrument as used for this study was 5.32 MHz. This bandwidth restricted the observable frequency range to frequencies that corresponded to the mass range of 17.3 amu or greater. This precluded the direct observation of CH_4^+, and CH_5^+. However, increasing the excitation frequency to above 2.667 MHz excited these ions and they could be observed as "reflected" peaks around 17.6 and 18.6 amu (Cody et al., 1987). These ions could also be observed by using the heterodyne detection mode. Ion frequencies were mixed with a carrier frequency of 3.135 MHz. Sum and difference frequencies resulted from this mixing and the selection of the difference frequency by a suitable low-pass filter resulted in frequencies corresponding to masses 16 and 17 that were lower than 2.667 MHz and could be observed directly. Both methods yielded the same rate coefficient for Reaction (3.2), and consequently the "reflection" technique was more commonly employed due to its simplicity. This reaction was measured over the pressure range from 1×10^{-7} to 1×10^{-6} Torr. The study was done at a variety of trapping voltages, but usually the trapping voltage was 1.0 V. The electron energy used to create CH_4^+ was nominally 15 V.

A second system factor determination was performed by connecting the capacitance manometer to a hollow stainless steel tube (i.d. = 10 mm) and inserting the tube through the solids probe inlet port into the vacuum chamber so that the

open end of the tube was within a few millimeters of the cell (as shown in Figure 3.2). Simultaneous pressure readings of the ionization gauge and the capacitance manometer were then obtained on the system with the gate valve in the 1/4th open position. This was accomplished by leaking in nitrogen, allowing the pressure to stabilize and then recording the readings on the ionization gauge and on the capacitance manometer. The slope of the plot of the capacitance manometer data versus the sensitivity corrected ionization gauge data was interpreted as the system factor. This differs from the normal sensitivity correction factor measurements because the gate valve connecting the system to the pumps was in the 1/4th open position. This experiment was repeated 10 times with nitrogen.

The final determination of the system factor involved placing a second ionization gauge at the location of the ICR cell, in place of the cell, in the absence of a magnetic field. First, a sensitivity correction factor was obtained for the standard ionization gauge (the gauge normally used for pressure measurement) by the usual sensitivity correction factor measurement routine involving the capacitance manometer. The gate valve was closed and a gas was leaked into the vacuum chamber. As the pressure gradually increased in the chamber, simultaneous pressure readings were taken from the ionization gauge and the capacitance manometer. The sensitivity correction factor for the standard ionization

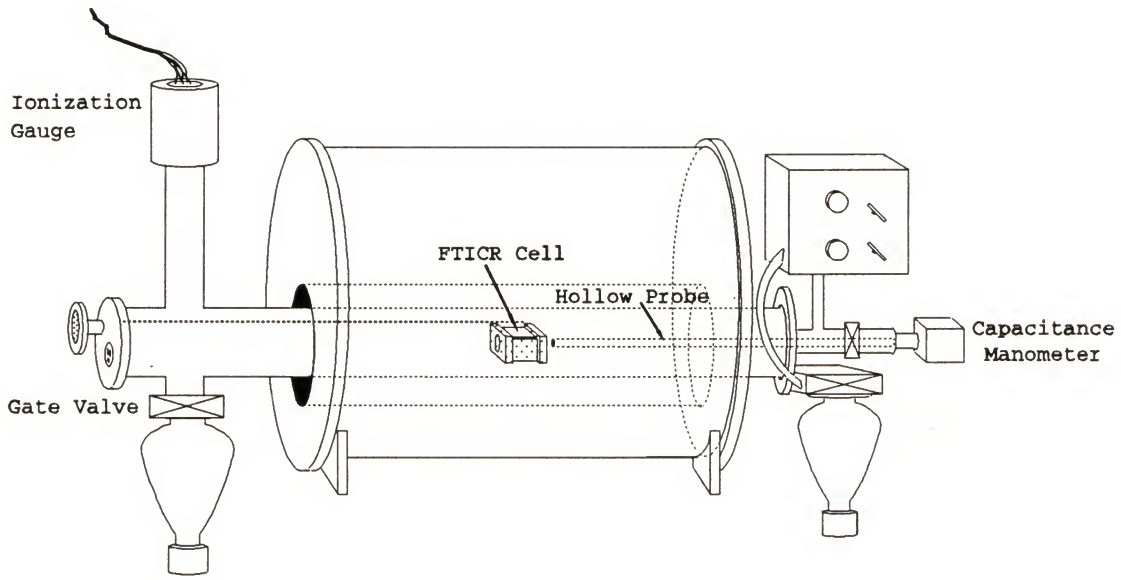

Figure 3.2. Illustration of the spatial relationship between the ionization gauge, FTICR cell, and capacitance manometer/hollow probe assembly used for system factor measurements.

gauge was obtained from the data, as was described in the previous paragraph. A similar process was performed to determine the sensitivity correction factor for the ionization gauge placed at the FTICR cell position (here termed the "cell ionization gauge", since it was located where the cell would normally be). Simultaneous pressure readings were then taken on both ionization gauges by leaking in a gas, allowing the pressure to stabilize, and then recording both pressure measurements, with the gate valve in an open position. A series of experiments of this type were done to determine the system factor with the gate valve in the 1/4th open and fully open positions. The slope of the plot of the readings of the ion gauge at the cell position versus those of the normal ion gauge (both gauges independently sensitivity corrected) yielded the system factor. This experiment was repeated with several different substances to determine if the nature of the compound being measured in any way affected the resulting system factor.

Results and Discussion

The first system factor measurement involved the kinetic energy-independent ion-molecule reaction, Reaction (3.2). Typical data for this reaction are shown in Figure (3.3). Illustrated in this figure are the normalized intensities of CH_4^+ and CH_5^+. The decaying CH_4^+ normalized intensities are fit to an exponential curve, typical of pseudo-first order

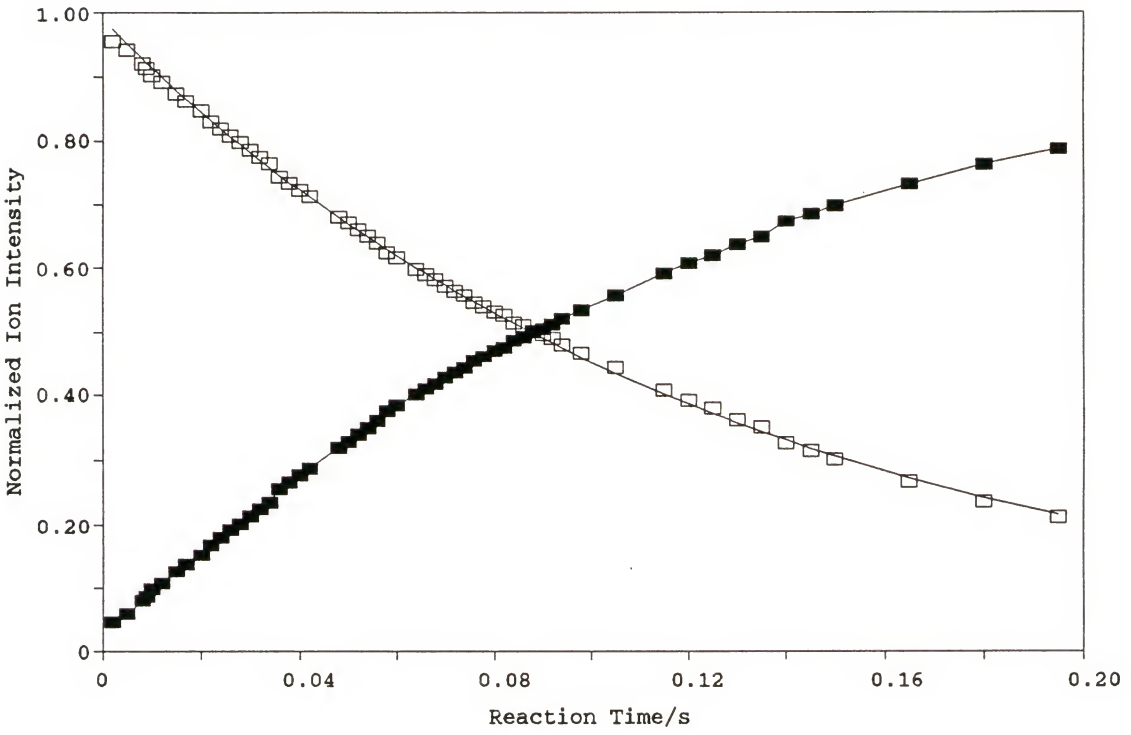

Figure 3.3. Typical data for the kinetic energy-independent Reaction (3.2). Empty rectangles are CH_4^+ normalized intensity, filled rectangles are CH_5^+.

kinetics. The pressure dependence of the rate constant for this reaction was also investigated; the results are shown in Figure (3.4). Also indicated in Figure (3.4) is the average of numerous previously published values (Ikezoe et al.,1987). The system factor estimate extracted from this work was obtained by dividing the average observed rate constant by the average literature rate constant. The average observed rate constant is (2.26 ± 0.1) x 10^{-9} cm^3s^{-1} and the average literature value is 1.13 x 10^{-9} cm^3s^{-1} (Ikezoe et al., 1987). This study indicates a system factor of 2.0, i.e., the pressure at the FTICR cell is twice as high as the pressure at the ionization gauge when the gate valve is adjusted to the 1/4th open position.

The second system factor estimate was obtained with experiments involving the capacitance manometer and the hollow solids probe, as discussed above. This experiment was done with nitrogen and the sensitivity correction factor measured for nitrogen was 1.05. The procedure to determine the system factor, which involved leaking in N_2, allowing the pressure to stabilize, and then recording the simultaneous pressure readings of the ionization gauge and the capacitance manometer, was repeated 10 times. The slopes extracted from each of these plots were virtually identical and the average of all ten determinations is represented in Figure 3.5. Also shown in this figure is the linear regression fit to these data. An excellent fit was obtained. The error associated

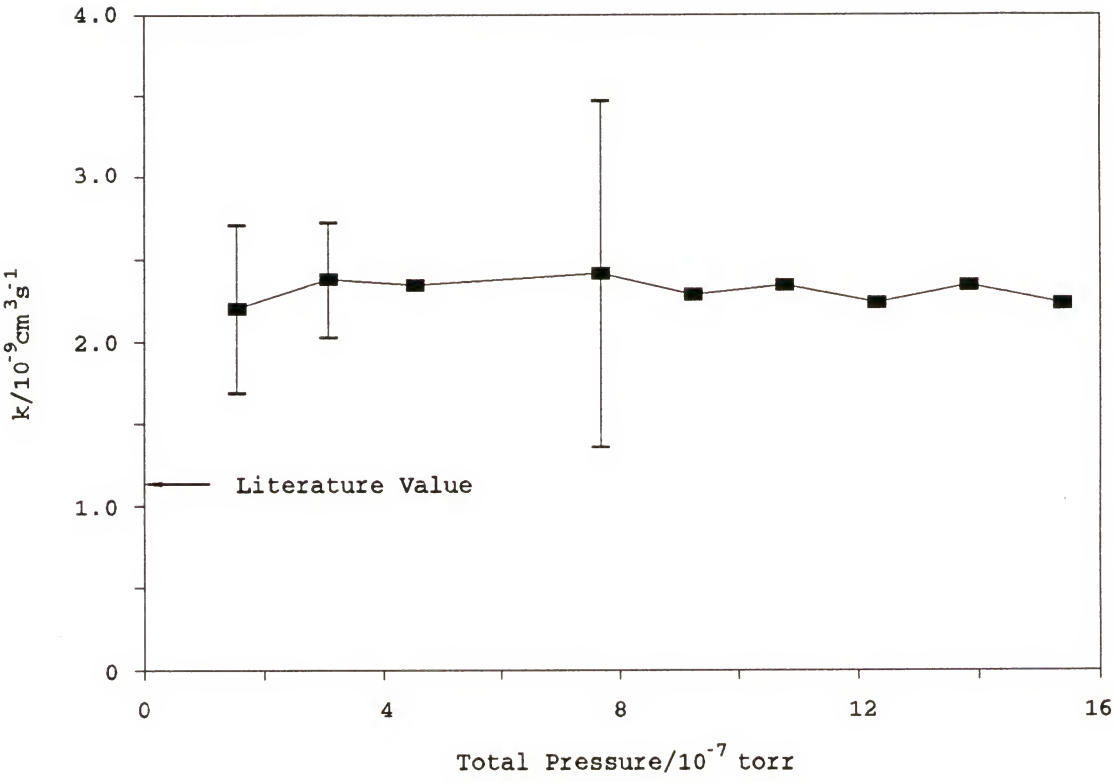

Figure 3.4. Reaction rate constant as a function of pressure for Reaction 3.2. Error bars shown are the 95% confidence limits of the mean for multiple determinations.

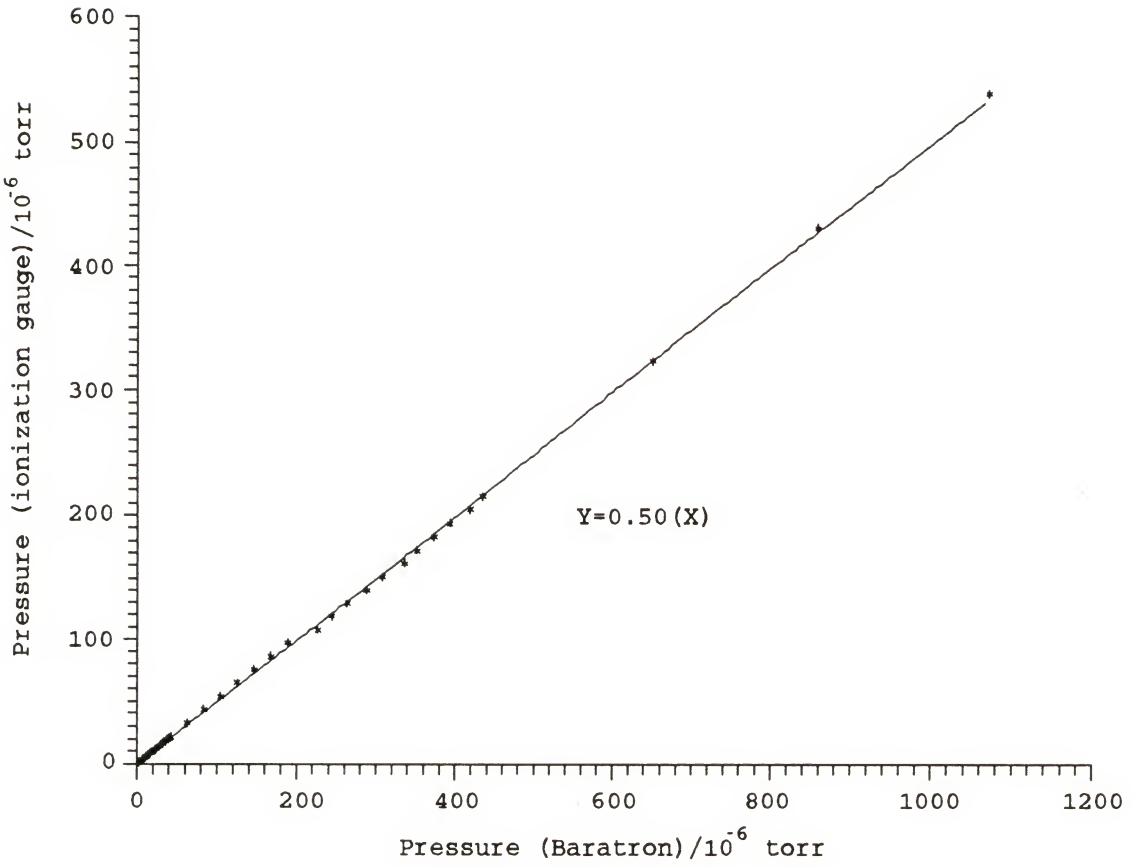

Figure 3.5. System factor measurement data obtained with the capacitance manometer/hollow solids probe and ionization gauge experiment done with nitrogen.

with the slope measurements was exceedingly small and is estimated to be less than 5%. The small deviations that were observed occurred when the ionization gauge changed scales i.e., from the 10^{-6} torr range to the 10^{-5} torr range. These variations are due to the inherent non-linear response of the ionization gauge. The slope that was obtained is 0.50 (the capacitance manometer readings are plotted on the abscissa) and thus the system factor estimate from these experiments is 2.0, in excellent agreement with the previous study utilizing the kinetic energy-independent reaction, reaction (3.2).

The final system factor determination involved dual ionization gauge measurements, in the absence of a magnetic field. Several different compounds were used in these experiments. Nitrogen and methane were used to further verify the previous results of the capacitance manometer/hollow probe and kinetic energy-independent ion-molecule reaction studies. Higher molecular weight and more "sticky" compounds were used to determine if the system correction factor was dependent upon the substance being measured. These experiments were performed with the gate valve adjusted to the 1/4th open position as well as the fully open position. Typical data for this type of experiment are shown in Figure 3.6. These data were obtained by leaking in nitrogen, allowing the pressure to stabilize, and then recording the pressure readings observed on both ion gauges, with the gate valve adjusted to 1/4th open. Sensitivity correction factors were obtained for each

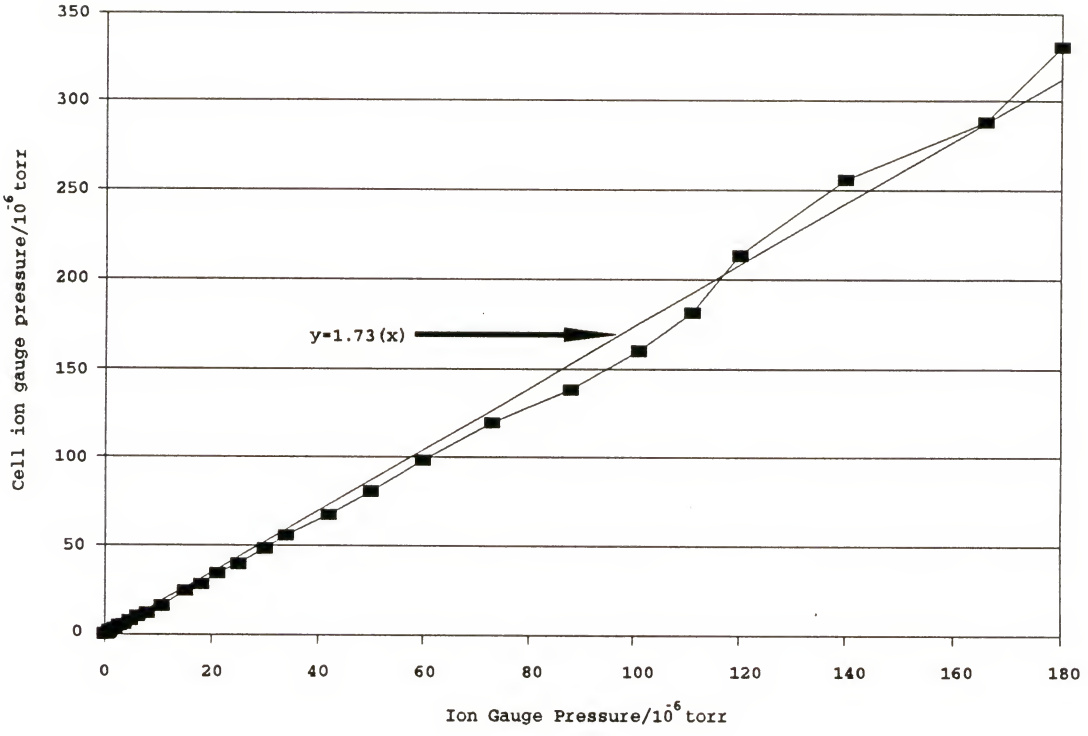

Figure 3.6. N_2 data obtained from the system factor measurements performed with two ionization gauges in the absence of a magnetic field and the gate valve in the 1/4th open position.

substance for both ionization gauges prior to performing system factor measurements, such as those shown in Figure 3.6. The sensitivity correction factors were usually nearly equal for both ionization gauges for a given substance since identical filaments and controllers were used for both measurements. The results of all the sensitivity correction factor measurements and for the 1/4th open gate valve system factor measurements are shown in Table 3.1. The 1/4th open gate valve system factor measurements are also shown graphically in Figure 3.7. The results for the fully open gate valve system factor measurements are shown in Table 3.2 and graphically in Figure 3.8. The variations in the observed system factors must be regarded as random noise since no trend is evident in both the 1/4th open and fully open gate valve studies. The average of all 1/4th open gate valve system factors is 1.9, in good agreement with the previous two determinations. The average value for the fully open gate valve system factor is 4.3. Thus this study indicates that the pressure at the FTICR cell is 4.3 times higher than the pressure at the ionization gauge when the gate valve is fully open. This study, as well as the two previous investigations, demonstrate very clearly that the pressure at the cell is twice as high as the pressure at the ionization gauge when the gate valve is in the 1/4th open position.

A serious discussion regarding pressure calibrations must include some reference to the work done by Bartmess and

Table 3.1. The results for ion gauge versus cell ion gauge study to determine the system factor with the 1/4th open gate valve.

Sub.	Abb.	IG/CM	CIG/CM	SEF	f_{sys}
N_2	N2	0.857 ± .07	0.803	1.07	1.73
CH_4	ME	0.947 ± .07	0.947	1.04	1.75
CH_3OH	MO	0.748 ± .13	0.686	1.02	2.00
Ar	AR	1.12 ± .07	1.04	1.08	1.71
Benzene	BZ	0.861 ± .14	0.963	0.894	1.61
Aniline	AN	0.781	0.839	0.931	2.10
Ferrocene	FE	0.800	0.741	1.08	1.96
$Fe(AcAc)_3$	FA	0.738	0.702	1.05	2.42

Sub. = Substance

Abb. = Abbreviation

IG/CM = Standard ion gauge sensitivity correction factor.

CIG/CM = Cell ion gauge sensitivity correction factor.

SEF = Sensitivity equalization factor (=(IG/CM)/(CIG/CM))

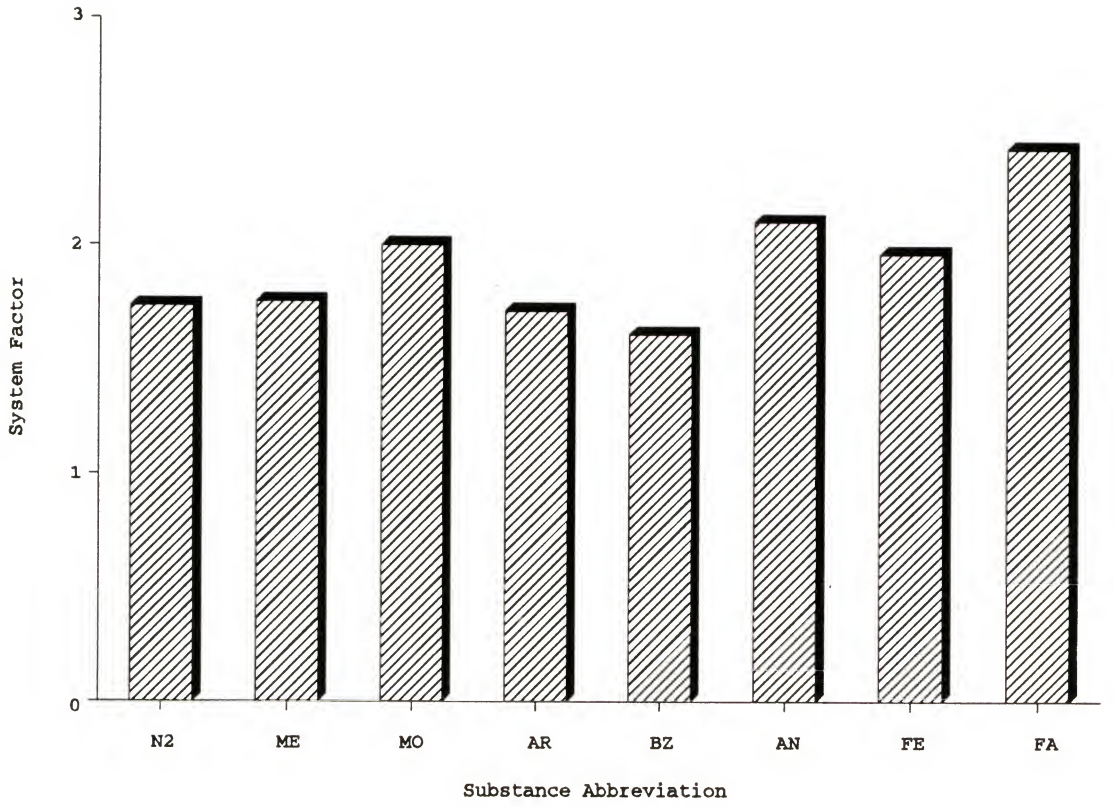

Figure 3.7. Results of system factor measurements performed with two ionization gauges in the absence of a magnetic field and the gate valve in the 1/4th open position.

Table 3.2. The results for the ion gauge versus cell ion gauge study to determine the system factor with the gate valve fully open.

Sub.	Abb.	IG/CM	CIG/CM	SEF	f_{sys}
N_2	N2	0.857 ± .07	0.803	1.07	3.77
CH_4	ME	0.947 ± .07	0.947	1.04	4.00
CH_3OH	MO	0.748 ± .13	0.686	1.02	4.65
Ar	AR	1.12 ± .10	1.04	1.08	3.91
Benzene	BZ	0.861 ± .14	0.963	0.894	5.00
Aniline	AN	0.781	0.839	0.931	4.72
Ferrocene	FE	0.800	0.741	1.08	4.57
$Fe(AcAc)_3$	FA	0.738	0.702	1.05	4.05

Sub. = Substance

Abb. = Abbreviation

IG/CM = Standard ion gauge sensitivity correction factor.

CIG/CM = Cell ion gauge sensitivity correction factor.

SEF = Sensitivity equalization factor (=(IG/CM)/(CIG/CM))

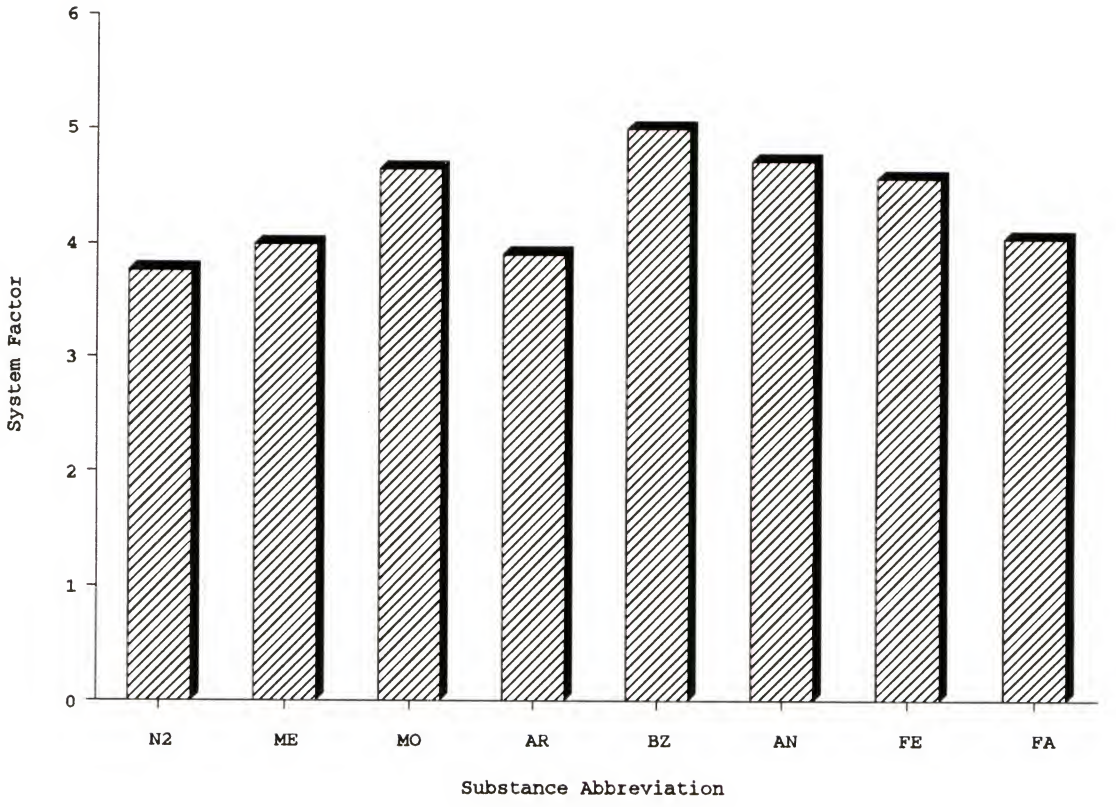

Figure 3.8. Shown are the results of the system factor measurements performed with two ionization gauges in the absence of a magnetic field and the gate valve in the fully open position.

Giorgiadis, (1983). This study was performed to develop an empirical method for determination of ionization gauge sensitivity correction factors. The sensitivity correction factors were found to correlate best with the polarizability, α, with $R_x = 0.36\alpha + 0.30$, where R_x is the sensitivity correction factor relative to N_2. The work was performed with a differently configured vacuum chamber and consequently, sensitivity correction factors were measured in a different manner. However, one would expect that the sensitivity correction factors relative to N_2 should at least be similar for the two experiments.

The primary goal of the work presented in this portion of the chapter was to take advantage of the absence of a magnetic field for the determination of system factors for this instrument. However, sensitivity correction factors were also determined and are given in Table 3.1 as IG/CM. These are absolute correction factors and must be divided by 0.857, the correction factor for N_2, for comparison to the data presented by Bartmess and Giorgiadis. Error limits indicate the 95% confidence limits for multiple determinations (n=3 for N_2, Ar and methane; n=2 for methanol and benzene). While N_2 (by definition) and Ar values agree quite well with those data from Bartmess and Giorgiadis, the values for the other compounds disagree by varying amounts (the present data are low in comparison by factors from 1.4 to 4.3).

The cause of the disagreement is unclear. One

possibility might be the presence of impurities in the inlet system. However, if this were the case one might expect to see these impurities in the mass spectrum of the examined compound. This is not the case with benzene. Benzene (the compound in Table 3.1 with the largest difference from previous data) has been calibrated on numerous occasions and no evidence has been observed to implicate a background contaminant. Another possibility is the existence of a pressure differential between the capacitance manometer and the ionization gauge with the system in a closed configuration. The differential might be larger for larger, slower moving compounds. If this were true, one would expect to observe a similar, but smaller pressure differential between the capacitance manometer and the ion gauge located at the cell position. This was not observed; sensitivity correction factors for the two ionization gauges were very similar (compare IG/CM to CIG/CM). Furthermore, later pressure calibrations done with the capacitance manometer located close to the ionization gauge resulted in similar sensitivity correction factors.

Conclusions

The work presented in this chapter shows that there does exist a large difference between the pressure at the ionization gauge and the pressure at the FTICR cell. This might be expected upon examination of the physical locations

of the gauge, the cell, and the pump. The evidence from three independent measurements of the pressure difference demonstrates that the pressure at the FTICR cell is a factor of two times higher than the pressure at the ionization gauge when the gate valve is in the 1/4th open position. Therefore, for all pressure measurements and rate constants presented throughout the remainder of this dissertation, a system factor of 2 will be applied. The data obtained with the dual ionization gauges in the absence of a magnetic field also indicate that neither the molecular weight, nor the "stickiness" of the substance alter the system factor significantly. Finally, one may conclude that the pressure difference increases to a factor of 4.3 when the gate valve is adjusted to the fully open position. The value is also supported by later measurements that were performed with the kinetic energy-independent reaction with the gate valve fully open. The rate constant obtained with the gate valve fully open was $(4.9 \pm 0.3) \times 10^{-9}$ cm^3s^{-1} (95% confidence limits, n=7). Assuming the same literature value as before, this indicates a system factor for the fully open gate valve configuration of 4.3.

CHAPTER 4
TIME-OF-FLIGHT KINETIC ENERGY MEASUREMENTS

Introduction

Perhaps the most logical method of determining trapped ion kinetic energies would be to measure them directly. Time-of-flight measurements, typically used for mass analysis, are based on the simple equation

$$KE=\frac{1}{2}mv^2 \qquad (4.1)$$

where KE is the kinetic energy of a particle, m is the mass of the particle, and v is its velocity. For mass analysis, as is performed with a time-of-flight mass spectrometer, the particles are usually singly charged ions. With proper application of voltages to acceleration electrodes, the kinetic energy of the particle is known. After acceleration, the time that elapses during the ion's free flight period through a defined distance is measured, yielding the velocity. Thus from Equation (4.1), one can easily solve for the mass of the particle, m. Conversely, if one knows the mass of the particle, this same equation can be applied to the measurement of ion kinetic energies. This is the basis for the experiments devised by Dunbar and Weddle (1988). They were interested in the photodissociation of ions trapped in a FTICR

mass spectrometer. More specifically, they were interested in measuring the amount of kinetic energy released upon photodissociation.

The measurement of the kinetic energy of fragment ions produced by photodissociation of trapped ions in an FTICR mass spectrometer is not an entirely new scientific endeavor. For many years, the technique known as kinetic energy release (KER) or kinetic energy spectroscopy has been used to measure the kinetic energy released upon photodissociation, in order to infer electronic state information (Rincon et al., 1988). A similar technique has been applied to the measurement of the kinetic energy released from exoergic ion-molecule reactions (Mauclaire et al.,1979). For experiments such as these, the ability or inability of the product ions, either from photodissociation or ion-molecule reactions, to escape from the FTICR cell along the z-axis is investigated. Measurements of the fraction of ions that escape at various applied trapping voltages provide information about the ions' velocity and thus, for a given mass, about the ions' kinetic energy. This method works quite well, as is evident from the many papers published utilizing KER measurements. However, this technique is contingent upon maintaining a well defined trapping well as the trapping potential is lowered. Unfortunately, the ability to do so is significantly decreased at trapping potentials below 100 mV. So, while the KER technique works well for higher energy ions, the approach is

inapplicable for the low energy ions produced by photodissociation which are of primary interest to the Dunbar group, and even more so for the near thermal ions that are produced by electron ionization which are of interest in this thesis.

The alternative method of time-of-flight kinetic energy measurements seems quite attractive for researchers interested in low energy ions. The basic approach in this type of experiment is to make the ions, allow them to be collisionally relaxed to the center of the ICR cell, drop the trapping potential to zero volts for a short time (on the microsecond time scale) so that ions with high kinetic energy are lost, restore the trapping potential to its original value, and measure the resulting ion intensity. Ion intensity decay curves are obtained by successively increasing the time at which the trapping plates are held at zero volts. Analysis of the shape of the decay curve provides information about the ion kinetic energies.

Experimental

These experiments were performed over a period of about two years. Consequently, both of the computers used for data acquisition and experiment control described in Chapter 2 were utilized for these experiments. Neither instrument had the ability to pulse the trapping potential (other than the quench pulse) and entirely different external trap plate voltage

pulsing circuits were used due to the different operating characteristics of each computer. Both pulsing circuits and interfaces are described below.

Early experiments were done with the Nicolet 1280 computer and associated electronics. The software for this computer did have a feature that allowed the user to pulse the trap plate potential to zero volts. However, the electronic components (and programming constraints) responsible for this pulse were far too slow for time-of-flight measurements. The minimum pulse width that could be attained from this feature was around 0.5 ms. However, this computer also had the ability to produce TTL pulses (still with a minimum pulse width of 0.5 ms) at any time during the experiment, and this feature was used to trigger an external circuit that controlled the trapping potentials for these experiments.

A schematic diagram of the circuit used for these early experiments is shown in Figure 4.1. The circuit is based on a one shot RC-timer. The only input required from the 1280 computer was the TTL pulse that was used to trigger the circuit. As is common to RC timer circuits, the duration of the zero volt pulse is controlled by the values of the resistor, R1, and capacitor, C1. This circuit followed the approximate law $t=0.45(R1)(C1)$, where t is the duration of the pulse. The resistor used for R1 was a ten turn potentiometer and the length of the zero volt pulse was adjusted by adjusting R1. The range over which adjustments could be made

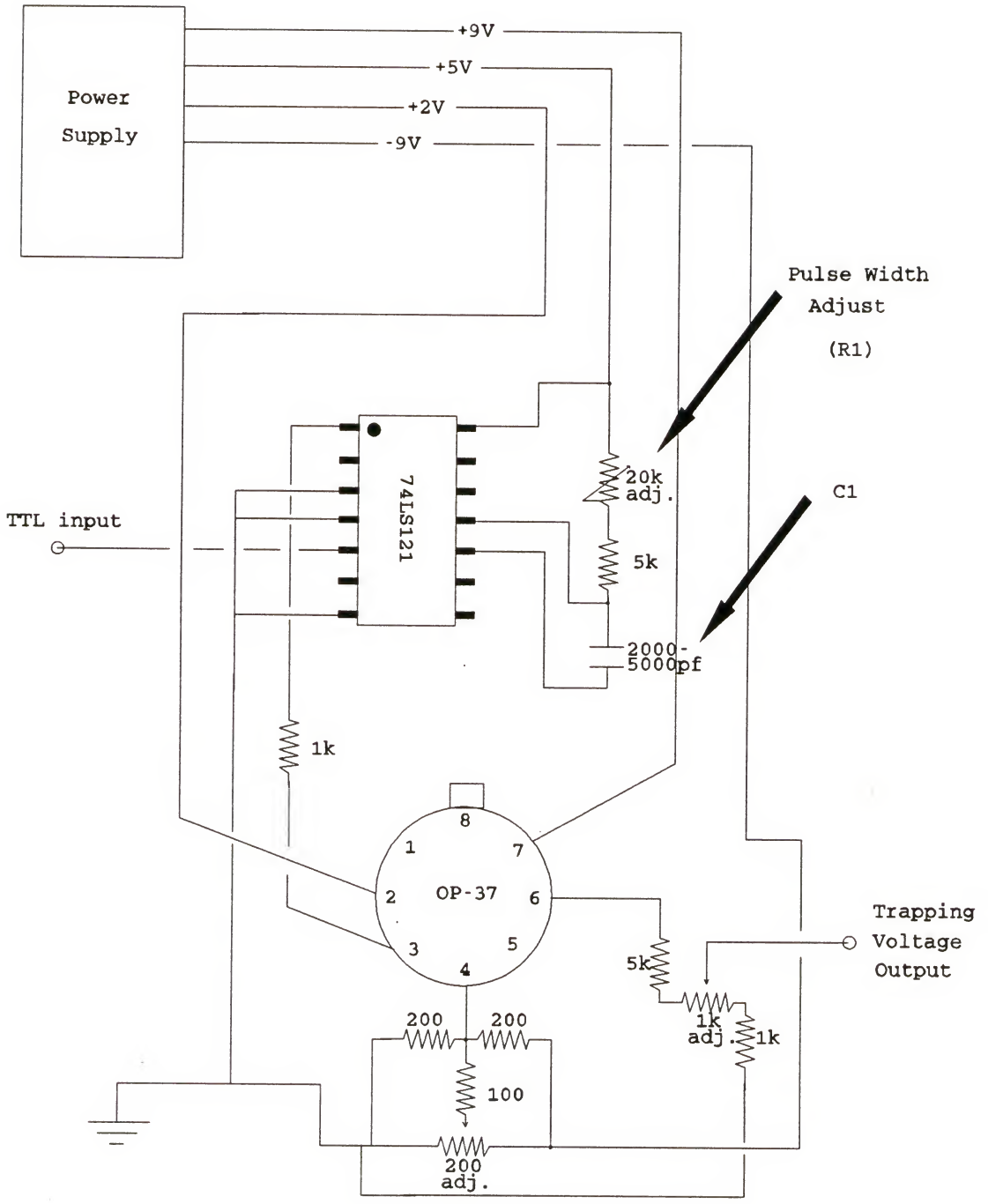

Figure 4.1. A schematic diagram of the circuit used to pulse the trapping potential to zero volts with the Nicolet 1280 computer system.

was controlled by C1. Zero volt pulses of a duration from 8 microseconds to several milliseconds were achieved with this circuit. The length of the pulse was measured with a LeCroy 125 MHz digital oscilloscope. The reference ground for the zero volt pulse was the common ground of the instrument. Several experiments were performed in which the potential was not pulsed to ground, but rather to a small positive or negative voltage. One peculiarity of this configuration in general was that the trapping voltage was completely controlled by the external circuit. The normal trapping voltage lines from the Nicolet computer were completely disconnected. This created the problem that the experiment had no quench pulse. However, the experimental sequence was altered so that after the detection period, when the quench pulse would normally occur, a long swept frequency eject of large amplitude was implemented. This eject covered the observed mass range and served to eject all ions.

Later experiments were done with an entirely different circuit. The IonSpec system was capable of producing microsecond width TTL pulses. However, this system was not capable of pulsing the trapping potential (other than the quench pulse) upon command. Therefore, an external circuit had to be used with this system to perform ion time-of-flight experiments as well. The circuit was quite different from that used with the Nicolet 1280 system, and is shown in Figure 4.2. It did not rely on a one shot RC timer to determine the

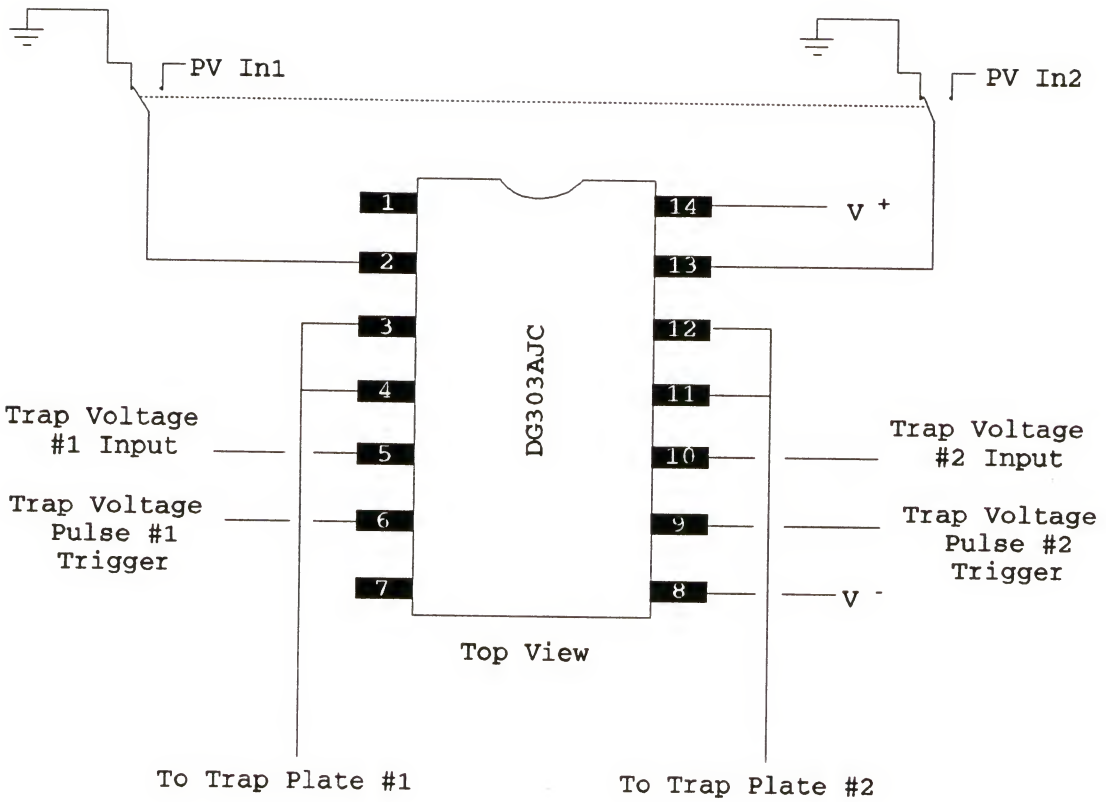

Figure 4.2. A schematic diagram of the circuit used to pulse the trapping voltage to zero volts with the IonSpec computer system.

pulse length; instead, the pulse length was set via the Omega software controlling the IonSpec system. As is shown in Figure 4.2, the external circuit was merely an analog switch that was used to switch the potential on the trapping plates. This circuit had two separate sets of inputs and switches that allowed the user to pulse each trap plate independently. The switch shifted between the trap plate voltage (pins 5 and 10 labeled as Trap Voltage #1 Input and Trap Voltage #2 Input in Figure 4.2), here controlled by the IonSpec system as in the normal configuration, and another input (pins 2 and 13 respectively). This input line had another switch (shown at the top of Figure 4.2) that allowed the user to switch from the ground common to the ac line to a voltage input on a BNC. In this figure, PV In1 is the pulse voltage input for trapping plate 1 that was connected to the BNC as mentioned above. PV In2 is a similar input for trapping plate 2. Quite frequently the switch was used in the "input voltage" position and the input voltage BNC was connected to an earth ground present in the laboratory.

The analog switch (DG303AJC) responsible for pulsing the trapping voltage to ground switched when the input line from the IonSpec was high. During the period in which the line remained high, the DG303 remained in its switched position and when the line went low, the DG303 switched back to its original position. The result of this switching was that the length of the zero volt pulse was equal to the length of the

pulse coming from the IonSpec system. This was advantageous in that the entire time-of-flight data collection procedure was completely under computer control, using a "user" pulse to control the DG303 and the width scan feature to control the width of the user pulse. (A "user" pulse is a user programmable TTL pulse that can be configured to occur at any time during the experimental sequence with practically any pulse width.) This configuration was also better than the Nicolet 1280 setup because the original quench pulse was still in operation, eliminating the need to implement a lengthy eject at the end of each experiment.

Also used in the later experiments was an electron collector to detect the electrons emitted from the filament during the electron beam event. The collector was positioned on the side of the cell opposite the filament. The collector itself consisted of a flat stainless steel plate upon which a 9 V potential was applied and upon which the electrons would impinge after traversing the cell. A limitation of the IonSpec system was the lack of an electron collector measurement circuit. The IonSpec system comes standard with a measurement system that measures the number of electrons lost from the filament, not the number traversing the cell. Hence, another external circuit was built to measure the number of electrons that passed through the cell. This circuit was housed in the same box that housed the trap voltage pulsing circuit and used the same power supply. A

schematic diagram for this circuit is shown in Figure 4.3. This circuit was essential to the time-of-flight kinetic energy measurements because it was found that the ion decay was greatly affected by space charge effects. To produce similar ion intensity decay curves, similar numbers of ions had to be initially be present. This required similar pressures, beam voltages, and emission currents. The collector was used during the setup procedure which included adjusting the filament to the desired emission current and allowing the system to equilibrate. When the current had stabilized, usually after 15-20 minutes, the collector was connected to the same earth ground that was input on the BNC "input voltage" line. This proved to be significant for obtaining smooth ion intensity decay curves. The collector circuit was also invaluable for the time-of-flight experiments performed with an external filament assembly. The filament was moved away from the FTICR cell and placed near the fringing fields of the magnet on a manipulator assembly. The collector was used to properly align the filament with the cell, indicating the best alignment with the largest detected emission current for a set filament current.

A typical pulse sequence used for time-of-flight kinetic energy measurements is shown in Figure 4.4. Ions were formed by electron ionization in the electron beam event. The relaxation period was the time in which the ions were allowed to collide with neutral molecules and lose kinetic energy,

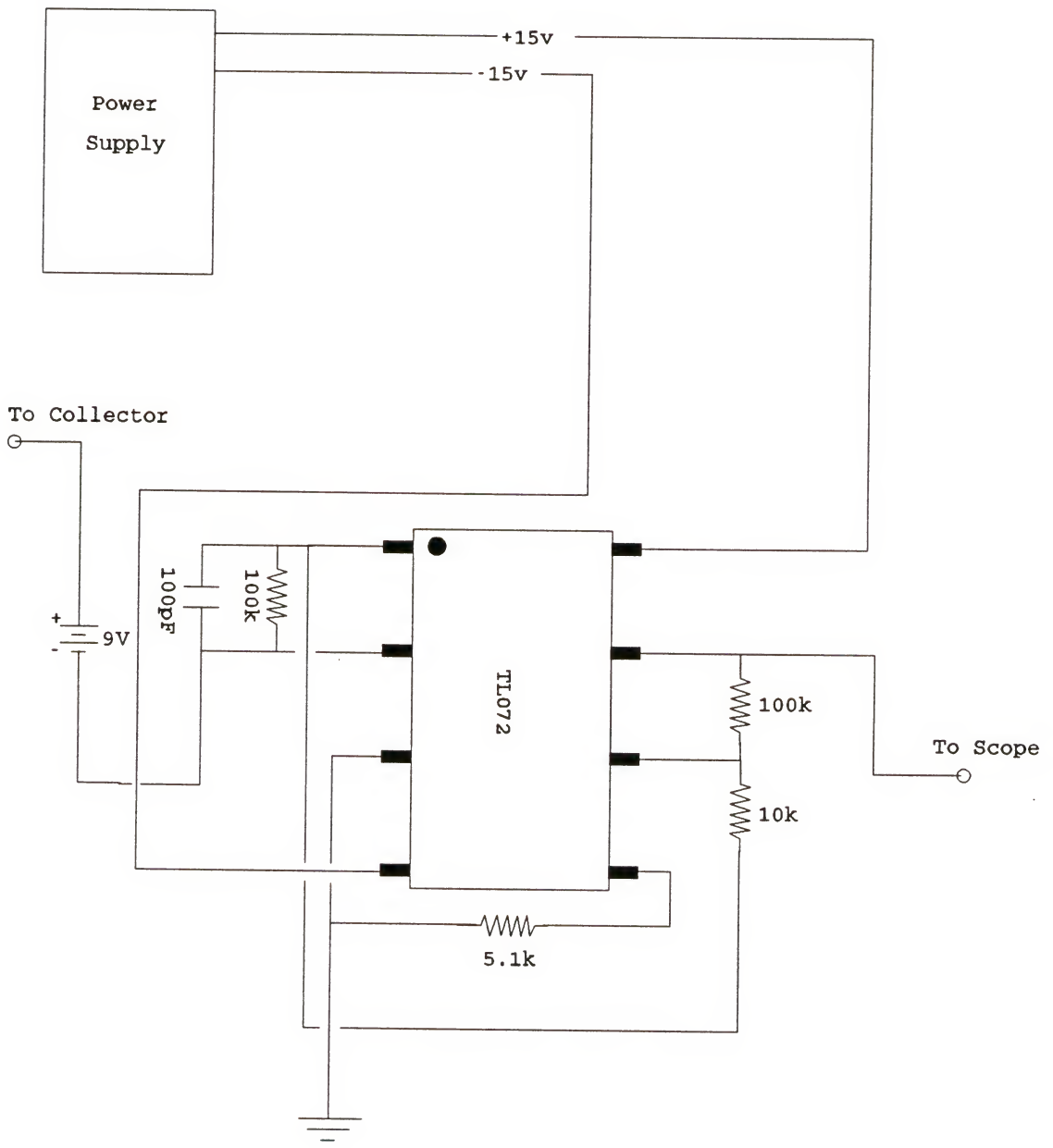

Figure 4.3. A schematic diagram for the circuit used to measure the electron emission current.

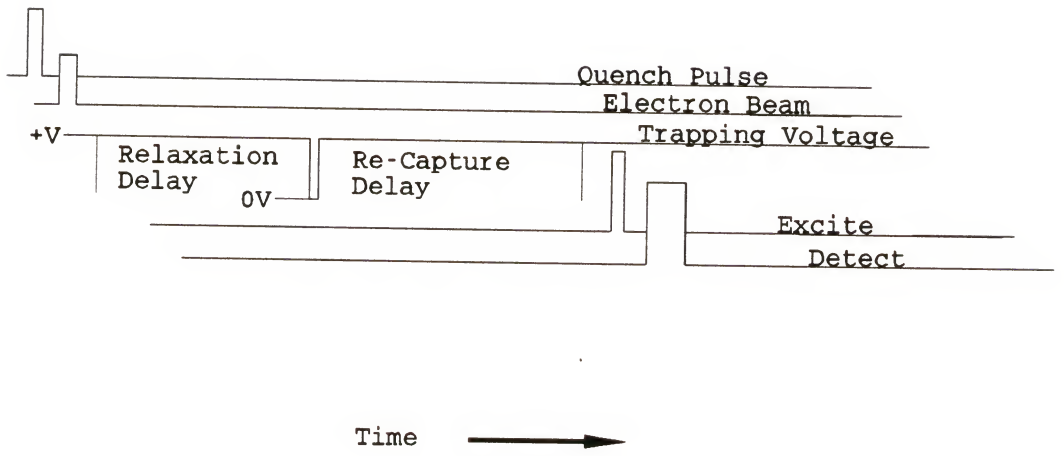

Figure 4.4. A typical pulse sequence used for time-of-flight kinetic energy measurements. The trapping voltage is pulsed to ground for periods on the microsecond time scale.

thus becoming relaxed along the z-axis. A usual value used for this delay was 200 milliseconds, which allowed for roughly 20 to 50 ion-molecule collisions to occur at the pressures employed. A user pulse was the trigger pulse which caused the switch (DG303AJC) to change the trapping voltage from the applied trapping potential to zero volts. A re-capture period, usually of length equal to the relaxation delay, then followed the zero volt pulse. This period was implemented to again allow ions to be relaxed to the center of the cell. This promoted higher detection efficiency and avoided the apparent decrease in ion intensity that would have been present at short zero volt pulse times if the ions moved off center, did not escape from the cell, and were not relaxed back to the center upon restoration of the trapping voltage. The quench pulse removed all ions from the cell.

Various trapping potentials were employed for the work presented in this chapter. Typically 1 or 2 volts were used. The ionizing electron energy was also varied, but was typically 20 volts. All other cell plates were held at zero volts, except when the excitation pulse was applied to the excite plates. Both excitation modes, chirp and impulse (defined in Chapter 2), were used; however, the chirp mode was more commonly used because lower masses were usually investigated. Ions were normally formed by electron ionization. For reasons discussed below, an external filament assembly was developed. However, several experiments were

also performed on ions produced by laser-desorption, such as C_{60}^+ and C_{70}^+.

Results and Discussion

Early results from the time-of-flight experiments were very interesting, but not promising. An example of the early results is shown in Figure 4.5. These data were gathered with benzene ions at a benzene pressure of 1 x 10^{-6} torr. The relaxation period and re-capture period were both 1 second. Thus the ions were allowed to undergo roughly 30 collisions prior to the zero volt pulse. This experiment was repeated several times with varying conditions; a "peak" near 100 microseconds was observed. Several (5) separate determinations are plotted in Figure 4.6. All determinations showed a disturbance (of varying intensity) near 100 microseconds. Next, experiments with Ar^+ ions were performed. These experiments showed similar behavior, except the "peak" was now shifted to 70 microseconds. Typical results for time-of-flight kinetic energy measurements performed with Ar^+ ions are shown in Figure 4.7. These data were taken with an argon pressure of 1 x 10^{-6} torr and a relaxation delay of 1 second. All these early experiments were performed without the use of an electron collector and as such the reproducibility of the T.O.F. profile curve was poor. However, the position of the peak was constant. Furthermore, this peak seemed to be

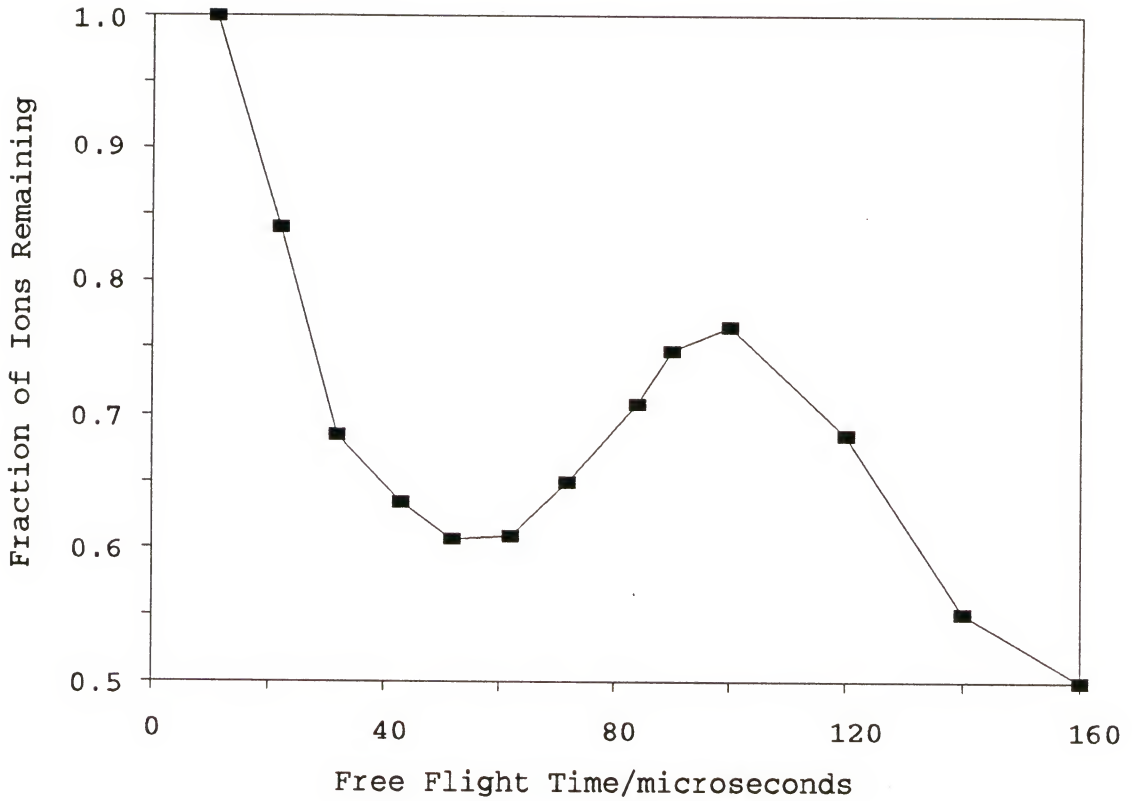

Figure 4.5. Typical results with benzene cations for the earlier TOF experiments using the Nicolet 1280 computer system.

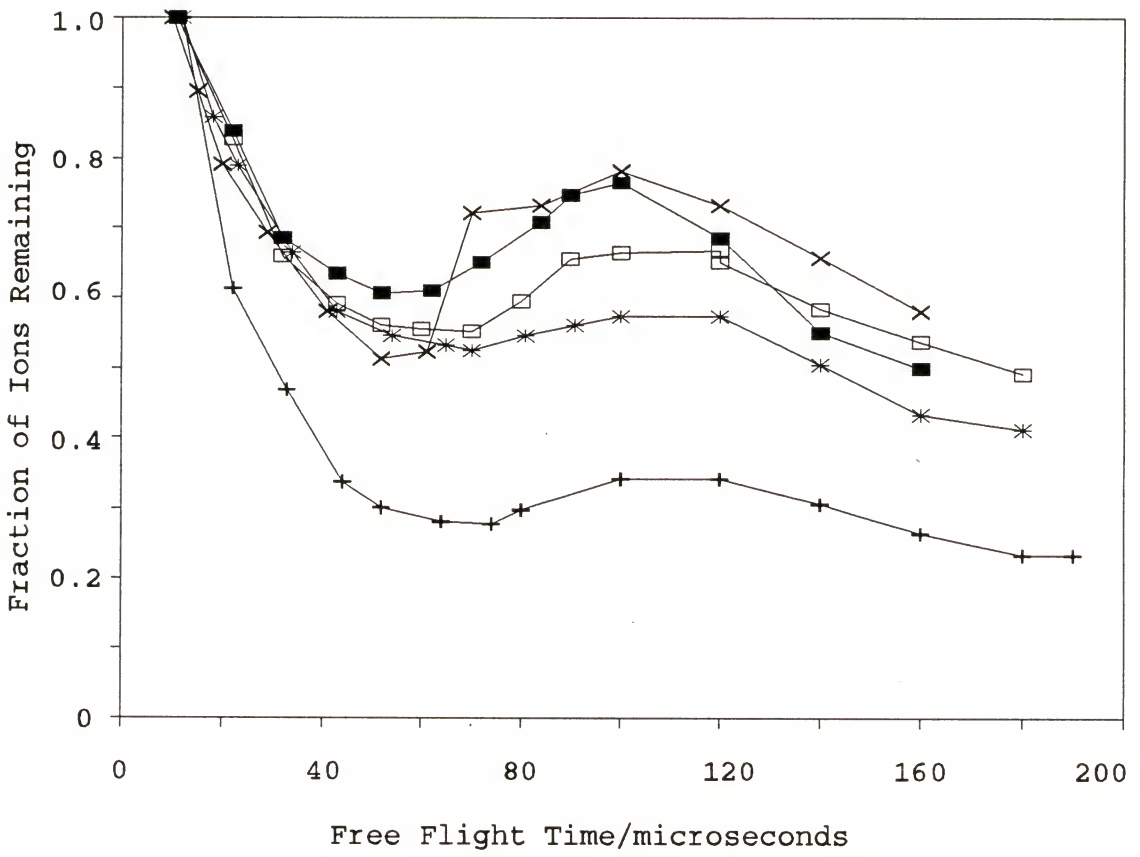

Figure 4.6. Simultaneous plot of five TOF kinetic energy determinations with benzene cations.

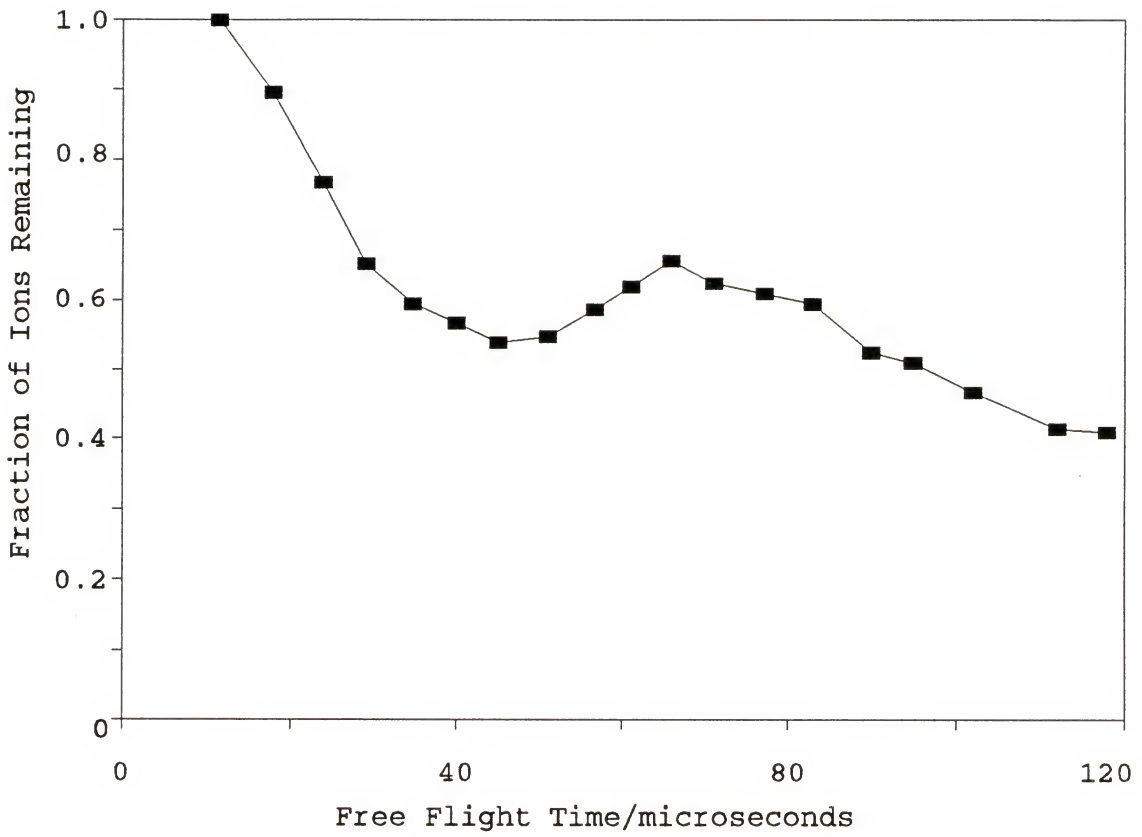

Figure 4.7. Typical results for time-of-flight kinetic measurements on Ar^+. The pressure and relaxation delay used for these data were 1 x 10^{-6} torr and 1 second, respectively.

dependent on the mass of the ion under study. It was postulated that peak was the result of ion reflection back into the cell, however it was unclear exactly what was the cause of the ion reflection. One possibility that was extensively investigated in this laboratory was related to the voltages applied to the filament assembly.

The filament is used as a source of relatively high energy electrons (up to 70 volts) that collide with neutral species and create ions. Normally, this filament is pulsed to a negative potential to repel electrons it emits through the cell during a well defined short time period that is commonly known as the beam event. Throughout the remainder of the experimental pulse sequence the filament is held at a positive potential, ca. +10 volts, so that no more ions are made. This is the state of the filament during the free flight period employed in these experiments for kinetic energy measurements. The filament was shielded so that the potentials present on it would not affect the ions trapped in the cell. A similar shielding electrode was reportedly used in the experiments described by Dunbar and Weddle (1988). However, the possibility that ions released from the cell during the free flight period could travel out of the cell far enough to experience the repelling positive potential of the filament does exist.

After formation and thermalization, ions trapped in an ICR cell will oscillate along the z-axis. The motion along

the other two axes is restricted by the Lorentz force due to the magnetic field and will be small for lighter ions. The thermal cyclotron radius for a m/z = 100 ion will be 0.1 mm at 500 K in a magnetic field of 3 T. Consequently, barring any sort of random walk process, the ions will remain near zero on the x and y axes of a three dimensional cartesian coordinate system with the origin defined as the center of the cell. With this in mind, one can predict that half of the ions that exit the cell during the free flight period exit via the filament end. These ions would encounter the positive potential and some might be reflected back into the cell.

SIMION (Dahl and Delmore, 1988) calculations have shown that ions are reflected back into the cell by the positive potential of the filament. Figure 4.8 shows the results of equipotential contour and trajectory calculations for a m/z=78 ion with 0.5 eV of total kinetic energy. Three trajectories with varying percentages of the total kinetic energy along the z-axis (100 %, 94 %, 77 %) are superimposed in this figure. The ions were all started at the center of the cell, heading toward the filament end of the cell. All ions were reflected back into the cell. Those ions with the largest percentage of kinetic energy along z penetrated into the filament potential the farthest before being reflected. The results of these simulations indicated that there is a problem with repelling potentials from the filament.

The next step that was taken to improve the T.O.F.

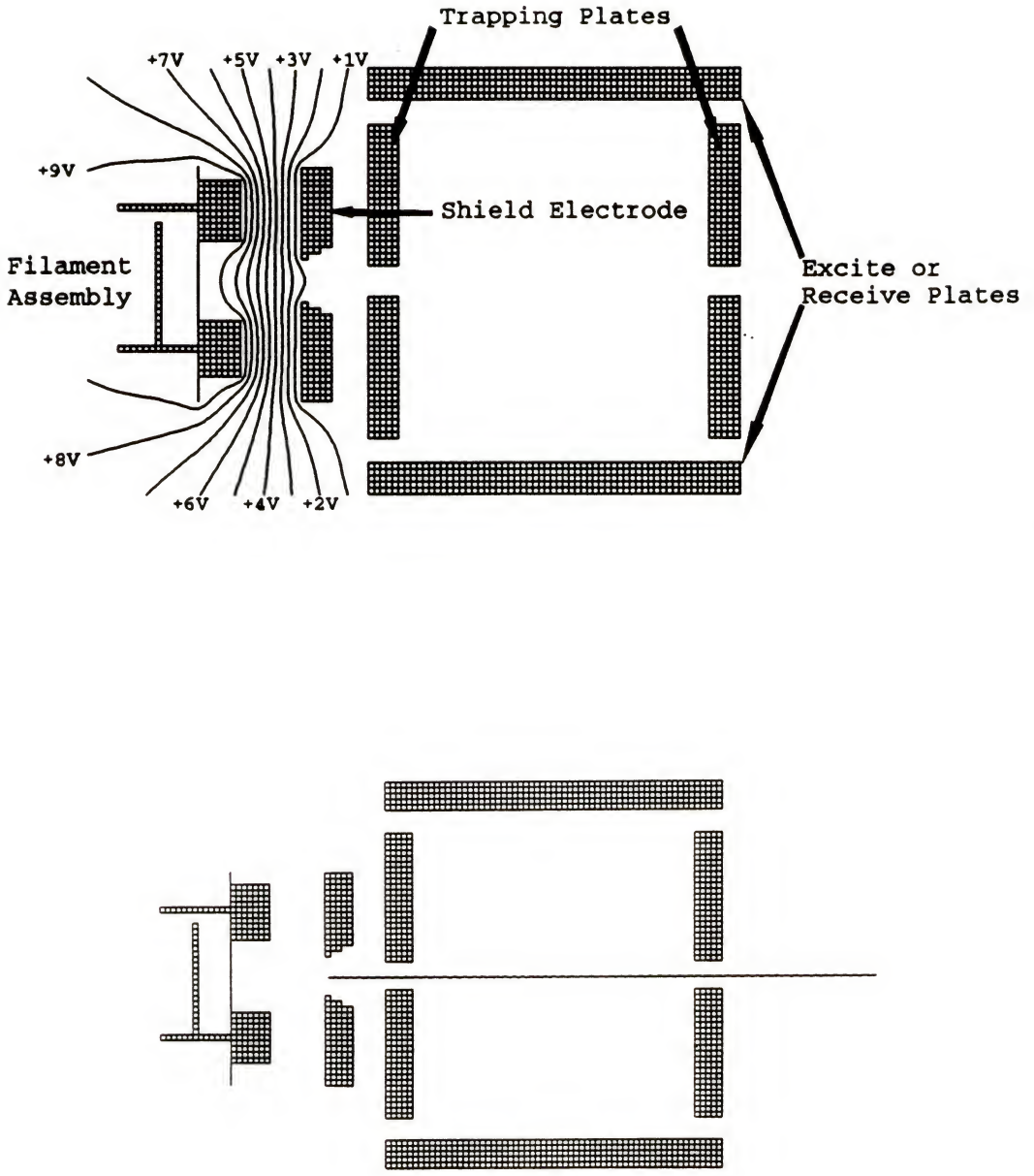

Figure 4.8. Results of SIMION calculations showing the equipotential lines present (TOP) and ion reflection from the filament potential (BOTTOM). The filament was at +10 V all other electrodes were at ground.

technique for kinetic energy measurements was to remove the filament assembly from the cell. Experiments were performed using a laser as an ion source. C_{60}^+ ions were generated by laser-desorption of a dried extract of commercially available C_{60} and C_{70}. These experiments did not show any reflection behavior but were subject to the poor shot-to-shot reproducibility common to laser experiments. Consequently, these experiments were abandoned in search of a more controllable ion source that did not also present possible stray potential problems.

An external filament assembly was developed for use with the time of flight experiments. This assembly consisted of an ordinary filament block, including the shielding electrode, and a manipulator bellows assembly. The filament block was attached to a stainless steel rod that was about 1 foot long. The rod was attached to the manipulator assembly which bolted to the vacuum chamber above the vacuum chamber diffusion pump as shown in Figure 4.9. The manipulator allowed movement of the filament block in any direction. An electron collector was situated on the opposite side of the cell so that proper alignment of the external filament could easily be detected. However, it should be noted that the collector was always held at ground potential during the actual time-of-flight data acquisition to prevent an ion reflection problem similar to that seen with the standard filament assembly.

Time-of-flight kinetic energy data taken with the

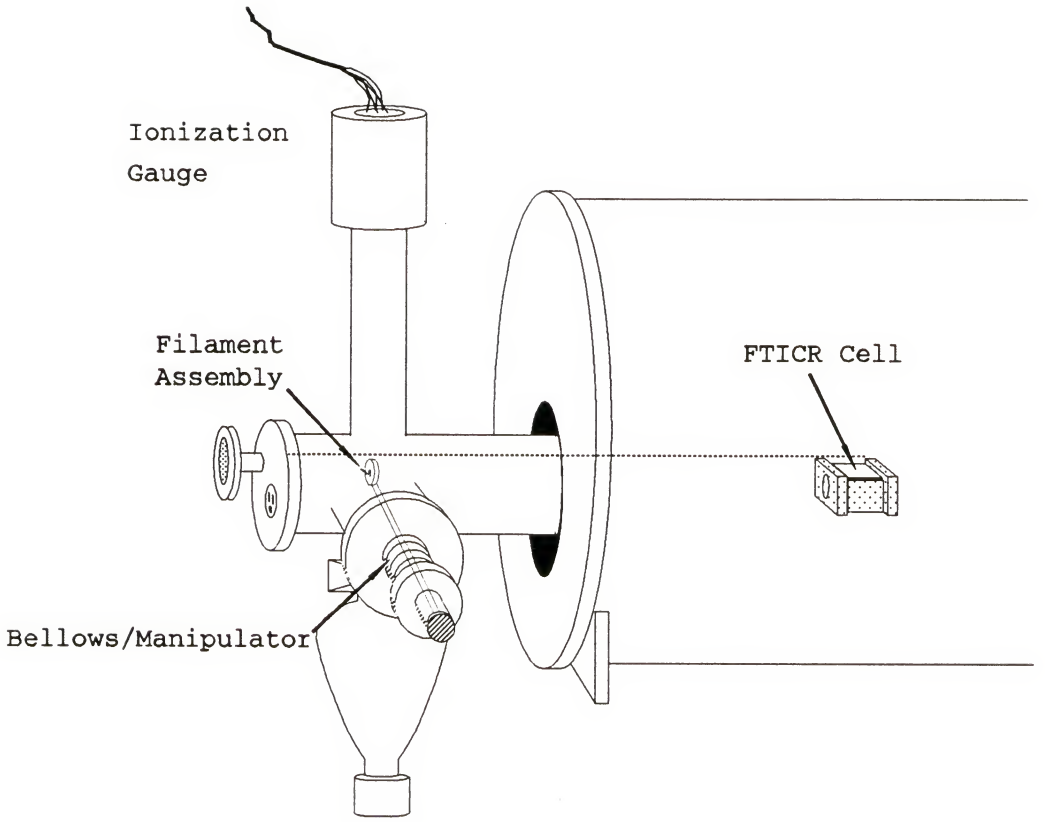

Figure 4.9. Location of external filament and manipulator assembly for improved time-of-flight experiments.

external filament configuration are shown in Figure 4.10. This figure shows the profile obtained for Ar^+ ions. These data were taken at an argon pressure of 6×10^{-6} torr with a relaxation delay and re-capture delay of 200 ms. These parameters allowed for roughly the same number of collisions as in the data in Figure 4.7. No peak is present in this data, suggesting that the previously observed peaks were indeed caused by ion reflection. Also shown in this figure is the decay predicted for a one dimensional Maxwell-Boltzmann distribution of ion velocities about a temperature of 500 K with Equation (4.2) (described below).

A more extensive study of the effects of various parameters on the ion intensity decay curve was performed with m-dichlorobenzene utilizing the external filament assembly. Data from these experiments are shown in Figure 4.11. These data were acquired at a pressure of 6.6×10^{-6} torr with a relaxation period of 200 ms. This provided for an average of ca. 40 ion-molecule collisions prior to the zero volt pulse. Also included in this figure is a fit based on the predicted curve from the analysis of Dunbar and Weddle,

$$N_{thermal}(\tau) = N_0 \, \mathrm{erf}\left(\left(\frac{1}{\tau}\right)\left(\frac{mr^2}{2kT}\right)^{\frac{1}{2}}\right) \qquad (4.2)$$

where $N_{thermal}(\tau)$ is the number of ions remaining trapped after a free flight time τ, N_0 is the original number of ions, erf is the error function, m is the mass of the ion, and r is the

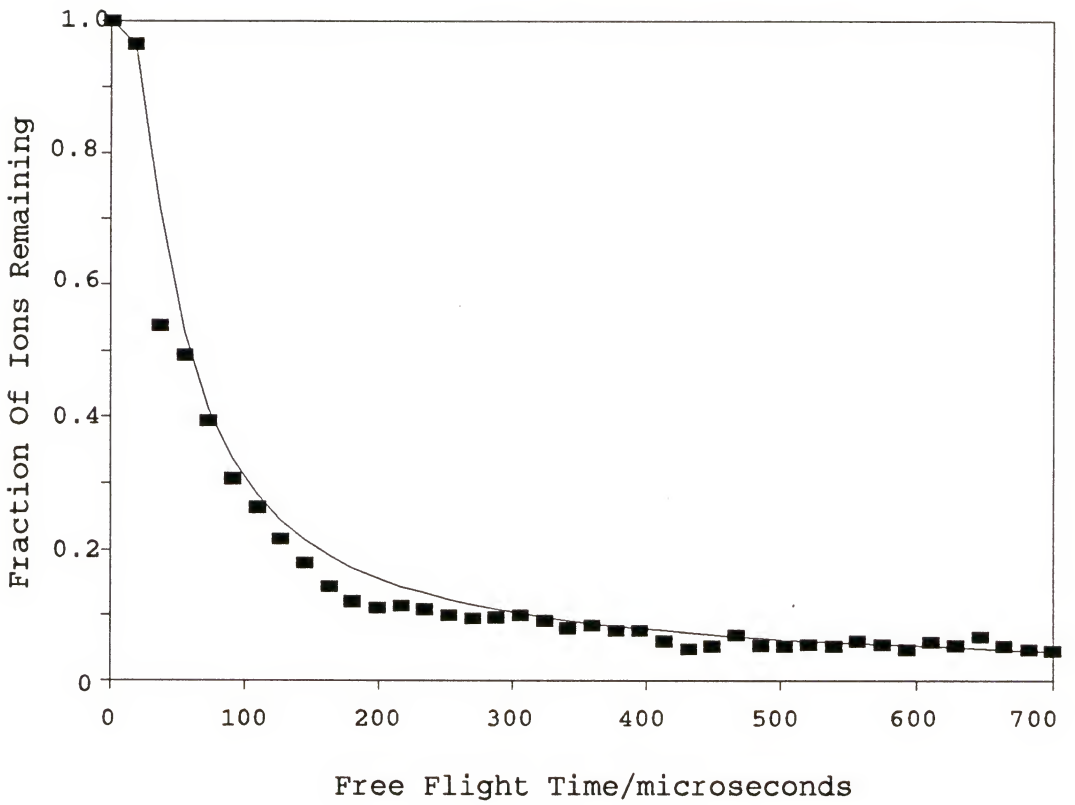

Figure 4.10. Time-of-flight kinetic energy measurements of argon cations at a pressure of 6 x 10^{-6} torr with the external filament assembly.

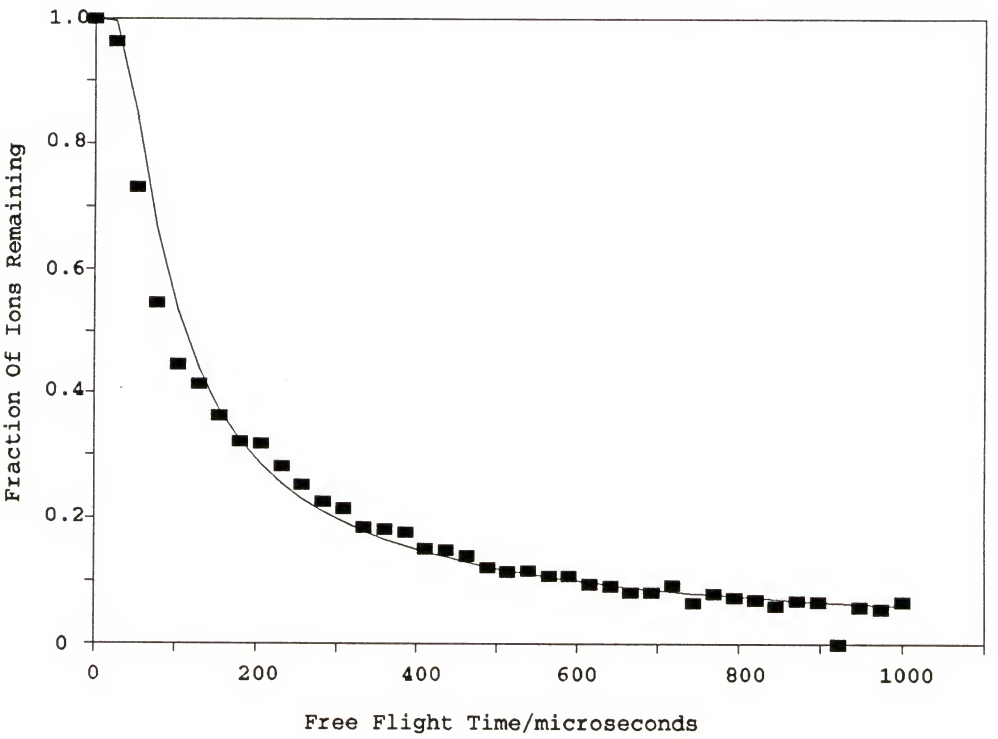

Figure 4.11. Time-of-flight kinetic energy data for m-dichlorobenzene. Pressure = 6.6 x 10^{-6} torr, relaxation delay = re-capture delay = 200 ms.

distance between the trapping plates.

The data presented in Figure 4.11 show that the ion velocities do closely resemble a Maxwell-Boltzmann distribution about a temperature of 500 K, a temperature estimate in good agreement with data to be presented in Chapter 6 of this dissertation. Also evident in this figure is a lower ion intensity than that predicted for free flight times less than 150 microseconds. This is believed to be due to the effects of ion-ion repulsion that are encountered immediately after the trapping voltage is dropped to zero, even for low ion intensities (the measured electron current through the cell was 20 nanoamperes for this figure). Collisional relaxation along the z-axis leads to compaction of the ions into a small region of the center of the cell. Even a small amount of ions might be compressed enough that the forces due to the repulsion between ions can cause acceleration of the faster ions exiting the cell. These forces become reduced due to the significant reduction in ion population that is experienced after the faster ions exit. As a result, the velocities of the slower ions are not as greatly affected as those of the faster ions and the data more closely resemble the predicted decay. The results from another experiment repeated at the same conditions, but with more data points at shorter free flight times (when the space charge effects should be the greatest) are shown in Figure 4.12. The decay curve fit to these data indicate that the ion

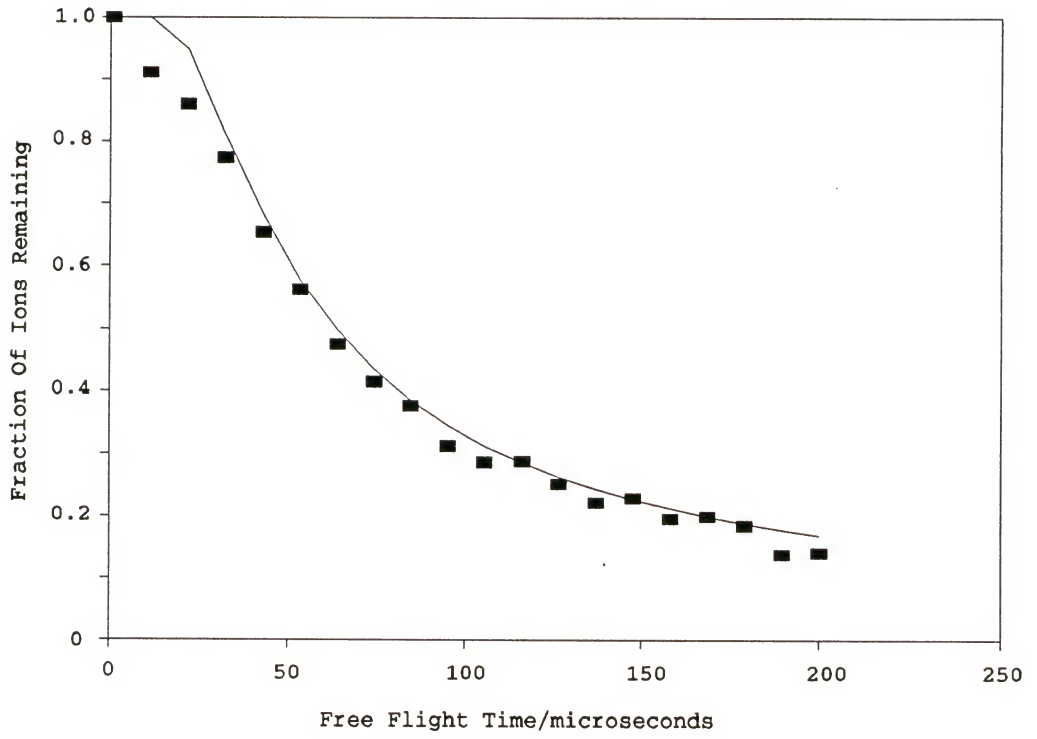

Figure 4.12. Data for the time-of-flight kinetic energy measurements for m-dichlorobenzene. The same conditions were employed for these data as were employed for those in Figure 4.10.

temperature is 1500 K. Thus, the effects of space charge on the ion velocities appear as large as three times the thermal value, even under low ion intensity conditions. The effects due to ion-ion repulsion become far more drastic at higher electron emission current, suggestive of a much higher ion density. Finally, data taken at minimum ion intensities, with a measured electron current through the cell of only 10 nanoamperes, are presented in Figure 4.13. Also shown in this figure is the fit based on Equation 4.2 with a temperature of 300 K. Again, the initial decay is faster than would be predicted for thermal ions although the agreement at longer times is good, with the exception of the points falling on the x-axis due to the very low numbers of ions used for these experiments.

Conclusions

The method of kinetic energy measurement based on the time-of-flight technique developed by Dunbar's group has been investigated. The technique seems conceptually to be quite plausible for the measurement of kinetic energies of near thermal trapped ions. Ideally, this technique would be applicable to the measurement of the kinetic energies of ions from many different sources; a general purpose ion velocity measurement device is desired. This device should be suitable for the measurement of the kinetic energies of ions produced by laser-desorption and/or laser ablation, multiphoton

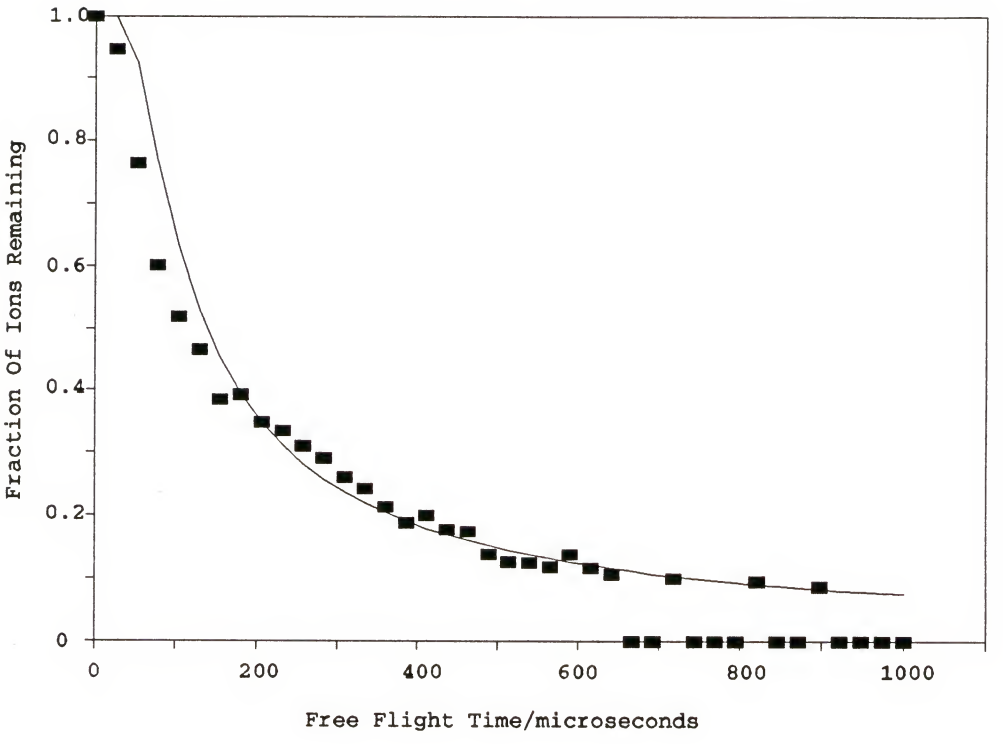

Figure 4.13. Data for the time-of-flight kinetic energy measurements for m-dichlorobenzene with the EMC set at 10 nanoamperes.

ionization, or ions injected from external sources. As has been shown in this chapter, the time-of-flight approach requires the ability to very precisely control the number of ions trapped in the cell. This requisite has proven to be an obstacle for the time-of-flight kinetic energy measurements that were attempted on laser desorbed C_{60}^{+} ions. The charges of the ions combined with the spatial compaction of ions inherent in FTICR cells serves to limit the applicability of this technique as a general purpose ion speedometer.

Finally, the time-of-flight technique has been successful in an effort to at least estimate the temperature of ions produced by electron ionization and trapped in an FTICR cell. These experiments have produced an ion temperature estimate of 300 to 600 K, a result that is supported in both Chapters 5 and 6. More importantly, however, these experiments have shown that the distribution of ion velocities, after a thermalization period, does very closely approximate a Maxwell-Boltzmann distribution.

CHAPTER 5
TRAPPED ION ENERGIES VIA EQUILIBRIUM MEASUREMENTS

Introduction

This dissertation presents the results of a series of investigations performed to determine the kinetic energy of ions trapped in a Fourier transform ion cyclotron resonance mass spectrometer. If these instruments were used for routine mass analysis only, the kinetic energy of the trapped ions would not be of great interest to researchers, with the exception of those researchers interested in optimization of the detection characteristics of these instruments. However, as was discussed in the introductory chapter of this dissertation, FTICR mass spectrometers are very commonly used to investigate physical properties of ions. The kinetic energy of trapped ions can affect many of these investigations and therefore, research performed to ascertain trapped ion kinetic energies is of extreme importance.

The basis for the ion kinetic energy determinations presented in this chapter is thermodynamic. The thermodynamic properties of ions have been the subject countless experimental inquiries. There exists in the chemical literature a vast reservoir of thermodynamic data related to ions, such as electron affinities, proton affinities, and

ionization potentials. The work presented in this chapter relies on the use of tabulated data such as that from Lias et al., (1988) to estimate trapped ion temperatures by chemical equilibrium measurements.

Ion kinetic energies can be investigated by utilizing several chemical methods, as will be discussed in greater detail in Chapter 6. Ion-molecule equilibria can be used to provide a crude estimate of trapped ion energies. Judicious choice of reactants for which the ΔG° of the reaction is known, in conjunction with measurement of the equilibrium constant, K, allows the temperature of the system to be evaluated with

$$\Delta G^\circ = -RT\ln(K) \qquad (5.1)$$

where T is the system temperature. This type of analysis requires that the system be at equilibrium and that the ion velocities truly form a Maxwell-Boltzmann distribution about T. This has been shown to be true for ions trapped in a FTICR mass spectrometer (see the preceding chapter on time-of-flight kinetic energy measurements). In this chapter, the results from three independent equilibrium investigations performed to estimate trapped ion energies are reported. Two proton transfer equilibria and one charge transfer equilibrium were studied. The two proton transfer equilibria investigated were between diethylamine and dipropylamine and between toluene and ethylbenzene. The charge transfer equilibrium employed was between fluorobenzene and m-dichlorobenzene. These equilibria

are represented below.

$$(C_2H_5)_2NH_2^+ + (C_3H_7)_2NH \rightleftharpoons (C_3H_7)_2NH_2^+ + (C_2H_5)_2NH \quad (5.1)$$

$$C_7H_9^+ + C_8H_{10} \rightleftharpoons C_8H_{11}^+ + C_7H_8 \quad (5.2)$$

$$C_6H_5F^+ + m\text{-}C_6H_4Cl_2 \rightleftharpoons m\text{-}C_6H_4Cl_2^+ + C_6H_5F \quad (5.3)$$

Experimental

Both data acquisition computers described in Chapter 2 were used for the equilibrium measurements presented in this chapter. The sequence of events used for equilibrium measurements was quite standard for FTICR experiments. Ions were formed by electron ionization with a typical beam voltage of 15 V. For the proton transfer equilibria, a long relaxation delay to allow translational relaxation and the formation of the protonated species was then implemented. This delay was normally 0.1 to 1 s. Chemical ionization was necessary for production of the protonated species for the substituted benzene proton transfer equilibrium, Reaction (5.2), experiments. Several chemical ionization (CI) reagents, of differing proton affinities, were used for this study to determine if the exoergicity of the proton transfer reaction between the CI reagent and the reactant ion could affect the observed equilibrium constant. CI reagents used included methane, methanol, and isobutane. No CI reagent was needed for the amine proton transfer equilibrium, Reaction

(5.1), due to the rapid self CI that typically occurs in ionized amine systems. For the charge transfer equilibrium, Reaction (5.3), the reactant ion was formed directly from electron ionization so no delay other than the relaxation delay (normally 0.1 seconds) was required. For all equilibrium studies, one of the two reactant ions was isolated using standard swept frequency ejects following the above mentioned delays. The selected ions were then allowed to undergo proton transfer or charge transfer with a constant pressure of the neutral reactant. The typical time allowed for equilibrium varied. For the amine proton transfer equilibrium, typical reaction times employed were 2 seconds. The pressures used for this equilibrium varied between 5.8×10^{-7} and 2×10^{-6} torr. These data were taken with mixtures of the two gases prepared prior to data acquisition with the ratio of diethylamine to dipropylamine varying from 3.08 to 5.07. The mixtures were prepared on a vacuum rack assembly and pressures were monitored during the mixing process with the aid of a capacitance manometer. As such, no pressure calibrations to correct for the ion gauge sensitivity differences of the two amines were required. For the toluene and ethyl benzene proton transfer equilibrium experiments, typical reaction times were 5 seconds. However in some cases, the reaction was allowed to proceed for as long as 30 seconds. The total pressures used for these experiments were from 1.6×10^{-6} torr to 4×10^{-5} torr. The pressure ratio of toluene to

ethylbenzene varied from 1:1 to 9.5:1. All three CI reagents mentioned above were employed for these experiments, however methanol was most commonly employed.

For the toluene-ethylbenzene proton transfer equilibrium studies, the pressures of each reactant were obtained by leaking each gas independently into the ICR vacuum chamber. The sensitivities of the ionization gauge for toluene and ethylbenzene were both determined by calibration with a capacitance manometer, as was described in Chapter 3. Toluene and ethylbenzene were found to have ionization gauge sensitivity correction factors, f_s, of 0.88 ± 0.16 and 0.93 ± 0.17 (95% confidence limits, n=3), where the true pressure for a closed system is equal to the ionization gauge reading multiplied by f_s. These numbers do not agreement with the ionization gauge calibration data presented by Bartmess and Georgiadis, (1983) (as was found for many of the compounds presented in Chapter 2). However, only the ratio of the sensitivity correction factors is important for the present work and this agrees quite well with their data (0.95 vs 0.93, for toluene correction factor divided by ethylbenzene correction factor). The pressure range for the fluorobenzene-dichlorobenzene charge transfer equilibrium experiments was from 5.6×10^{-7} torr to 2.0×10^{-6} torr. The reactants for these experiments were leaked in independently, as in the toluene-ethylbenzene studies, and pre-mixed, as in the amine experiments. As might be predicted, the sensitivity

correction factors for fluorobenzene and dichlorobenzene were nearly equal, 0.95 ± 0.10 and 0.91 ± 0.22, respectively. Different results were obtained with these two methods, as will be mentioned below. Although the pre-mixed data led to predictions of temperatures that were closer to thermal values, these data were suspect due to the observed condensation of some of the reactant inside the mixture container. This caused some uncertainty in the actual administered pressure ratio. The ratio of fluorobenzene to m-dichlorobenzene was varied between 1.5:1 to 4.93:1. Typical reaction times were up to 1 second; however, some studies allowed for reaction times up to 10 seconds. The trapping voltages employed for all equilibrium measurements presented in this chapter varied between 1 and 2 volts.

In all systems studied, the equilibrium constant was obtained using the ratio of the measured ion peak heights after the system had reached equilibrium. A temperature estimate was then performed utilizing Equation (5.1). Error limits on the temperature estimates were produced with

$$\lambda_T = \sqrt{\left(-\frac{1}{R \ln K}\right)^2 \lambda_{\Delta G^\circ}^2 + \left(\frac{\Delta G^\circ}{R(\ln K)^2}\frac{1}{K}\right)^2 \lambda_K^2} \qquad (5.2)$$

which was derived with standard error propagation methods. In Equation (5.2), λ_T is the estimated error in the temperature approximation, $\lambda_{\Delta G^\circ}$ is the reported error in the tabulated free energy change for the reaction, and Δ_K is the calculated 95 % confidence limits for the determined equilibrium constant for

the reaction. R is the gas constant which is equal to 8.314 $JK^{-1}mol^{-1}$.

Results and Discussion

Diethylamine and Dipropylamine Proton Transfer Equilibrium

Typical results for the proton transfer equilibrium experiments with the amine mixtures are shown in Figure 5.1. These data were taken with a total pressure of 4×10^{-6} torr and a diethylamine to dipropylamine ratio of 5.07:1. The standard Gibbs free energy change for this reaction is 1.9 ± 0.5 kcal/mol. Table 5.1 illustrates all the results for this system. The average equilibrium constant obtained for this system is 0.019 ± 0.003. Thus, a temperature estimate based on the amine proton transfer equilibrium study is 280 ± 70 K. Since the ICR cell has been measured to be in the range of 350 to 375 K during normal operation under electron ionization conditions, one would expect that at equilibrium, the ion temperatures should reflect the same value. The reason for this low value is not clear. This could simply indicate an error in the published standard free energy change for this reaction. However, the error limits on the temperature, which include the error from both the free energy value as well as the determined 95% confidence limits on the equilibrium constant, do encompass the expected near thermal quantity.

Toluene and Ethylbenzene Proton Transfer Equilibrium

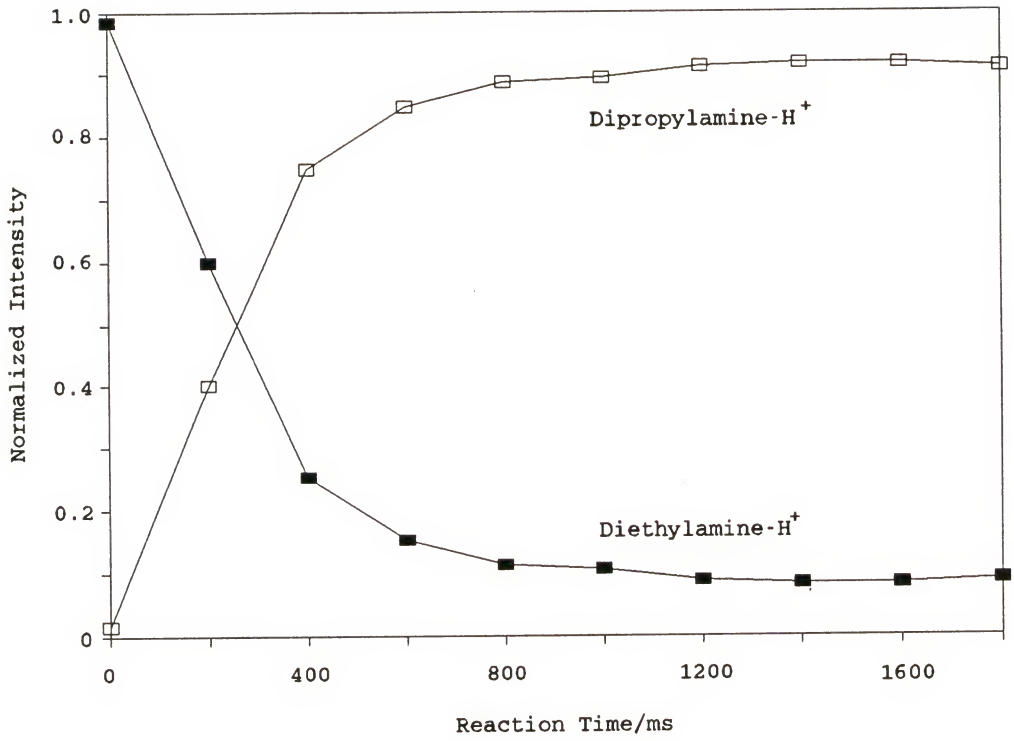

Figure 5.1. Typical results for the proton transfer equilibrium experiments with diethylamine and dipropylamine. Diethylamine-H^+ represents the normalized $(C_2H_5)_2NH_2^+$ intensities.

Table 5.1. All the results for the diethylamine and dipropylamine proton transfer equilibrium experiments. PRESSURE is the total pressure/10^{-7} torr.

FILENAME	PRESSURE	K	T/Kelvin
JB910606.A01	5.8	0.014	258
JB910606.A03	40	0.019	279
JB910606.A04	32	0.022	288
JB910606.A05	32	0.022	286
JB910606.A12	30	0.017	265
JB910606.A13	30	0.015	262
JB910606.A14	30	0.022	289
JB910606.A15	32	0.026	302
JB910606.A16	32	0.027	303
JB910607.A09	10	0.024	286
JB910607.A09	20	0.015	261
JB910607.A10	20	0.014	256

Typical results for the proton transfer equilibrium studies with toluene and ethylbenzene are shown in Figure 5.2. These data were taken with methanol as the chemical ionization (CI) reagent. The pressures of toluene, ethylbenzene, and methanol were 9.5×10^{-7} torr, 1.0×10^{-6} torr, and 1.1×10^{-6} torr, respectively. Little effect on the system temperature was observed as the CI reagent was varied. Table 5.2 shows the three CI reagents used, the proton affinity of the CI reagent, and the average equilibrium constant for the toluene-ethylbenzene proton transfer reaction obtained with each CI reagent. If the system temperature estimate were affected by the proton affinity of the CI reagent, one should expect to see the temperature decrease as the proton affinity of the CI reagent increases (imparting a smaller quantity of energy into the reactant ion). Clearly, no effect of the CI reagent on the equilibrium constant was observed that could be correlated to the proton affinity of the CI reagent. This indicated that the excess kinetic and/or internal energy delivered to the reactant ion by the lower proton affinity CI reagent is absorbed by the system on a time scale that is fast in comparison to the reaction. Table 5.3. presents all the results obtained on the proton transfer equilibrium between toluene and ethylbenzene. The average equilibrium constant for this reaction from the present data is 0.20 ± 0.02, where error limits indicate the 95% confidence limits about the mean of all determinations. The published

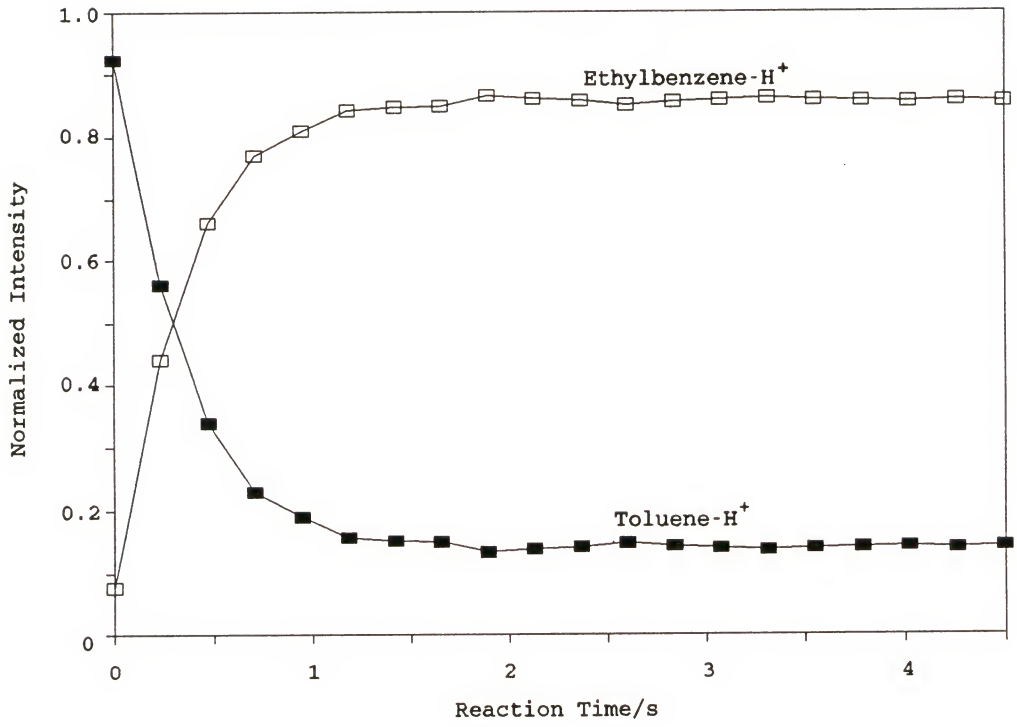

Figure 5.2. Proton transfer data for toluene and ethylbenzene system. Toluene-H^+ represents the normalized $C_7H_9^+$ intensities.

Table 5.2. The three CI reagents used in the toluene-ethylbenzene proton transfer equilibrium experiments. P.A. = the proton affinity of the CI reagent in kcal/mol.

CI Reagent	Proton Affinity	K	T/Kelvin
Methane	131.6	0.25 ± 0.088	360 ± 205
Isobutane	163.3	0.15 ± 0.032	270 ± 140
Methanol	181.9	0.21 ± 0.025	320 ± 170

Table 5.3. Results for toluene and ethylbenzene proton transfer equilibrium studies. CIR = Chemical Ionization Reagent.

FILENAME	CIR	K	T/Kelvin
125651	Methane	0.31	427
125661	Methane	0.18	290
125662	Methane	0.22	335
127691	Methane	0.26	378
127692	Methane	0.34	469
129071	Isobutane	0.17	288
129072	Isobutane	0.16	270
129073	Isobutane	0.15	267
129101	Isobutane	0.17	285
129102	Isobutane	0.11	234
128041	Methanol	0.24	357
128042	Methanol	0.25	366
128043	Methanol	0.26	368
125052	Methanol	0.19	303
125053	Methanol	0.20	312
JB910918.A01	Methanol	0.17	280
JB910918.A02	Methanol	0.17	282
JB910918.A03	Methanol	0.17	287
JB910918.A04	Methanol	0.18	289
JB910919.A02	Methanol	0.30	425
JB910919.A03	Methanol	0.33	458
JB910919.A04	Methanol	0.32	444
JB910919.A05	Methanol	0.31	429
JB910919.A06	Methanol	0.26	369
JB910919.A07	Methanol	0.23	341
JB910919.A08	Methanol	0.24	351
JB910919.A09	Methanol	0.16	270
JB910919.A10	Methanol	0.15	266
JB910919.A11	Methanol	0.17	287
JB910919.A12	Methanol	0.31	428
JB910919.A13	Methanol	0.15	262

standard Gibbs free energy change for this reaction is 1.0 ± 0.5 kcal/mol, which indicates a temperature for this system of 315 ± 160 K. This result is in good agreement with the data presented in Chapter 4 on time-of-flight kinetic energy measurements and the results to be presented in the following chapter on the $Ar^+ + N_2$ charge transfer reaction.

Fluorobenzene and Dichlorobenzene Charge Transfer Equilibrium

Typical results for the fluorobenzene and m-dichlorobenzene charge transfer equilibrium investigations are presented in Figure 5.3. These data were taken with a total pressure of 1.13×10^{-6} torr and a fluorobenzene to m-dichlorobenzene ratio of 1.63. The equilibrium constant extracted from the data in Figure 5.3 is 6.84. Table 5.4 presents all the results for this reaction taken by independently introducing each reactant into the vacuum system. The average equilibrium constant for this reaction from these data and the standard Gibbs free energy are 6.6 ± 1.0 and -2.08 ± 0.2 kcal/mol, respectively. In conjunction with Equation 5.1, these values produce an average temperature of 550 ± 70 K. The pre-mixed data gave somewhat different results. The average K for these studies was 11.4 ± 3.6. This rather large change in K corresponded to a 120 K decrease in the average temperature. However, the pre-mixed data were not used for the temperature estimate due to the uncertainties regarding the mixture ratios discussed earlier. This

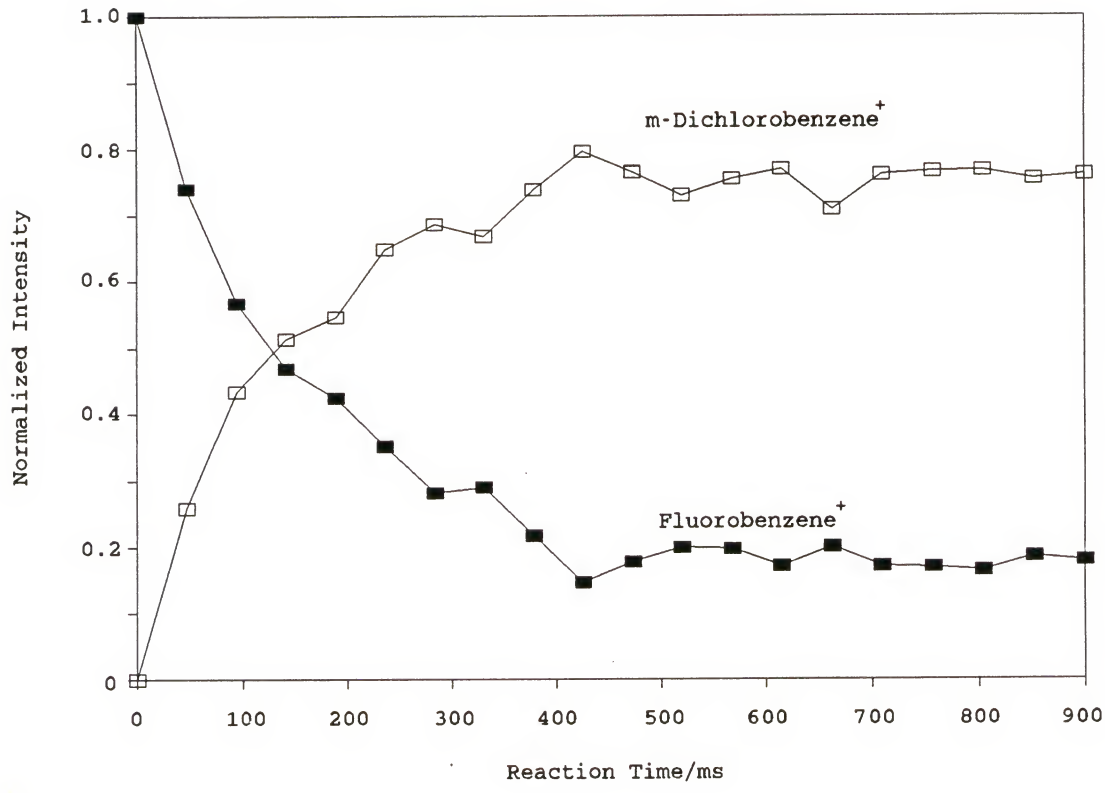

Figure 5.3. Charge transfer equilibrium data for fluorobenzene and m-dichlorobenzene.

Table 5.4. Summary of results for the fluorobenzene and dichlorobenzene charge transfer equilibrium experiments. PRESSURE is the total pressure/10^{-7} torr.

FILENAME	PRESSURE	K	T/Kelvin
JB910822.A01	11.3	6.84	543
JB910822.A02	11.3	5.98	584
JB910822.A03	11.3	5.08	643
JB910822.A06	5.6	7.34	524
JB910823.A00	5	7.5	518
JB910823.A01	5	5.51	612
JB910823.A03	40	7.67	513
JB910823.A04	40	7.11	532

investigation produced results that overlap quite well with those from the toluene and ethylbenzene proton transfer equilibrium study and the results from the chapters mentioned in the discussion of the toluene and ethylbenzene results above.

No effects on the equilibrium constants due to pressure were observed for any of the systems presented in this chapter. This indicates that by the time equilibrium is reached, the ions have become thermalized. The low pressure experiments performed on these systems can yield an indication of the number of collisions that are required to produce equilibrium behavior, and thus thermalization. Figure 5.4 illustrates low pressure data for the amine proton transfer reaction and the fluorobenzene and m-dichlorobenzene charge transfer reaction taken at 5.8×10^{-7} torr and 5.6×10^{-7} torr, respectively. No low pressure comparison for the toluene-ethylbenzene proton transfer system could be performed since this system required the use of a CI reagent (the lowest total pressure studied was 1.6×10^{-6} torr). The amine mixture reached equilibrium with a total delay of 3 seconds from the time of the beam event. The fluorobenzene and m-dichlorobenzene mixture arrived at equilibrium in only two seconds. These times represent the maximum time required for thermalization since thermalization can be achieved prior to equilibrium. Therefore, these data suggest, based on a Langevin collision cross section (Langevin, 1905), that

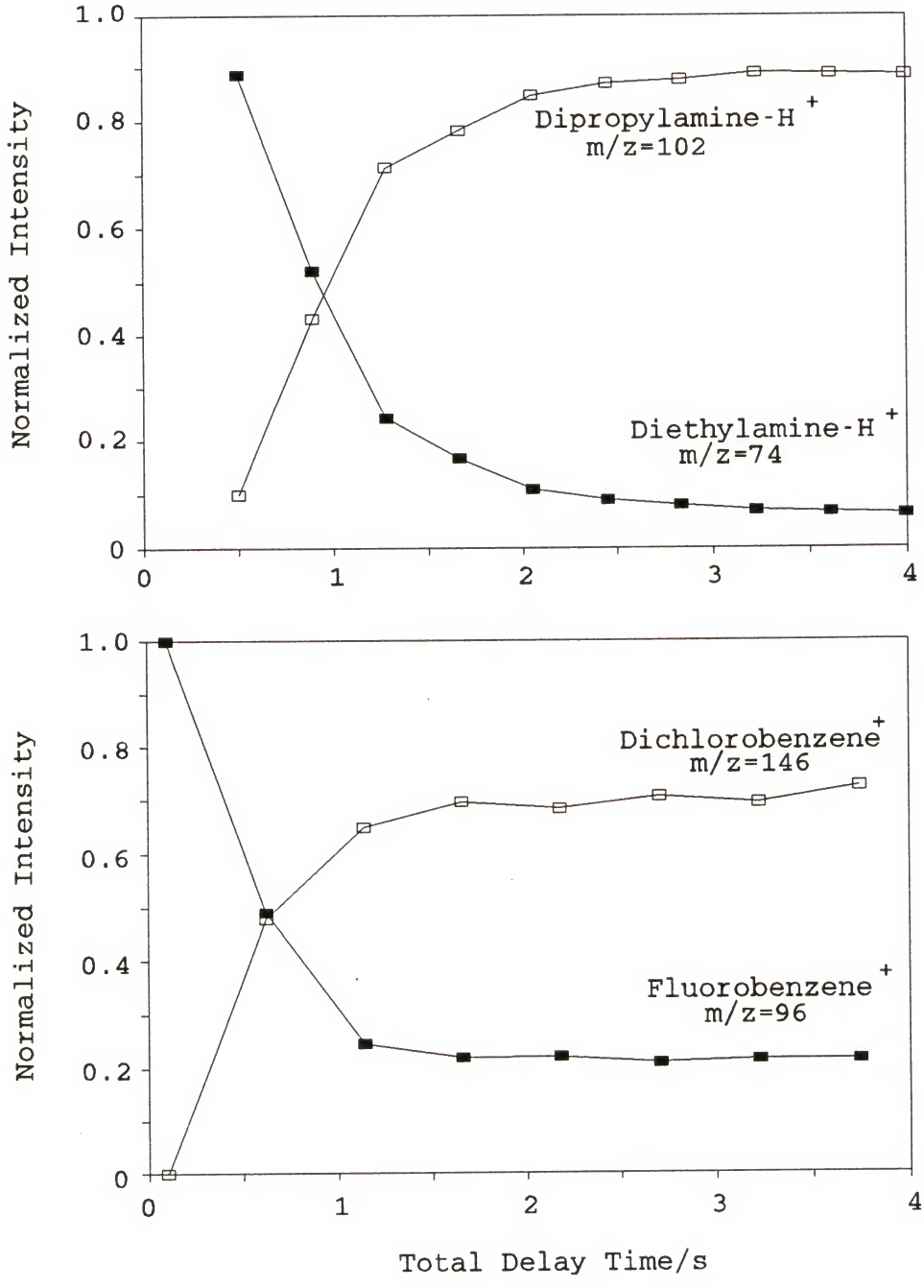

Figure 5.4. Low pressure data for the diethylamine-dipropylamine reaction (TOP) and the fluorobenzene-dichlorobenzene reaction (BOTTOM).

thermalization is reached with 40 to 60 ion-neutral collisions or less. The results obtained in the previous chapter on time-of-flight kinetic energy measurements indicated a requirement of approximately 30 ion-molecule collisions, or less, necessary for thermalization. Thus, this chapter exhibits results that support those results presented in both the preceding and following chapters.

Conclusions

These equilibria were investigated to estimate trapped ion energies. While only a rough estimate of the ion temperature can be obtained from this type of study, due to the errors associated with the tabulated physical properties of the involved ions, several important conclusions can be extracted from these results. The average temperature for all of these systems is 382 K. If one disregards the sub-thermal result obtained with the amine mixture study, the average temperature result is 432 K, again still in good agreement with the preceding and following chapters. Thus, these results at least discredit the alarmingly high temperature estimate of 1000 K from Henchman, (1987). Furthermore, the results from these investigations provide some evidence regarding the thermalization process, an elusive subject of study. The results presented in this chapter demonstrate that the ions trapped in the FTICR cell do reach thermal equilibrium in a number of collisions that is 60 or less.

This result is slightly higher than the number of collisions that were found to be required for the thermalization of Ar^+ ions (to be reported in the following chapter). However, a greater number of collisions might be expected for the complete equilibration of internal and translational energy of the relatively large polyatomic ions utilized in this chapter. This is contrasted to the study of Chapter 6, where conditions were adjusted such that only the translational energy of Ar^+ ions was involved.

CHAPTER 6
TRAPPED ION ENERGIES VIA ION-MOLECULE REACTION KINETICS

Introduction

Several chemical methods for measuring ion kinetic energies were proposed at a panel meeting to review ion kinetic energies at a NATO conference (Bartmess, 1987). The systems for study included proton transfer equilibria, negative ion equilibria, and the charge exchange reaction of Ar^+ with N_2. Some of these equilibria have been investigated, and the results of those investigations are reported in Chapter 5. The latter charge transfer reaction seemed most convenient for an ion-molecule kinetics study because of the simplicity of both the reaction and reactants. Furthermore, this reaction has been extensively studied and considerable data exist on its energy dependence. It can be studied with relative ease in FTICR mass spectrometers as well as in other mass spectrometers (A parallel study was done by Cecilia Basic of the Yost research group at the University of Florida using a quadrupole ion trap).

In this chapter, the $Ar^+ + N_2$ reaction rate coefficient obtained in an FTICR mass spectrometer is compared to determinations in previous work where the reaction was studied

as a function of kinetic energy (Dotan and Lindinger, 1982; Viggiano et al., 1990). A center of mass kinetic energy is estimated for FTICR ions by this direct comparison. Assuming that both the ion and the neutral have independent Boltzmann distributions of velocities, one can calculate the estimated temperature of the Ar^+ ions. This approach may neglect some fundamental differences between FTICR mass spectrometers and those that are typically used to measure kinetic energy dependent ion-molecule reactions, such as the flow tube (McDaniel et al., 1962) or the selected ion flow tube (SIFT) (Adams and Smith, 1976). In fact, it is these types of comparisons and the general lack of agreement among different instruments that have aroused interest in kinetic energy of ions, not just for FTICR researchers, but throughout the entire mass spectrometric community. However, the comparison does allow a crude estimate of FTICR ion kinetic energies to be made. The estimates are crude because it completely ignores the possibility that ions may be cooled, but to some non-Boltzmann distribution. More importantly, however, the studies of this system presented in this chapter permit the relative assessment of ion energies resulting from differing experimental conditions. With this knowledge in hand, researchers may adjust parameters that reduce or minimize ion kinetic energy for situations in which low energy ions are critical. Also, examination of the reaction rate coefficient for the effects of thermalizing collisions by varying the

total pressure gives an indication of the average number of collisions necessary to produce varying degrees of thermalization for this reaction system.

Experimental

All experiments reported here were carried out on a Nicolet FTMS-1000 system (Nicolet 1280 computer and vacuum controlling electronics, Oxford 3T superconducting magnet, vacuum chamber pumped by a 300 l/s oil diffusion pump). The actual pumping speed of this system as used for data presented here was somewhat less than 300 l/s because the main gate valve that isolates the vacuum chamber from the pump was partially closed (reproducibly to a 1/4 open position). Operation with a partially closed valve was beneficial because it reduced pressure fluctuations and the system factor greatly, as was discussed in detail in Chapter 3. Typical background pressures were in the low 10^{-9} torr region even with the valve partially closed. The basic principles of FTICR and details regarding this instrument can be found in Chapter 2 of this dissertation.

Ion-molecule reactions are examined in the FTICR instrument by observing the time dependence of the intensity of reactant ions produced by electron ionization in a constant pressure of reactant gas. Rate constant extraction from the raw data ultimately involves division by the pressure of the neutral reactant; therefore, determination of this pressure is

crucial for accurate ion-molecule reaction rate constant measurements. Pressure was monitored by an ionization gauge mounted approximately 1.5 meters from the ICR cell, external to the magnetic field. The pressure readings taken from the ionization gauge were corrected by two multiplicative factors. The first factor corrected the ionization gauge for sensitivity differences of different gases. This factor was measured by comparing simultaneous ionization gauge pressure readings and capacitance manometer pressure readings on a sample of trapped gas. A sensitivity correction factor for each gas used in this work was obtained in this manner. The second factor corrected the ionization gauge readings for the difference in pressure between the ionization gauge and the ICR cell. This factor is called the system factor, f_{sys}, and is defined by

$$f_{sys} = \frac{P_{cell}}{P_{ion\ gauge}} \quad . \tag{6.1}$$

The system factor was evaluated by performing three separate experiments. The results of those experiments were presented in Chapter 3 and a system factor of 2.0 was applied to all pressure measurements and rate constants reported in this chapter.

As mentioned above, the kinetic energy-dependent charge exchange reaction,

$$Ar^+ + N_2 \rightarrow N_2^+ + Ar \tag{6.1}$$

was investigated for the determination of ion energies. For this reaction, ions were formed by electron ionization and then allowed a "relaxation period", usually around 100 ms, during which they collided with neutral molecules, lost excess kinetic energy, and relaxed along the z (magnetic field) axis to the center of the FTICR cell where detection efficiency has been shown to be the highest [Rempel et al., 1986; van der Hart and van der Guchte, 1988). This relaxation period precludes the observation of any kinetic energy or electronic energy effects during the first 100 ms after ion formation on the reactivity of Ar^+ ions. However, such a relaxation period was necessary to avoid an initial increase in ion intensity due to collisional relaxation of ions to the center of the cell. As discussed later, only after this period of time could reproducible exponentially-decaying Ar^+ signals, indicative of a pseudo-first order reaction, be obtained.

The electron energy used to form the ions was usually around 15.5 volts. The trapping voltage normally used for the study of this reaction was around 1 V; however, effects of the trapping voltage on ion energy were examined over the range 0.5 to 5 V. The effect of collisional cooling on ion energy was also investigated by varying the total pressure over a range from 4×10^{-6} to 2×10^{-5} Torr. This was done by independently varying the pressure of N_2 and Ar over the range from 2×10^{-7} to 1.4×10^{-5} Torr. All gases were of ultra high purity grade and were used as obtained.

The ion transient response signals obtained consisted in most cases of 16 K data points and were in the broadband mode, covering the frequency range that corresponded to the mass range of 17.3 to 1000 amu (the lower limit was set by the maximum analog to digital converter rate possible with our electronics). Ar^+ ions and N_2^+ ions were formed by electron ionization. The N_2^+ ions formed by the electron beam as well as those produced by Reaction (6.1) must be removed continually by single frequency excitation of the N_2^+ cyclotron frequency to prevent the possible reverse of Reaction (6.1) from taking place (exothermic for N_2^+ formed in excited vibrational levels (Liao et al., 1986)). A schematic representation of the time sequence of events used to monitor this reaction is shown in Figure 6.1. Since only Ar^+ ions are present in the cell after this ejection (with the exception of a small amount of m/z=18), ion loss must be carefully monitored. Normalization to account for non-reactive Ar^+ ion loss is not possible and for each pressure and trapping voltage, the electron beam current and or beam length was adjusted so that little or no Ar^+ signal loss was seen when no N_2 was present in the chamber. Ion energies were extracted from rate data by comparison with flow-drift tube (Dotan and Lindinger, 1982) and variable temperature selected ion flow drift tube (VT-SIFDT) (Viggiano et al., 1990) results for the kinetic energy dependence of the rate constant of Reaction (6.1).

$$Ar^+ + N_2 \rightarrow N_2^+ + Ar$$

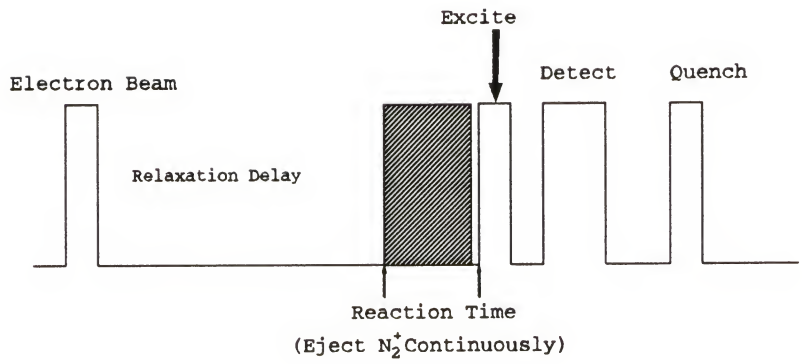

Figure 6.1. A diagram of the time sequence used to monitor Reaction (6.1).

Results and Discussion

Ar^+ ions produced by electron ionization in the 15-17 eV range should have $^2P_{1/2}$ and $^2P_{3/2}$ states populated in a statistical 1:2 ratio based on the total angular momentum multiplicities. Hamdan et al., (1984) have shown that both states are produced by electron ionization and that the reactivity (for charge transfer with N_2) of the higher energy J=1/2 state is approximately three times that of the J=3/2 state at collision energies below 0.2 eV. However, they also reported that the J=1/2 state has a quenching rate constant that is nearly equal to the reaction rate constant. Kinetic modelling of this reaction system was performed without the inclusion of an additional buffer gas using the following reactions:

$$Ar^+(^2P_{3/2}) + N_2 \rightarrow N_2^+ + Ar \qquad (6.2)$$

$$Ar^+(^2P_{1/2}) + M \rightarrow Ar^+(^2P_{3/2}) + M \qquad (6.3)$$

$$Ar^+(^2P_{1/2}) + N_2 \rightarrow N_2^+ + Ar \qquad (6.4)$$

The rate constants used (Hamdan et al., 1984) were $k_4 = 1.1 \times 10^{-11}$ cm^3s^{-1}, $k_5 = 3.2 \times 10^{-11}$ cm^3s^{-1}, and $k_6 = 3.6 \times 10^{-11}$ cm^3s^{-1}. The possibility of spin conversion from the J=3/2 state to the J=1/2 state through collisions with neutrals was neglected. The results of the modelling are shown in Figure 6.2.

This model showed that while minor deviations from the

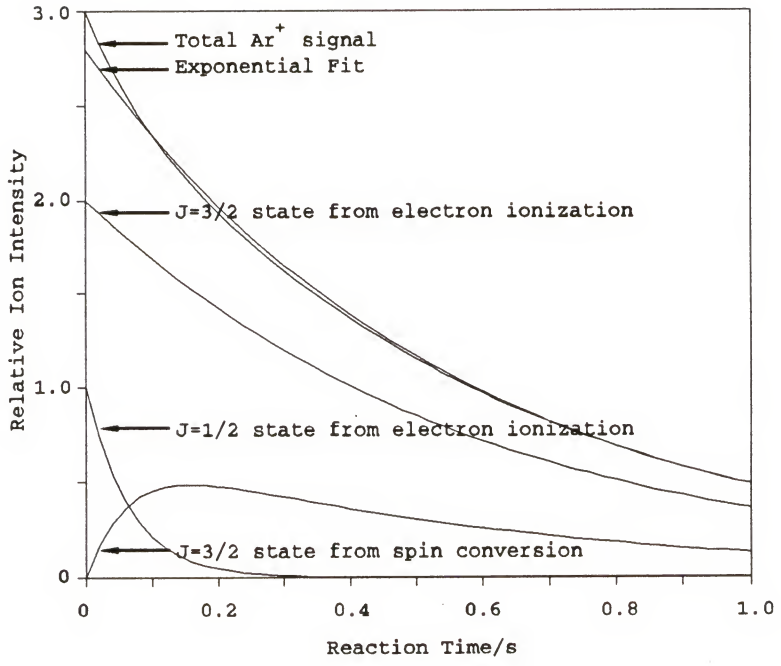

Figure 6.2. Results of the model on the $Ar^+ + N_2$ system including contributions from the two spin states of Ar^+, J=3/2 and J=1/2.

exponential fit did occur at longer times, the primary effect of the higher energy spin state was an increase in reactivity at short reaction times. The change in the rate constant between the $Ar^+(^2P_{3/2})$ only decay and the total Ar^+ decay was only a three percent increase. As shown in Figure 6.2, the largest deviation of the total Ar^+ signal from an exponential fit is for reaction times less than 100 ms. This time period corresponds to the relaxation period, which was always implemented in our work to allow collisional relaxation of ions to the center of the cell. Since our data collection began after this time period, we did not observe curvature due to the difference in reactivity of the two spin states when the $\ln(Ar^+)$ signal was plotted as a function of reaction time.

The charge exchange Reaction (6.1) was investigated to estimate ion temperatures or kinetic energy as well as to assess the effects of various experimental parameters on ion energy. Typical data for this reaction are shown in Figure 6.3. In this figure, the filled rectangles are H_2O^+ relative ion intensities and the empty rectangles are Ar^+ relative ion intensities. Figure 6.4 shows the increase in ion signal that was observed when no relaxation delay was implemented. Ar^+ relative ion intensities are plotted in this figure. As ions were relaxed to the center of the cell (the bottom of the trapping well) by collisions with neutrals, the signal obtained increased due to the higher detection efficiency for ions at this position. Note that there is no observed growth

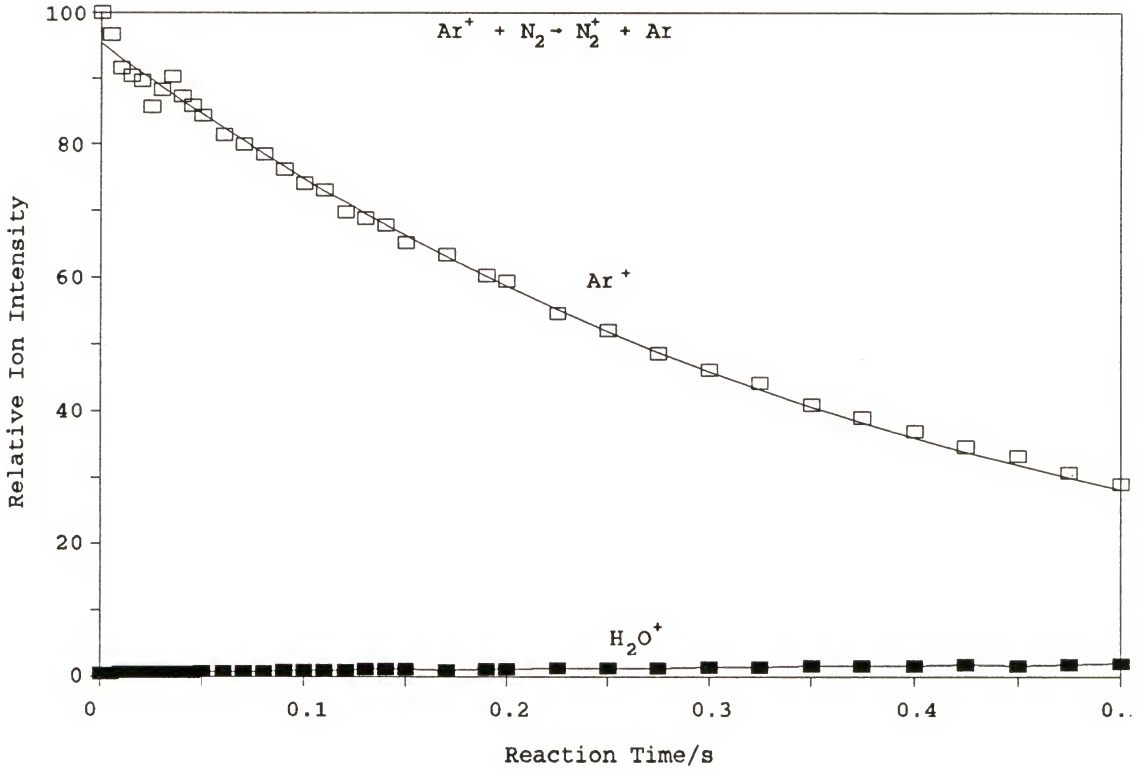

Figure 6.3. Data for the kinetic energy dependent reaction (6.1) taken with 100 ms relaxation delay. These data were obtained with pressures of 2×10^{-6} Torr of each gas.

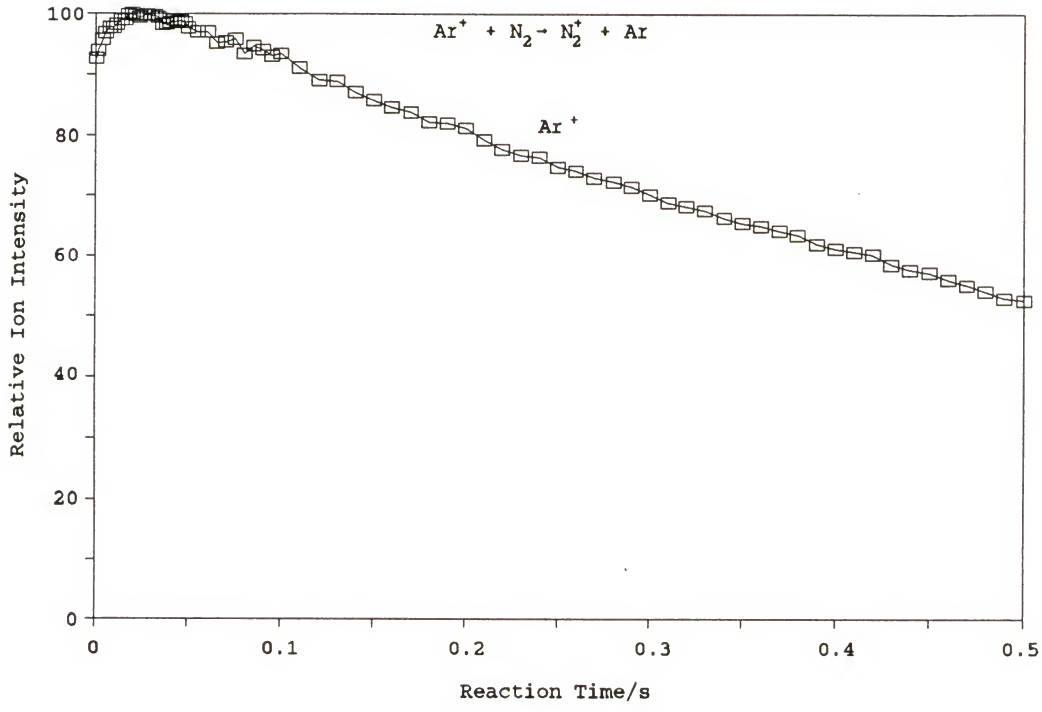

Figure 6.4. Data for the kinetic energy dependent Reaction (6.1) taken without the standard 100 ms relaxation delay. These data were obtained with pressures of 2×10^{-6} Torr of each gas.

of N_2^+ since N_2^+ was continually ejected by a single frequency cyclotron resonance ejection to prevent the possible reverse charge exchange reaction from occurring. A small quantity of m/z=18 formed with time from the charge transfer between Ar^+ and trace quantities of H_2O.

The results of a pressure dependence study of the rate coefficient for Reaction (6.1) are shown in Figure 6.5. In this study, the argon pressure and the nitrogen pressure were varied independently over the range from 2×10^{-7} to 1.4×10^{-5} torr. Error limits indicate the 95% confidence limits of the mean of multiple determinations (n=4 to 32) at a constant total pressure. The large fluctuations in these data are probably due to the slow rate of the reaction, which requires operation in a pressure region somewhat high by FTICR standards. If the Ar^+ ions were translationally excited, one would expect the rate constant to decrease at high pressures due to the increased collisional cooling. Clearly, there is no significant effect of total pressure on the rate coefficient. Therefore, one may conclude that the delay to allow ions to relax to the center of the cell is also sufficient to allow ions formed with higher than thermal kinetic energy to be thermalized. Kinetic data for this reaction could not be collected without the relaxation delay because of the observed effect on the ion intensity illustrated in Figure 6.4. Since the total pressure (corrected both for gas sensitivities as well as for a system

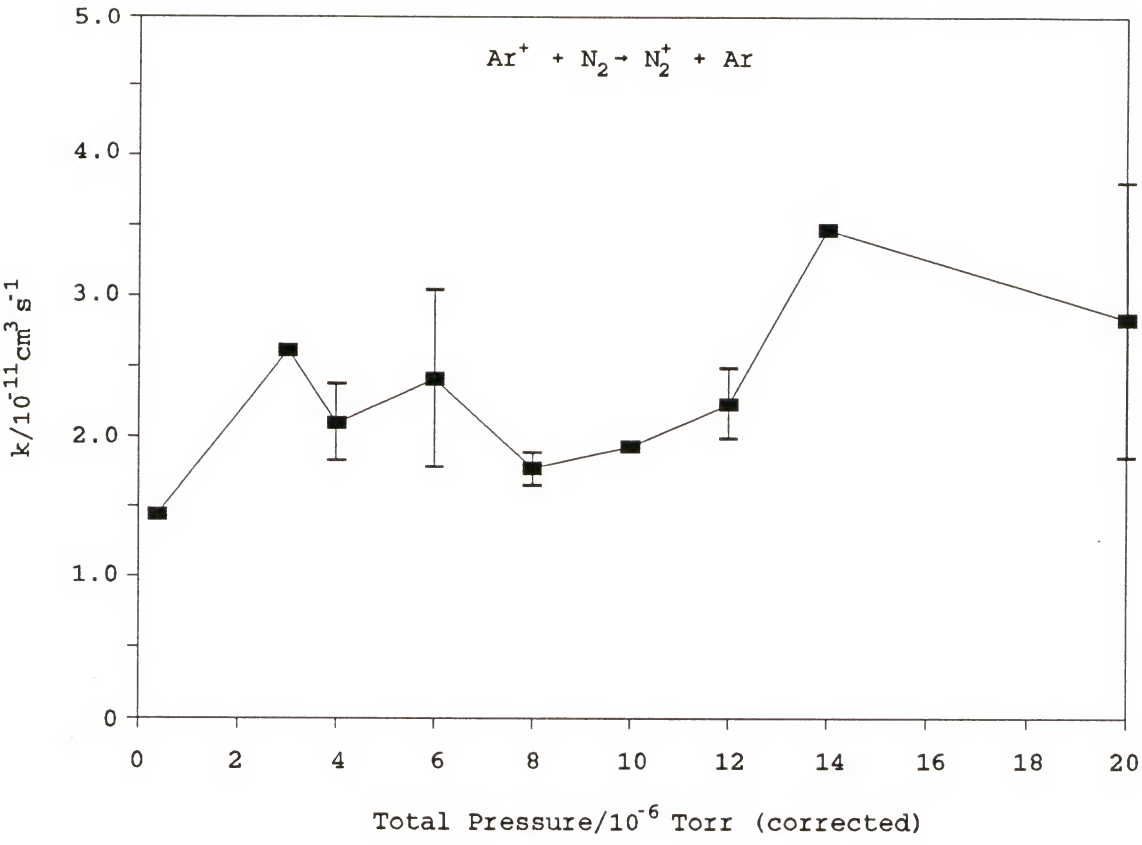

Figure 6.5. Rate constant for Reaction (6.1) as a function of pressure. Shown along the x-axis is total pressure. Each gas was independently varied over the range from 2 x 10^{-7} Torr to 1.4 x 10^{-5} Torr.

factor of 2.0) was $4x10^{-6}$ torr or higher, one may estimate, based on a Langevin (Langevin, 1905) cross section, that with an average of as few as 13 collisions, Ar^+ ions were collisionally cooled to some kinetic energy that could not be reduced by additional collisions.

Because the trapping voltage is believed to be a major source of translationally excited ions (Bartmess, 1987), its effect on the charge exchange reaction rate coefficient was also examined. The results of this study are shown in Figure 6.6. This experiment was done at constant argon and nitrogen pressures by changing the trapping voltage and systematically adjusting the electron ionizing time and or current to produce approximately the same signal intensities and presumably approximately the same number of ions at all trapping voltages. Data are shown for trapping voltages between 0.3 and 5 V. Error limits indicate 95% confidence limits of the mean for multiple determinations (n=3 to 8) for a single trapping voltage. The results show no dependence of the rate coefficient on the trapping voltage. This means that even though ions may be formed with considerable excess kinetic energy, they are rapidly collisionally relaxed to the center of the cell within the first 100 milliseconds after formation.

An effective ion temperature may be extracted from this work by averaging all the rate coefficient determination results and comparing them to the flow-drift tube work of Dotan and Lindinger (1982). Our average value for the charge

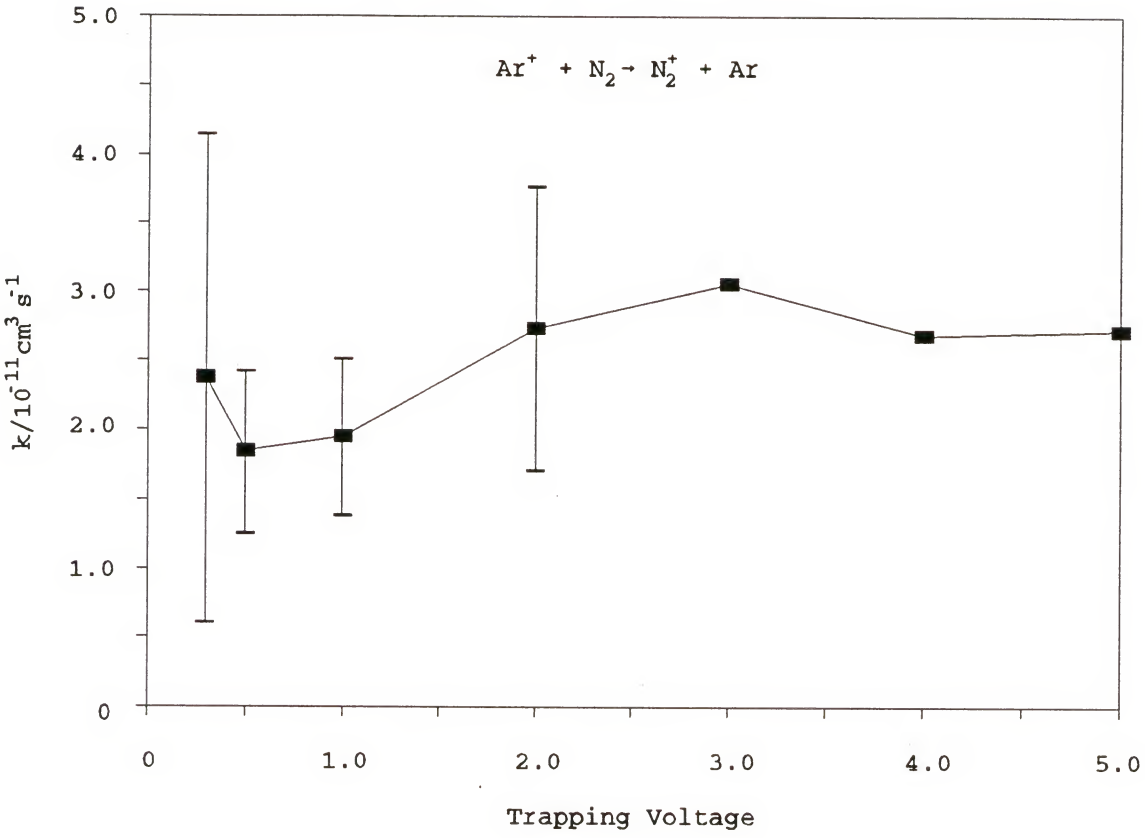

Figure 6.6. Rate constant of Reaction (6.1) as a function of trapping voltage. All determinations were done at a total pressure of 1.2 x 10^{-5} Torr.

exchange reaction coefficient is (2.4 ± 0.2) × 10^{-11} cm^3 s^{-1} (in good agreement with (2.2 ± 0.2) x 10^{-11} cm^3s^{-1} determined in earlier ICR studies (Laudenslager et al., 1974)). By comparison to the flow-drift tube data (Figure 3 of Dotan and Lindinger, 1982), this leads to a center of mass kinetic energy, KE_{cm}, of 0.065 ± 0.010 eV. KE_{cm} is defined by

$$KE_{cm}=\tfrac{1}{2}\mu v_r^2 \qquad (6.2)$$

where μ is the reduced mass of the colliding pair and v_r^2 is the square of the relative velocity. One can then solve for v_r^2 since μ is easily obtained from the ion and neutral masses. The square of the relative velocity is related to ion and neutral temperatures by

$$v_r^2=3k(T_1/m_1+ T_2/m_2) \ , \qquad (6.3)$$

if one assumes that the colliding neutrals and ions have separate Boltzmann distributions of velocities about temperatures T_1 and T_2, respectively (Kennard, 1938; McFarland et al., 1973). Using a value of 375 K (the temperature of the ICR cell as measured with a resistive temperature device) for T_1, the temperature of N_2 molecules, one can solve for T_2, the temperature of the Ar^+ ions using Equation (6.3). By doing this, one obtains a temperature of 690 ± 190 K. This temperature seems suspiciously high.

Chesnavich et al., (1976) calculated the temperature for ions generated along the trapping potential surface by approximating this surface with

$$V_z=(V_T/2)(z^2+1) \qquad (6.4)$$

where z is the distance along the z (magnetic field) axis with the origin at the center of the cell and V_T is the applied trapping voltage. Using this and assuming a thermal distribution for the neutral species and integrating over all z points of ion formation their group estimated the velocities of ions to be only 50% greater than thermal for a 1 volt trapping voltage, in the absence of any thermalizing collisions. It is doubtful that the temperature of the Ar^+ ions would be this high after 10 collisions with argon atoms or nitrogen molecules.

Alternately, one may compare the obtained rate constant to the more recent VT-SIFDT (Variable Temperature -Selected Ion Flow Drift Tube) work of Viggiano and co-workers (1990). They investigated the kinetic energy dependence of the $Ar^+ + N_2$ reaction by varying the drift voltage at constant temperature as well as the temperature at constant drift voltage. While some uncertainties remain in their interpretation, the results showed that the effect of varying the temperature on the rate constant was not equivalent to the effect produced by altering the drift voltage at lower values of KE_{cm}. They concluded that increased temperatures probably lead to an increase in the rotational energy of N_2. When plotted as a function of total energy, their data showed that, with a rotational contribution of kT, all points (see Figure 3 of Viggiano et al., 1990) fell on the same curve. Comparing the present FTICR data with that from the VT-SIFDT instrument indicates that the total energy

for the reaction in the ICR cell is in the range 0.080 to 0.10 eV, which is defined as the average center of mass kinetic energy plus the average rotational energy. Again using 375 K for T_1 and subtracting kT_1 (the rotational energy of N_2) from the total energy range given above, one obtains 0.048 to 0.068 eV for KE_{cm}. These kinetic energies correspond to a temperature (T_2 from Equation (6.3)) of 545 ± 190 K. Although still somewhat high, this range does encompass the thermal value.

Conclusions

Measurements of the kinetic energies of ions produced in a FTICR instrument are crucial to the interpretation of data obtained from ion-molecule reactions. Several conclusions can be obtained from the present study. First, electronic states of Ar^+ of energy equal to or higher than that of $^2P_{1/2}$, if present, react with the same rate constant as $^2P_{3/2}$ or are rapidly relaxed. Second, no additional collisional cooling was observed after the 100 ms relaxation period, indicating that by that time ions have been cooled to some level unaffected by additional collisions. The value of this kinetic energy plateau is still not well defined; however, based on recent VT-SIFDT measurements, it is believed to be only slightly above thermal. The initial growth of ion intensity avoided in our work by allowing a relaxation period, could itself serve as a "thermometer", indicating that ions

have reached thermalization when the ion intensity maximizes. Since the detection efficiency has been shown to be position dependent and the average position in the trapping well is kinetic energy dependent, one can conclude that the detection efficiency is itself kinetic energy dependent with a maximum efficiency observed for a minimum kinetic energy. Finally, the pressure dependence study indicates that the Ar^+ ions are collisionally relaxed with as few as 13 collisions.

CHAPTER 7
APPLICATION OF ION-MOLECULE REACTIONS TO THE STUDY OF CLUSTERS

Introduction

The study of clusters has recently grown to become the focus of much experimental and theoretical research (Weltner and van Zee, 1989). With the revelation of the new form of carbon exemplified by the carbon clusters commonly referred to as the fullerenes, cluster investigations have reached epidemic proportions. Considerable research has dealt with characterization of the physical properties of clusters. A goal of these studies has been to produce a better understanding of the bonding involved in clusters and to comprehend how the bonding behavior and physical properties of clusters evolve as the number of atoms is varied. The "holy grail" of cluster research has been to witness the transition of physical properties from those of atoms and molecules to those of bulk materials (Eckardt, 1984; Yang et al., 1988; Kappes et al., 1986).

A large portion of cluster research has been performed in the gas phase, involving laser ablation, supersonic pulsed nozzle sources (Alford et al., 1986), tunable laser spectroscopy (Kitsopoulos et al., 1991), and ultrahigh vacuum chambers and mass spectrometers (Cox et al., 1988). The

experimental gas phase study of clusters has, to a large extent, dealt with cluster ions, since the charge of the ion provides a unique "handle" to control these clusters. The charge of the cluster ion has been essential for the selection of one particular size cluster (for experiments involving the spectroscopy or reactions of clusters ions), for the acceleration of cluster ions (for collision experiments such as the Coulomb explosion technique), and for the detection of cluster ions (almost all cluster studies is mass spectrometric detection).

Two relatively common experiments involving cluster ions are photoelectron spectroscopy (Cheshnovsky et al., 1987) and photoionization spectroscopy (Honea et al., 1990; Rohlfing et al., 1984; Zhang et al., 1986). As well as detailed electronic structure information, these experiments yield electron affinities and ionization potentials, respectively. These techniques have become a standard method for the determination of IP's and EA's of clusters. However, the same physical properties of clusters can also be probed by ion-molecule reactions.

For several years, experiments have been underway at the University of Florida to determine the ionization potentials of clusters using ion-molecule reaction bracketing techniques (Bach and Eyler, 1990; Zimmerman , Watson et al., 1991). These experiments utilized the ion trapping ability common to Fourier transform ion cyclotron resonance mass spectrometers

to store cluster cations formed by laser ablation (McElvany, Nelson et al., 1987; Moini and Eyler, 1987; Moini and Eyler, 1988). In general, the agreement between the bracketing and the photoionization experiments has been excellent. Furthermore, in some cases the charge transfer bracketing work has reported the first measured ionization potential of a cluster, new evidence for structural isomers (as for the P_4 cluster) (Zimmerman et al., 1991a), and stimulated at least one new theoretical study on clusters. Clearly, this work has been of great value to the scientific community interested in the properties of clusters.

FTICR mass spectrometers are particularly well suited to the charge transfer bracketing technique because of their previously mentioned ion trapping ability. Also crucial to the measurement of ionization potentials has been the ion ejection capability (Comisarow et al., 1978). This feature allows the isolation of all clusters of a single mass-to-charge ratio and the unambiguous assignment of reaction pathways of complex reaction systems with the continuous ejection of the products from competing channels. Finally, the facile adaptation of lasers for laser desorption/laser ablation makes FTICR instruments particularly tractable for cluster experiments.

We have recently extended the bracketing technique to include negative cluster ions and thus to provide electron affinities. In this chapter, the electron affinities of small

carbon clusters, C_n (n=4 to 8), C_{60}, C_{70}, and the silicon cluster Si_2, as measured by the charge transfer bracketing experiment, are reported. These values are compared to the results obtained by more traditional methods, such as photoelectron spectroscopy and threshold photodetachment spectroscopy. Also reported in this chapter are interesting results obtained on the hydrogen atom abstraction reactions of the smaller carbon cluster anions with various compounds.

Experimental

The reactions of all the cluster anions mentioned above were investigated with the Nicolet FTMS-1000 vacuum system and 3 T superconducting magnet and IonSpec personal computer based data system described in Chapter 2. All clusters were formed by laser ablation or laser desorption of a target material. For smaller carbon clusters, the target material was a graphite rod machined into the shape of a removable solids probe tip. For Si_2 clusters, a sample of silicon wafer was adhered with Torrseal to a removable stainless steel probe tip. For the production of gas phase fullerenes a pure C_{60} and C_{70} extract (Haufler et al., 1990) was dissolved in toluene which was then dried on a removable stainless steel probe tip.

The lasers used to form the clusters varied. For the smaller carbon clusters as well as Si_2, the laser employed was a Quantel (now Continuum) Nd:YAG. The second harmonic output of the laser was used for carbon clusters while the

fundamental output was used for silicon cluster formation. The output power was in the range of 10-100 mj/pulse. In both cases, the laser beam was focussed with the aid of a three inch focal length quartz lens mounted inside the vacuum system in front of the cell, so that the laser beam was focussed through the cell onto the target material. A similar configuration was employed for the study of fullerene clusters. However, the laser used in this case was a pulsed CO_2 laser operating at 10.6 microns with ca. 1 joule/pulse. The three inch focal length quartz lens was replaced in this study with a ZeSe lens of equal focal length. Only two clusters were seen from the laser-desorption of the dried extract. These were C_{60} and C_{70}, indicating that either no other clusters were present in the extract, the CO_2 laser did not fragment C_{60} or C_{70} into smaller clusters, or that these smaller clusters were not efficiently trapped.

For all cluster studies presented here, the corresponding cluster anion was trapped in the ICR cell with trapping potentials in the range of -1 to -2 volts. These negative ions were presumably formed by the attachment of free electrons generated in the plasma created by the laser. Cluster anions with kinetic energies along the z-axis higher than the applied trapping voltage are able to enter the cell. During the traversal of the cell, a small fraction of these anions collide with neutral species and either lose kinetic energy or have some of the z-axis kinetic energy distributed

into the other two components. The resulting anions have kinetic energies along the z-axis less than the applied trapping voltage and remain trapped in the cell.

The general pulse sequence for results presented here is shown in Figure 7.1. Very shortly after the laser was fired, a pulsed valve was triggered which allowed argon to enter the vacuum chamber to a peak pressure of ca. $5x10^{-6}$ torr. The time that was required for the pressure to rise and fall back to the original pressure was around 2 seconds. This time period served as the thermalization period. Several eject pulses were implemented after the valve was triggered, but before the argon pressure had risen significantly. All cluster anions with the same mass-to-charge ratio were isolated by the application of these swept and single frequency ejects to the excitation plates. Generally, ions with a mass-to-charge ratio near the ion of interest were removed with low intensity, ca. 2 V_{pp}, 10 ms single frequency ejects to avoid imparting excess kinetic energy into the isolated ion. However, after the isolation step, all remaining ions were thermalized with the relatively high pressure of argon from the earlier valve pulse. Argon was used for thermalization, rather than the SF_6 used in the previous carbon cluster IP determinations, due to the rapid formation of SF_5^- and SF_6^-.

After isolation and thermalization, the cluster anion was allowed to react with a charge transfer bracketing compound. The reference compounds used and their electron affinities are

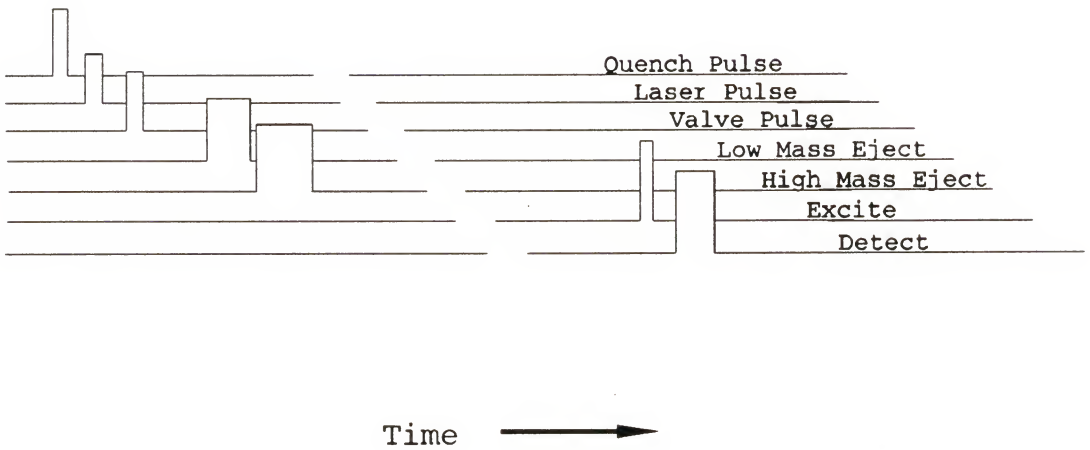

Figure 7.1. Typical pulse sequence used for electron affinity bracketing experiments.

given in Table 7.1. For electron affinity bracketing, the compound used was varied, starting with lower electron affinity compounds, until a compound was found that would remove an electron from the thermalized cluster anion. Starting with lower EA compounds was necessary to prevent their interference as a residual background contaminant in subsequent experiments. The first observation of electron transfer indicated that the cluster had an electron affinity that was less than the EA of the reference compound but greater than that of the previously utilized compound.

All reference compounds used were of laboratory grade or better and were obtained commercially. Liquid compounds were subjected to several freeze-pump-thaw cycles and solid reference samples were evacuated to the millitorr range for several minutes prior to use.

Results and Discussion

Electron Affinities

The first clusters studied by this process were the fullerenes, C_{60} and C_{70}. Figure 7.2 shows a typical low resolution spectrum of the two cluster anions. With more data points and careful tuning, the ^{13}C peaks for C_{60} at 721, 722, and 723 can easily be resolved with this instrument. Both of these clusters were reacted with many compounds, six of which are shown in Table 7.2. The results of the electron transfer investigation are also shown in this table. The electron

Table 7.1. Reference compounds used for all electron affinity bracketing experiments.

EA/eV[a]	Compound
0.69	azulene
0.86	3-nitro-o-xylene
0.92	2-nitrotoluene
0.95	4-nitrotoluene
0.99	3-nitrotoluene
1.10	1,4-dicyanobenzene
1.23	1-fluoro-3-nitrobenzene
1.41	3-nitro-α,α,α-trifluorotoluene
1.56	3-nitrobenzonitrile
1.61	2-nitrobenzonitrile
1.65	1,3-dinitrobenzene
1.72	4-nitrobenzonitrile
1.81	1,4-naphthoquinone
1.91	1,4-benzoquinone
2.00	1,4-dinitrobenzene
2.16	3,5-dinitrobenzonitrile
2.19	2,3-dichloro-1,4-naphthoquinone
2.44	2,5-dichloro-1,4-benzoquinone
2.48	2,6-dichloro-1,4-benzoquinone
2.70	tetrafluoro-1,4-benzoquinone
2.78	tetrachloro-1,4-benzoquinone
3.17	tetracyanoethylene

[a]Lias et al., 1988

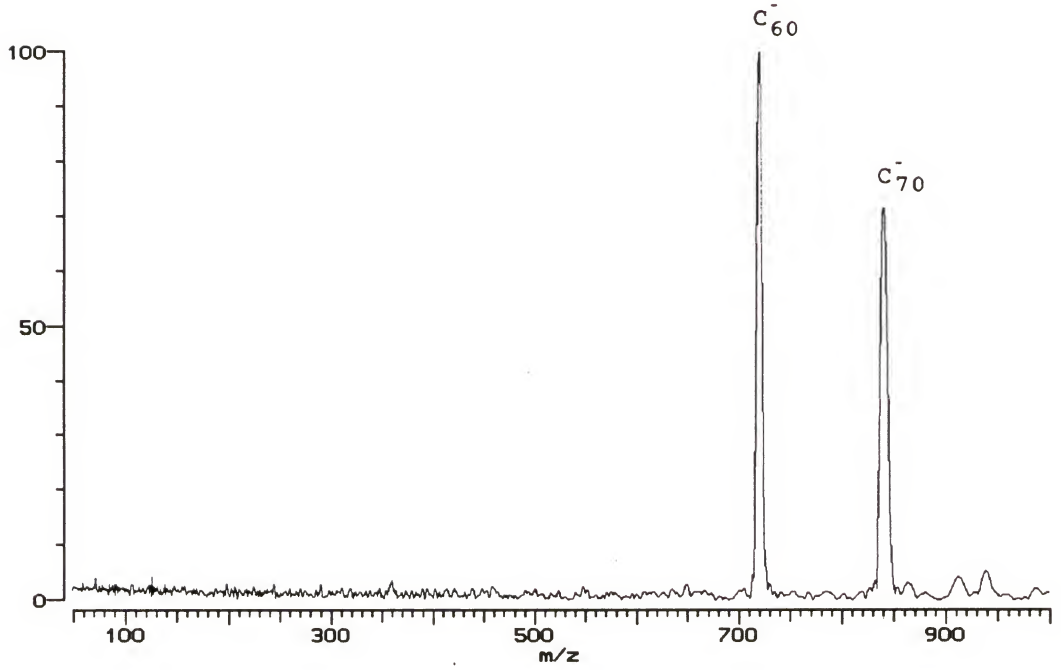

Figure 7.2. Typical low resolution spectrum of C_{60}^- and C_{70}^- produced by CO_2 laser desorption.

Table 7.2. Results for the electron transfer reactions of C_{60}^- and C_{70}^-. Y indicates that electron transfer did occur from the cluster anion to the reference compound.

Reference Compound	EA/eV	C_{60}^-	C_{70}^-
3,5-Dinitrobenzoquinone	2.1	N	N
2,3-Dichloro-1,4-naphthoquinone	2.19	N	N
2,6-Dichloro-1,4-benzoquinone	2.48	N	N
Tetrafluoro-1,4-benzoquinone	2.70	Y	Y
Tetrachloro-1,4-benzoquinone	2.78	Y	Y
Tetracyanoethylene	3.17	Y	Y

affinities of both clusters were bracketed to be 2.59 ± 0.15 eV in this study. The rates for electron transfer of these clusters with tetrafluorobenzoquinone, the lowest EA compound found to remove an electron from these clusters, were also investigated. Figure 7.3 shows C_{60}^- undergoing electron transfer with tetrafluorobenzoquinone at a pressure of 5.6 x 10^{-8} torr. Also shown in this figure is an exponential fit, characteristic of pseudo-first order kinetics, to the decaying cluster signal. Figure 7.4 shows a similar result for C_{70}^-, at a pressure of 4.3 x 10^{-7} torr. Even though these clusters exhibit very similar electron affinities, their rate constants for the reaction with tetrafluorobenzoquinone are remarkably different. The rate constants extracted from the data shown in Figures 7.3 and 7.4 are 7.0 x 10^{-11} cm^3s^{-1} and 4.7 x 10^{-12} cm^3s^{-1}, respectively. The rate constant for the reaction of C_{60}^- is about 15 times larger than that of C_{70}^-. This is surprising given that the rates based on Pure Polarization Theory (Langevin, 1905) are nearly equal, 7.1 x 10^{-10} cm^3s^{-1} and 7.0 x 10^{-10} cm^3s^{-1} for C_{60}^- and C_{70}^-, respectively. The molecular polarization of tetrafluorobenzoquinone was calculated for these rate constant estimates based on the method described by Miller and Savchik, (1979). The observed rate constants not only differ from each other, but are also substantially slower than predicted. This implicates a relatively large barrier along the reaction coordinate due to the geometry change of the tetrafluorobenzoquinone upon electron attachment, such

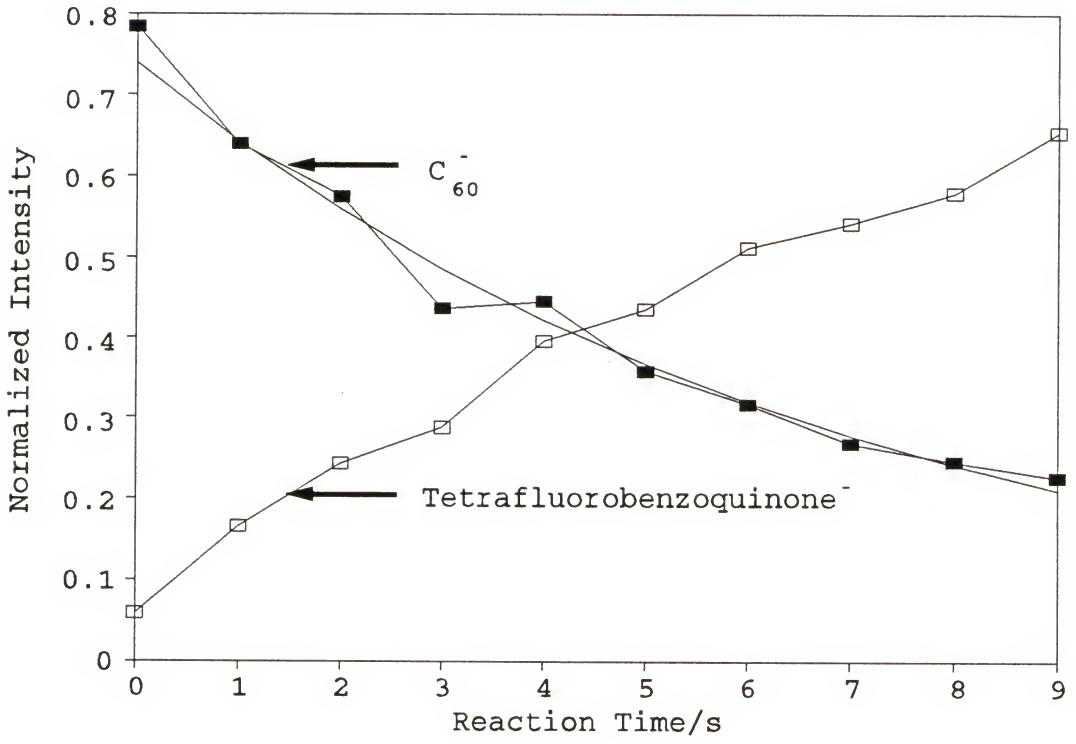

Figure 7.3. C_{60}^- reacting with tetrafluorobenzoquinone at a pressure of 5.6×10^{-8} torr.

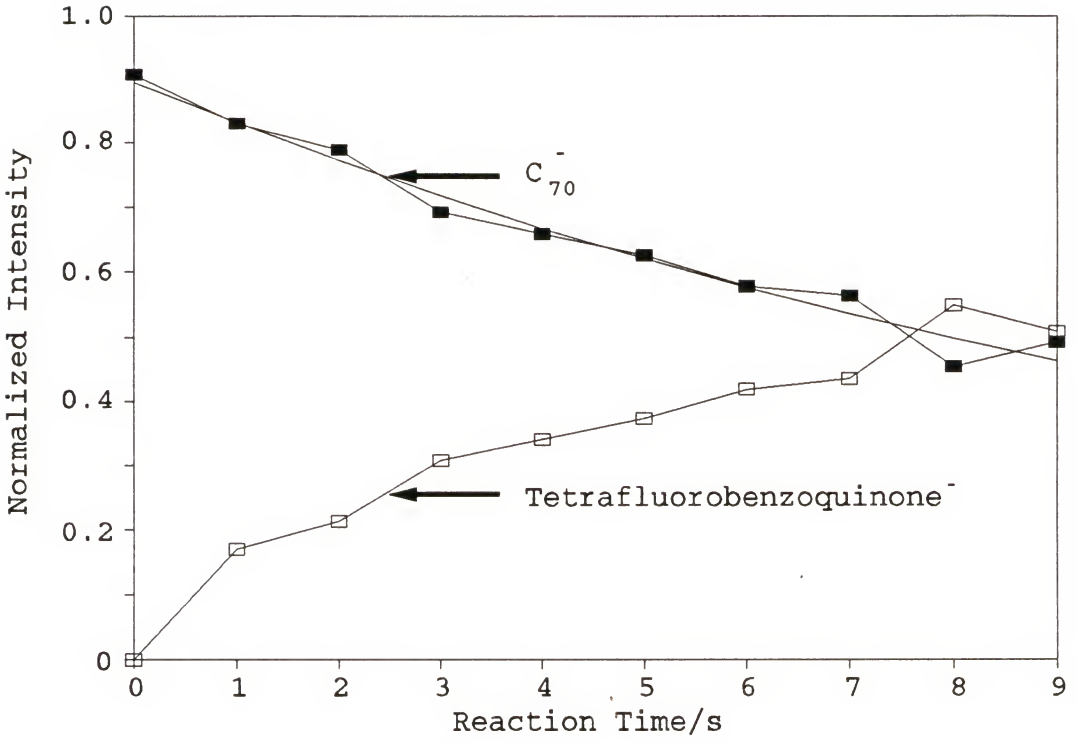

Figure 7.4. C_{70}^- reacting with tetrafluorobenzoquinone at a pressure of 4.3×10^{-7} torr.

that few of the complexes have sufficient energy to proceed to products, as has been discussed for many gas phase electron transfer reactions by Nelsen et al., (1987) and Richardson et al., (1987). Even though the electron affinity estimates obtained by bracketing were the same for these two clusters, the electron affinity of C_{70} may be slightly higher than that of C_{60}. This not only reduces the exothermicity, which may slow the reaction, but may also serve to increase the barrier height, thus further reducing the electron transfer rate constant, as discussed by Dodd and Brauman, (1986).

Silicon cluster anions were formed by laser ablation of a silicon target with the 1064 nm output of a Nd:YAG laser as discussed above. A typical distribution of clusters is shown in Figure 7.5. Small peaks m+1 and m+2 are evident in this spectrum and are due to the two isotopes of silicon Si^{29} (4.7%) and Si^{30} (3%). From this manifold, Si_2^- was isolated and thermalized as described earlier. Data for an electron transfer reaction of Si_2^- are shown in Figure 7.6. This figure shows the reaction of Si_2^- with 3-nitrotoluene, the first reference compound observed to remove an electron from this cluster anion. Although not shown in this figure, the rate was seen to double when the pressure was increased by a factor of two, providing further evidence for electron transfer. The resulting bracket for the EA of Si_2 was 0.96 ± 0.10 eV.

Small carbon clusters were formed by laser ablation of a carbon rod. A representative distribution of carbon cluster

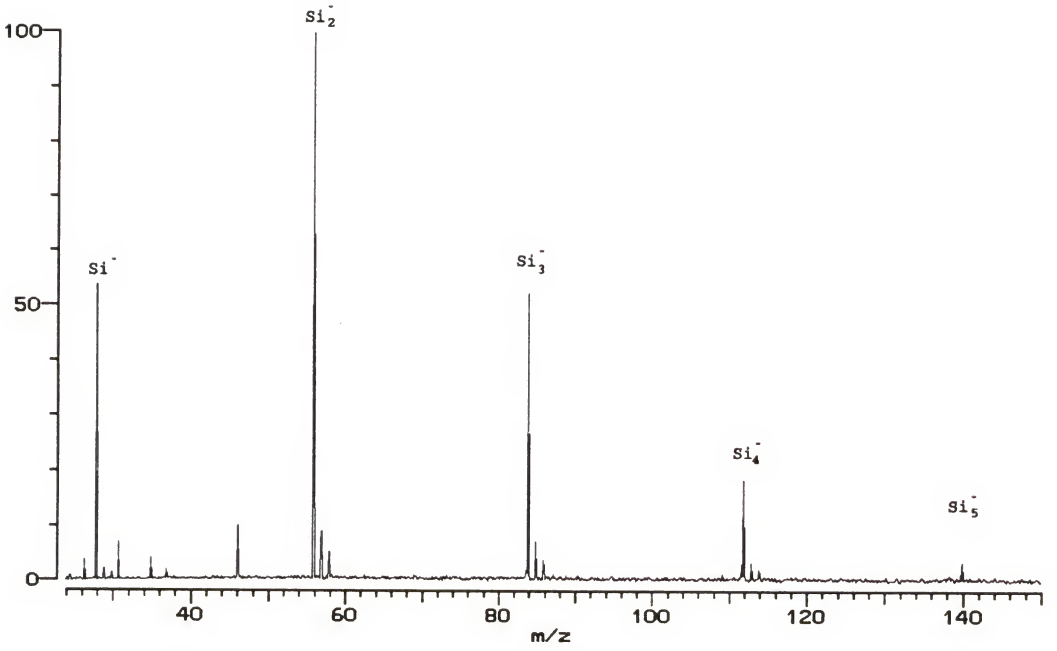

Figure 7.5. Typical silicon cluster anion distribution obtained from 1064 nm laser ablation of a silicon target.

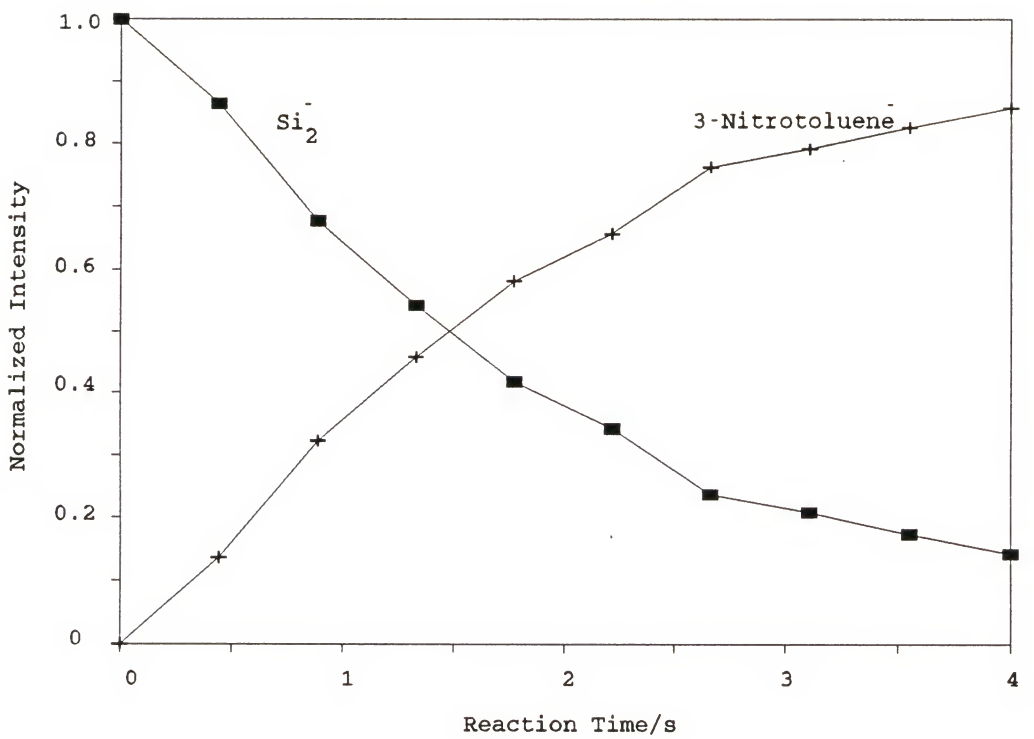

Figure 7.6. Electron transfer data for Si_2^- reacting with 3-nitrotoluene at 2.2 x 10^{-7} torr.

anions obtained with this configuration showing cluster peaks for anions from C_3^- to C_{13}^- is presented in Figure 7.7. The electron affinities of C_n clusters for n=4-8 were investigated with the electron transfer bracketing technique as described previously. Figure 7.8 shows typical timeplot data obtained with C_4^- and 3-nitro-α,α,α-trifluorotoluene at a pressure of 3.7×10^{-7} torr. All reactions were seen to go to completion, thus eliminating the possibility of two structures of the same cluster with markedly different electron affinities. Furthermore, the bracketed electron affinity remained constant regardless of whether the clusters were thermalized or not, indicating that kinetic and internal energies of the cluster anions played little or no role in the electron affinity measurements. This is probably a result of the rapid collisional relaxation of ions trapped in a FTICR cell that was observed in Chapters 4, 5, and 6.

Table 7.3 summarizes all the electron affinity measurements presented in this work and compares them to previous values. Excellent agreement was observed between the present study and the previous photoelectron data from Yang et al., (1987) for C_{60} and C_{70}, which indicates that the measurement of electron affinities of clusters with electron transfer bracketing is a feasible technique. However, a total lack of agreement was observed for all the small clusters presented in this work. The smaller carbon cluster electron affinities were previously reported by Yang et al., (1988) and

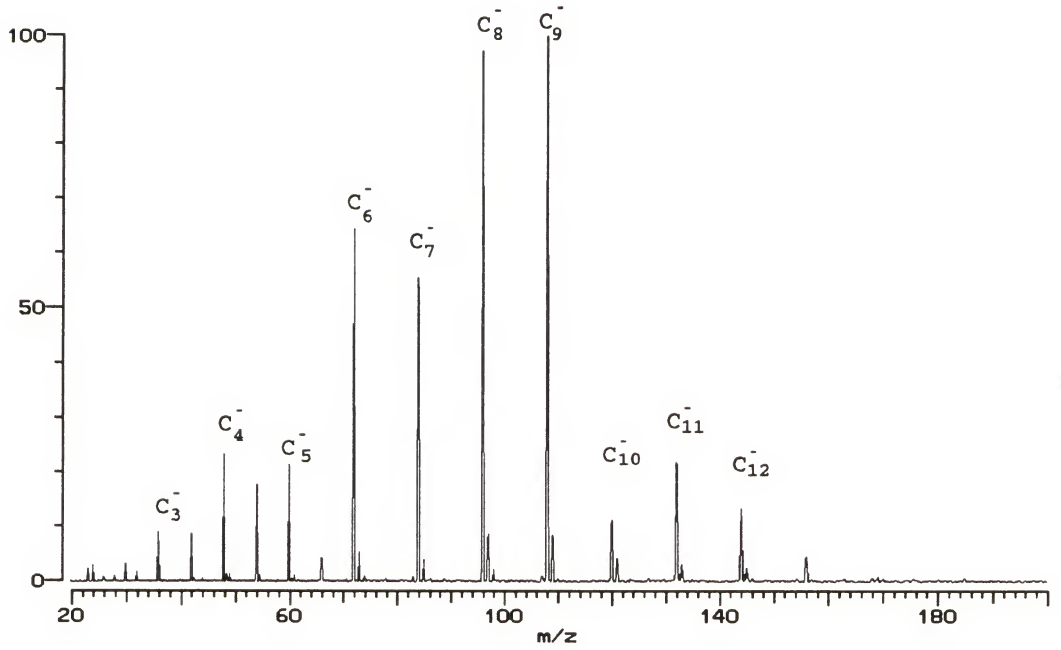

Figure 7.7. Carbon cluster anion distribution obtained from 532 nm laser ablation.

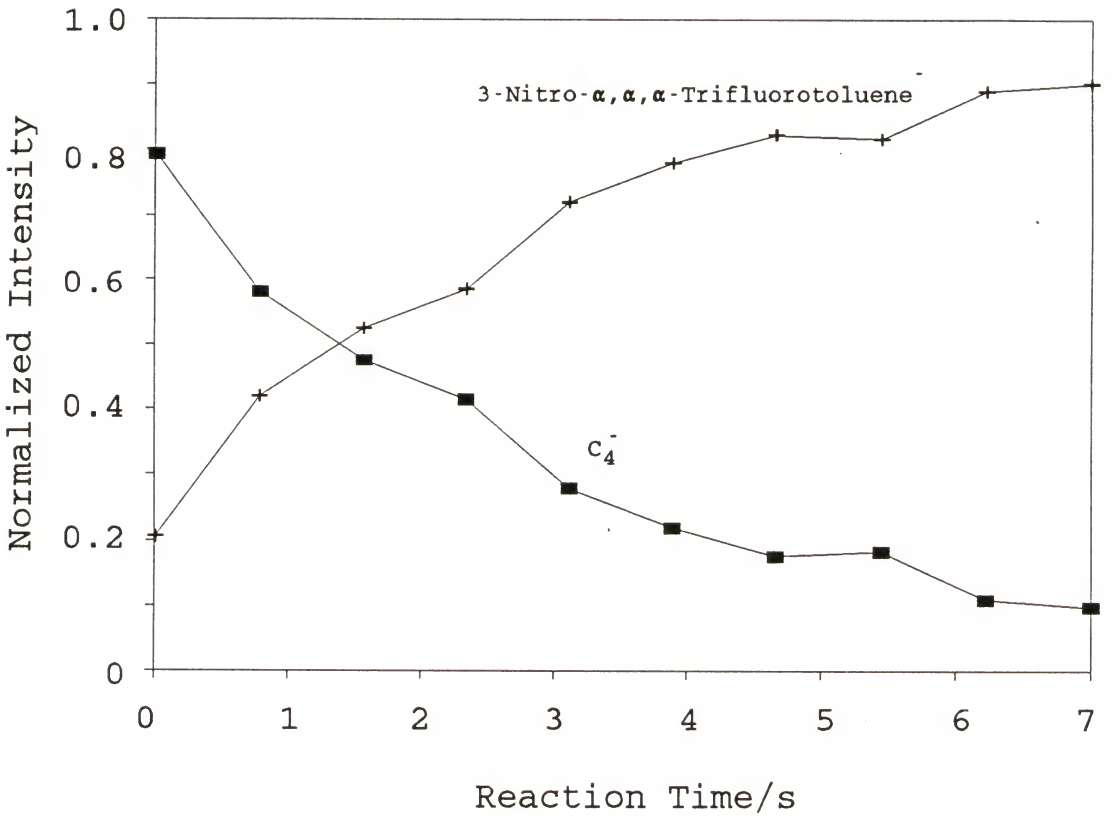

Figure 7.8. Electron affinity bracketing data showing C_4^- electron transferring to 3-nitro-α,α,α-trifluorotoluene.

Table 7.3. The results of all electron affinity bracketing experiments.

Species	EA/eV (this work)	EA/eV (lit) Exp'l.	Theory
Si	< 0.69	1.385 ± 0.005[a]	1.35[d]
Si_2	0.96 +/- 0.1	2.176 ± 0.002[b]	2.09[d]
		2.199 ± 0.012[c]	
C_4	1.3 +/- 0.1	3.70[e]	3.41[f]
			3.29[h]
			2.02[h]
C_5	1.5 +/- 0.1	2.80[e]	2.43[f]
C_6	1.5 +/- 0.1	4.10[e]	3.69[f]
C_7	1.6 +/- 0.1	3.10[e]	
C_8	1.6 +/- 0.1	4.42[e]	
C_{60}	2.6 +/- 0.1	2.6-2.8[g]	
C_{70}	2.6 +/- 0.1	2.6-2.8[g]	

[a]Kasdan et al.,1975.
[b]Kitsopoulos et al.,1991a.
[c]Nimlos et al., 1987.
[d]Raghavachari and Rohlfing, 1991.
[e]Yang et al., 1988.
[f]Adamowicz, 1991.
[g]Yang et al., 1987.
[h]Higher value is for linear structure and lower is that of the cyclic C_4 from Bernholdt et al., 1988.

were determined by photoelectron spectroscopy preformed on the negative clusters. Those values as presented by Smalley's group are not guaranteed to be free from systematic error. However, in the present study not even the alternation between even and odd clusters was observed. Perhaps even more troublesome is the lack of agreement between the present data on Si_2 and the threshold photodetachment data presented by Kitsopoulos et al., (1991a).

The reason for the disagreement is unclear. The method seems to work well for the larger clusters, yet has problems for the smaller ones. Several possible explanations for this observation exist. A large geometry shift may exist between the ground state of the anion and the ground state of the neutral cluster such that predominantly the excited states of the neutral are produced in the vertical P.E.S. process. The resulting photoelectron would have less kinetic energy than it would if it had originated from the ground state causing the electron affinity to appear larger than it is. Another possibility is that the experiment performed by Smalley's group in fact led to dissociation of the cluster as well as photodetachment of the electron. This seems possible since the photodissociation of these cluster anions has been previously investigated by Deluca and Johnson, (1988) and the threshold for photodissociation was found to be far below the 7.9 eV used in the photoelectron experiment. However, the data from Smalley's group is further confirmed in a recent

publication from Neumark's group which presented higher resolution photoelectron spectra of the smaller carbon cluster anions (Kitsopoulos et al., 1991b). In addition, Neumark's data show some vibrational resolution, lending little credence to the possibility of simultaneous photodissociation / photodetachment (which would be expected to be structureless).

The possibility that the differences can be completely ascribed to higher kinetic energy ions being present in the bracketing study can be ruled out. If this possibility were in fact real, at least a subtle shift in the bracketed electron affinity would be observed when comparing thermalized vs nonthermalized data. No such shift was encountered. Furthermore, the difference between the photoelectron data and the present data is, in some cases, larger than the applied trapping potential, indicating that these ions should probably not even be trapped. The possibility that the difference is due to an excited electronic state of the anion in the present study also seems unlikely, considering that this state would require a radiative lifetime that is greater than the 2 second thermalization period.

One problem with the FTICR experiment that can't be neglected is the possibility of trapped electrons. Electrons could be trapped in the FTICR cell and slowly attach to the reference compound, creating the anion. However, this would appear as electron transfer without the corresponding loss of the cluster anion. This possibility can be discredited by

ejecting the isolated cluster anion before the reaction period. This was done and the results showed no growth of the reference compound anion. This indicated that the trapped electrons, if there were any, were removed from the cell, either by electron attachment or trapping loss, by the end of the thermalization period.

Other Reactions

Occasionally, side reactions can occur in these bracketing reactions and create complications for the IP or EA determination. These complications can usually be surmounted, however, by utilizing the ejection capabilities of the FTICR mass spectrometer. For example, in addition to the formation of the reference compound anion, R^-, another product $C_n(R-X)^-$ may form, where $C_n(R-X)^-$ is the adduct anion with the loss of some neutral X. This can lead to uncertainty regarding the formation of R^-. However, FTICR mass spectrometers possess the ability to continually eject a product of a reaction, as was shown in Chapter 6 with the ejection of N_2^+, thus allowing unambiguous assignment of reaction channels.

Sometimes the side reactions are themselves of interest. An interesting side reaction was observed during the course of the small carbon cluster electron affinity study. Reaction of all the cluster anions with 3-nitrotoluene revealed an interesting phenomenon. The slow formation of C_nH^- and $C_nH_2^-$ was observed, but only for even n. Figure 7.9 shows the

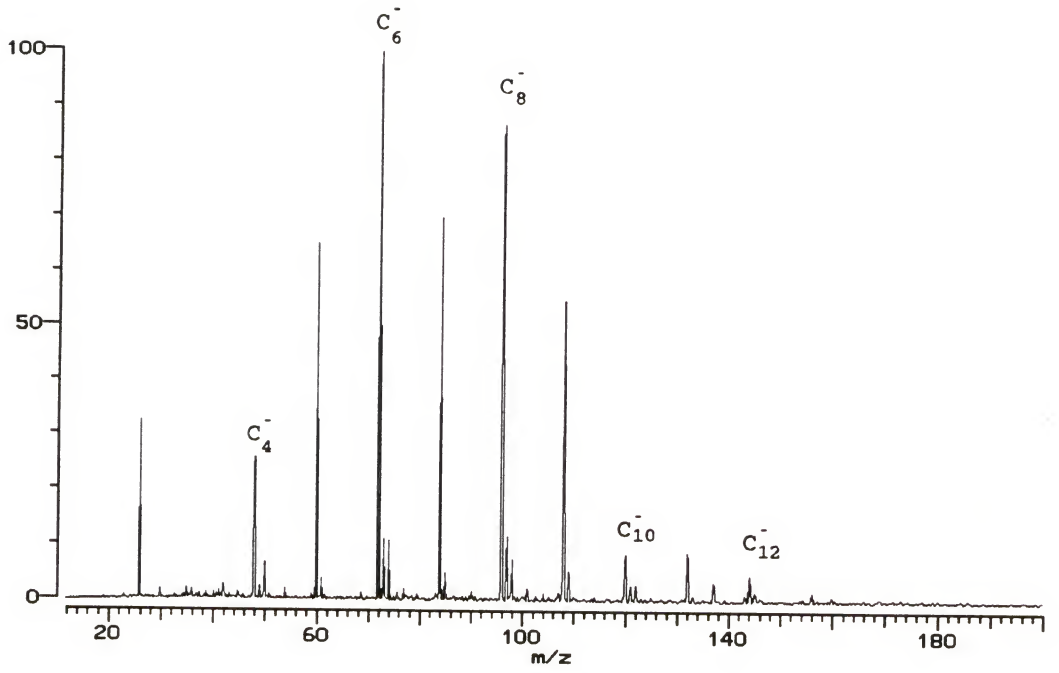

Figure 7.9. Results obtained after reacting all cluster anions for 10 seconds with 3-nitrotoluene at a pressure of 9.0 x 10^{-8} torr.

results obtained for the reaction of all clusters from C_4^- to C_{12}^-. This spectrum was observed after a ten second reaction period with 3-nitrotoluene at a pressure of 9.0×10^{-8} torr. Clear evidence for the propensity of the even numbered clusters to abstract 1 and 2 hydrogen atoms is seen. With the relatively low resolution employed for these experiments, it was not possible to distinguish between $^{12}C_nH^-$ and $^{12}C_{n-1}{}^{13}C^-$. However, the peaks at m+1 for the odd clusters did not grow in with reaction time (the intensity of these C_n+1 peaks remained constant at the expected n% intensity, where n% is n% of the C_n^- peak), nor was any peak at m+2 observed. These facts indicated that the odd clusters did not undergo the same hydogen-atom abstraction that was observed for the even clusters. It was unclear, however, whether the small amount of product observed for the even clusters was due to the presence of two structures, one reactive and one unreactive, or if the small amount was simply indicative of a very slow reaction. Consequently, a better source of hydrogen atoms was sought.

It has long been known that radicals are very reactive and consequently are the cause of the short shelflives of many food items. Food preservatives are designed to be radical scavengers; radicals are scavenged by hydrogen atom abstraction reactions. A common preservative that is used to scavenge radicals is tri(tertbutyl)phenol. It is an efficient source of hydrogen atoms because of the radical stabilizing

ability of the conjugated ring. Believing that this type of radical stabilization should also apply to phenol, a more common laboratory reagent with a significantly high vapor pressure, we chose to react the cluster anions with this compound.

The results of an initial investigation of the clusters with phenol is shown in Figure 7.10. This was performed with a pressure of 2 x 10^{-8} torr of phenol and the spectrum shows the results after a 6 second reaction period. The greater hydrogen atom affinity of the even numbered clusters was still evident. Furthermore, the reaction proceeded to a greater extent than with the 3-nitrotoluene. However in this case, the even numbered clusters were seen to primarily abstract only one hydrogen atom. Also apparent in this study is the peak at m/z=93. This ion is from the proton transfer from neutral phenol to the cluster anion resulting in a neutral C_nH and the $(m-1)^-$ ion for phenol. This ion is the phenoxide ion, the conjugate base of a fairly strong Brønsted-Lowry acid. Electron transfer from the clusters to phenol does not take place, i.e. the mass at m/z=94 is not observed, possibly because the electron affinity of phenol is too low.

These reactions provide some tantalizing possibilities for structural information regarding these smaller carbon cluster anions. Hydrogen-atom abstraction reactions for the cationic clusters have previously been reported (McElvany et al., 1987a). For the cations, no such dramatic even-odd

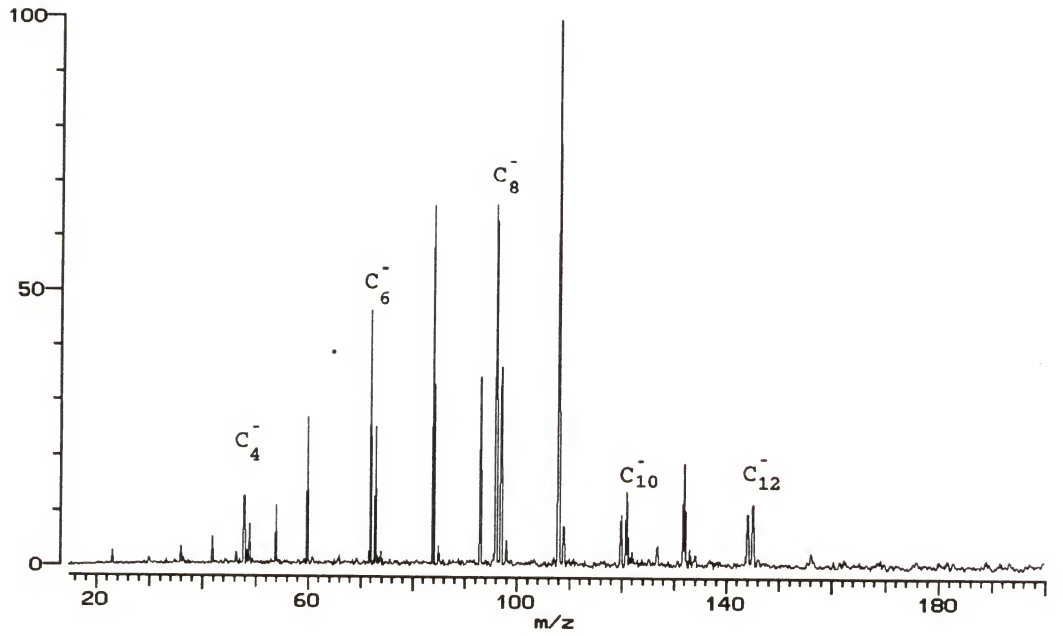

Figure 7.10. Results obtained by reacting all clusters with phenol at a pressure of 2.0×10^{-8} torr for 6 seconds.

alternation was observed in their reactions with D_2 and H_2. However, several interesting fluctuations in the rate constants for these reactions, indicative of cluster geometry changes, did occur. A large shift in the rate constants was encountered at n=10 for the C_n^+ clusters which was considered to be suggestive of a shift from linear structures (for the n<10 cluster cations) to a cyclic structures for n=10 and larger. Furthermore, Yang et al., (1988) reported an abrupt change in the observed photoelectron spectra of the negative clusters C_n^- for n=2 - 30 at n=10. This shift was also considered to be due to the change to cyclic structures. This group also reported the observation of two structures for C_{11}^-, presumably one linear the other cyclic. The results of the present study seem to be suggestive of linear structures for the anions from C_4^- to C_{12}^-. If the hydrogen-atom abstraction reactions are indicative of a more radical nature for the even numbered clusters, then these data seem to support the earlier concept that the clusters are linear structures with the even numbered chains possibly possessing an acetylene-like structure, with a radical electron on both ends, and a cumulene-like structure, thus a carbene, for the odd numbered structures. The above discussion presumes that the extra electron, present in the negative carbon clusters, occupies a π^* orbital, as is suggested in the theoretical study by Adamowitz (1990), and does not drive the observed reactions. This conflicts with the data of Smalley's group in that they

postulated termination of linear structures at C_9 and we have observed these reactions out to C_{12}.

Conclusions

The ion trapping ability of the FTICR mass spectrometer has proven to be a great asset in the study of ion-molecule reactions of cluster anions. This chapter has demonstrated the successful application of the charge transfer bracketing scheme, first developed to measure the ionization potentials of carbon clusters, to the estimation of the electron affinities of clusters of silicon and carbon. Although the agreement between the present data and previously reported data has in some cases not been good, there does not seem to be any simple explanation that can account for these anomalies.

Finally, even more intriguing has been the observation of the selective hydrogen atom abstraction reactions of the carbon cluster anions. The present data seem to support the earlier postulate that the even clusters are linear acetylenes and that the odd clusters are cumulenes.

CHAPTER 8
CONCLUSIONS

The primary focus of this dissertation was to obtain a reliable estimate of the kinetic energies of ions that are trapped in a Fourier transform ion cyclotron resonance mass spectrometer. Also driving this work was the desire to develop an efficient all purpose ion velocity meter. The demand for determining accurately the kinetic energies of ions in a Fourier transform ion cyclotron resonance mass spectrometer exists in nearly every application. This demand has not yet been fully satisfied due to the difficulties encountered in measuring such a quantity. Consequently, unsubstantiated claims regarding the kinetic energies of ions trapped in a Fourier transform ion cyclotron resonance mass spectrometer are frequently made. The controversy pertaining to kinetic energies is far from over. The results from three independent efforts to ascertain the kinetic energies of trapped ions have been presented in this dissertation. At least two of these experiments do have the potential to be developed into the desired all-purpose velocity meter. Despite the fact that only crude estimates for ion kinetic energies were produced in the work presented in Chapters 4, 5, and 6, several interesting conclusions can be extracted from

these experiments.

The three most important conclusions derived from the kinetic energy experiments concern ion kinetic energies, ion velocity distributions, and the thermalization process. All three of the experiments performed to estimate ion kinetic energies produced results that indicated a trapped ion kinetic energy corresponding to temperatures slightly above thermal (< 500 K). These results contradict the claims (Henchman, 1987) that ions trapped in a FTICR mass spectrometer have velocities that are characteristic of temperatures above 1000 K. Clearly, in those temperature-dependent studies there is some other explanation for the lack of agreement between FTICR data and other higher pressure studies. Perhaps there are unconsidered factors affecting the reactions' temperature dependence as was observed to be the case when the rotational energy dependence of the $Ar^+ + N_2$ charge transfer reaction was discovered. This example shows the lack of a complete understanding of the energy dependence for even simple reactions.

The time-of-flight technique, although exceptionally susceptible to the trapped ion densities, illustrated not only that the trapped dichlorobenzene ions had low kinetic energies, but also that the ion velocity distribution did approximate a Maxwell-Boltzmann distribution. This fact was of extreme importance to the other two chapters on kinetic energy measurements. Both of these chapters relied on the

assumption that the ions were present in this type of distribution for the kinetic energy analysis. This time-of-flight technique has the potential for additional investigations on ion kinetic energies and will be discussed again later in this chapter as one of the suggestions for further study.

The three techniques all provided information about the collisional thermalization process. Using Langevin collisional cross-sections, the maximum number of collisions needed to produce near-thermal distribution of ion kinetic energies was calculated. These calculations were based on the pressures employed and the times required or allowed for thermalization and as such the values obtained represent only an upper limit. The studies indicate that for atomic ions such as Ar^+ the number of ion-molecule collisions required for thermalization may be as low as 13 while for polyatomic aromatics this number may be as high as 50.

Another important conclusion gained from this work resulted from an anomaly observed in the $Ar^+ + N_2$ reaction study. The result was an application of a previously described effect to the kinetic energy problem. This work showed that the collisional relaxation of ions along the z-axis (magnetic filed axis) and its effect on the observed ion signal could function as a built-in ion thermometer, indicating that ions had thermalized when the ion intensity maximized. This thermometer also has potential and will be

discussed in the following section.

The ability to measure ion kinetic energies presents the researcher with a wealth of further possible investigations. The time-of-flight technique could be applied to study the kinetic energies of ions injected into the ICR trap from an external source. This could produce information essential to the fine tuning of the injection optics. Also, this arrangement could be used to narrow the energy range of injected ions by properly timing a short duration zero volt pulse. This technique could be useful for studying laser desorbed ions. The kinetic energy of ions formed by laser desorption has been of great interest. One could employ trapping potentials high enough that little or no ions are able to enter the cell except during a very short zero volt pulse. By scanning the delay of this pulse, a temporal profile of the ions emitted from the surface of the probe could be acquired, thus presenting information about the ions' kinetic energy. By this same procedure, one could allow access to ions of a selected kinetic energy for the study of kinetic energy dependent processes. In addition to ions formed by laser desorption, ions injected from any external ion source with the aid of guiding optics could be studied in this same manner. Decreasing the delay between when the ion source is pulsed and when the trapping voltage is pulsed to ground will result in selecting ions with higher kinetic energies. The thermometer that relies on peak intensities to

measure ion kinetic energies could be used in conjunction with the trapping ejection capability of the IonSpec system to study kinetic energy dependent processes. Application of the ions trapping frequencies to the trapping plates for varying periods of time will impart varying amounts of kinetic energy into the motion of the ions along the z-axis. This energy could be detected by means of the peak intensity variations. However, a set of calibration experiments must first be performed to determine the relationship between peak height and z-axis kinetic energy. This could be accomplished by observing the effect on the peak height as an increasingly longer trapping frequency excite pulse is applied to the trapping plate. The peak height will experience a maximum when the ions have only thermal kinetic energy. The height will decrease as the ions gain kinetic energy until they gain kinetic energies that are greater than the applied trapping potential. At this point, the ion intensity will decrease to zero due to the ions exiting the cell. This experiment would be useful for the study of low energy CID processes and for the measurement of reaction barrier heights. In addition, the peak height thermometer could be extremely effective for the study of some fundamental aspects of FTICR. This thermometer could be applied to examine the interesting z-axis ejection phenomenon reported by van der Hart and van der Guchte, (1988).

A secondary goal of this dissertation was related to the

application of ion-molecule reactions. Although Chapters 5 and 6 both dealt with fundamental ion-molecule reactions, Chapter 7 presented the results of the application of ion-molecule reactions to the study of clusters. This was an extension to negative ions of prior work performed with the FTICR instrument on positive cluster ions. Several interesting conclusions arose from these studies. The first conclusion was that an electron affinity ladder could be constructed to bracket the electron affinities of carbon and silicon clusters, analogous to earlier ionization potential bracketing experiments.

Agreement with previously published photoelectron spectroscopy data for the larger clusters was excellent. However for smaller clusters of carbon and silicon, a general lack of agreement with both theoretical, as well as photoelectron data was encountered. The reasons for this disagreement are unclear. If this is a vertical versus adiabatic difference due to the differences in the experimental techniques, further study of the middle sized clusters should show a convergence of the bracketing data with the photoelectron data. One might expect the geometry change experienced upon electron attachment to be the greatest for the smaller clusters, thus producing some disagreement between photoelectron data and bracketing data. However, the observed shift should decrease as the clusters become larger, until the point is reached when the vertical and the adiabatic process

are the same, as may be the case for C_{60} and C_{70}.

An obvious suggestion for further study in this area is to determine the electron affinity of some of the middle range clusters (C_n, n=20 to 30) by electron transfer bracketing experiments. Comparison of these data to the photoelectron data (Smalley et al. have studied C_n, n=2 to 30) should reveal evidence to support or contradict the above hypothesis regarding the electron attachment induced geometry change.

Another set of experiments that should be investigated relies on the ion injection capability of some FTICR mass spectrometers for the production of ions external to the magnetic field and separated from the high vacuum requirement common to these instruments. Essentially the same bracketing experiment could be performed with the exception that the ions are produced in a relatively high pressure region, extracted, and injected into the FTICR cell. This would allow the incorporation of a supersonic type source, similar to that used for the photoelectron studies. These experiments could possibly address the question regarding different cluster structures being produced under different production conditions.

BIBLIOGRAPHY

Adamowicz, L. J. Chem. Phys. 1990, 93, 6685.

Adamowicz, L. J. Chem. Phys. 1991, 94, 1241.

Adams, N. G.; Smith, D. Int. J. Mass Spectrom. Ion Phys. 1976, 21, 349-359.

Alford, J. M.; Weiss, F. D.; Laaksonen, R. T.; Smalley, R. E. J. Phys. Chem. 1986, 90, 4480.

Anicich, V. G.; Kim, J. K.; Huntress, W. T. Int. J. Mass Spectrom. Ion Phys. 1977, 25, 433.

Anicich, V. G.; Sen, A. D.; Huntress, W. T., Jr.; McEwan, M. J. J. Chem. Phys. 1990, 93, 7163.

Anicich, V. G.; Sen, A. D.; Huntress, W. T., Jr.; McEwan, M. J. J. Chem. Phys. 1991, 94, 4189.

Arnold, D. W.; Bradforth, S. E.; Kitsopoulos, T. N.; Neumark, D. M.; J. Chem Phys. 1991, 95, 8753.

Bach, S. B. H. and J. R. Eyler, J. Chem. Phys. 1990, 92, 358.

Bartmess, J. E. in "Structure/Reactivity and Thermochemistry of Ions"; Ausloos, P. ; Lias, S. G., Ed.; Plenum: New York, 1987; p 368.

Bartmess, J. E. and Geogiadis, R. M. Vacuum 1983, 33, 149.

Baykut, G. and Eyler, J. R. Trends in Anal. Chem. 1986, 5 44.

Beggs, C. B.; Kuo, C. H.; Wyttenbach, T.; Kemper, P. R.; Bowers, M. T. Int. J. Mass Spectrom. Ion Processess. 1990, 100, 397.

Bernholdt, D. E.; Magers, D. H.; Bartlett, R. J. J. Chem. Phys. 1988, 89, 3612.

Buchanan, M. V.; Comisarow, M. B. In "Fourier Transform Mass Spectrometry: Evolution, Innovation, and Applications"; ACS Symp. Series 359; Buchanan, M. V.,Ed.; American Chemical Society: Washington, DC, 1987.

Cheshnovsky, O.; Yang, S. H.; Pettiette, C. L.; Craycraft, M. J.; Liu, Y.; Smalley, R. E. Chem. Phys. Lett. 1987, 138, 119.

Chesnavich, W. J.; Su, T.; Bowers, M. T. J. Chem. Phys. 1976, 65, 990.

Cody, R. B.; Kinsinger, J. A.; Goodman, S. D. Anal. Chem. 1987, 59, 2567-2569.

Comisarow, M. B.; Grassi, V.; Parisod, G. Chem. Phys. Lett. 1978, 57, 413.

Comisarow, M. B. and Marshall, A. G. Chem. Phys. Lett. 1974, 25, 282.

Cox, D. M.; Reichmann, K. C.; Kaldor, A. J. Chem. Phys. 1988, 88, 1588.

Dahl, D. A.; Delmore, J. E. "SIMION PC/PS2 Version 4.0", EGG-CS-7233 Rev. 2, April 1988; Idaho National Engineering Laboratory, EG&G Idaho Inc.,P.O. Box 1625, Idaho Falls, ID 83415.

Deluca, M. J. and Johnson, M. A. Chem. Phys. Lett. 1988, 152, 67.

Devlin, J. L. III; Wolf, J. F.; Taft, R.; Hehre, W. J. J. Am. Chem. Soc. 1976, 98, 1990.

Dodd, J. A. and Brauman, J. I. J. Phys. Chem. 1986, 90, 3559.

Dotan, I.; Lindinger, W. J. Chem. Phys. 1982, 76, 4972.

Dunbar, R. C. Int. J. Mass Spectrom. Ion Processess. 1990, 100, 423.

Dunbar, R. C. and Weddle, G. H. J. Phys. Chem. 1988, 92, 5706.

Eckardt, W. Phys. Rev. B 1984, 29, 1558.

Fisher, J. J. and McMahon, T. B. Int. J. Mass Spectrom. Ion Processess. 1990, 100, 701.

Grosshans, P. B.; Shields, P.; Marshall, A. G. J. Am. Chem. Soc. 1990, 112, 1275-1277.

Hamdan, M.; Birkinshaw, K.; Twiddy, N. D. Int. J. Mass Spectrom. Ion Processes 1984, 57, 225-231.

Hanson, C. D.; Kerley, E. L.; Castro, M. E.; Russell, D. H. Anal. Chem. 1989, 61, 2040-2046.

Haufler, R. E.; Conceicao, J.; Chibante, L. F. F.; Chai, Y.; Byrne, N. E.; Flanagan, S.; Haley, M.M.; O'Brien, S. C.; Pan, C.; Xiao, Z.; Billups, W. E.; Ciufolini, M. A.; Hauge, R. H.; Margrave, J. L.; Wilson, L. J.; Curl, R. F.; Smalley, R. E. J. Phys. Chem. 1990, 94, 24.

Henchman, M. in "Structure/Reactivity and Thermochemistry of Ions"; Ausloos, P. ; Lias, S. G., Ed.; Plenum: New York, 1987; p 376.

Hipple, J. A.; Sommer, H.; Thomas, H. A. Phys. Rev. 1949, 76, 1877.

Honea, E. C.; Homer, M. L.; Persson, J. L.; Whetten, R. L. Chem. Phys. Lett. 1990, 1718, 147.

Ikezoe, Y.; Matsuoka, S., Takebe, M., and Viggiano, A. A. "Gas Phase Reaction Rate Constants Through 1986", Maruzen Co.: Tokyo, Japan, 1987.

Kappes, M. M.; Schar, M.; Radi, P.; Schumacher, E. J. Chem. Phys. 1986, 84, 1863.

Kasdan, A.; Herbst, E.; Lineberger, W. C. J. Chem. Phys. 1975, 62, 541.

Katrizky, A. R.; Watson, C. H.; Dega-Szafran, Z.; Eyler, J. R. J. Org. Mass Spectrom. 1989, 24, 1017.

Katritzky, A. R.; Watson, C. H.; Dega-Szafran, Z.; Eyler, J. R. J. Am. Chem. Soc. 1990, 112, 2471.

Kennard, E. H. "Kinetic Theory of Gases, With an Introduction to Statistical Mechanics" 1st ed.; McGraw-Hill Book Company, Inc.: New York and London, 1938; p 105-109,

Kitsopoulos, T. N.; Chick, C. J.; Zhao, Y.; Neumark, D. M. J. Chem. Phys. 1991a, 95, 1441.

Kitsopoulos, T. N.; Chick, C. J.; Zhao, Y.; Neumark, D. M. J. Chem. Phys. 1991b, 95, 5479.

Langevin, P. M. Ann. Chim. Phys. 1905, 5, 245. Translated in:

Laudenslager, J. B.; Huntress, W. T. Jr.; Bowers, M. T. J. Chem. Phys. 1974, 61, 4600.

Liao, C. L.; Shao, R.; Xu, G. D.; Flesch, Y. G.; Ng, C. Y. J. Chem. Phys. 1986, 85, 3874.

Lias, S. G.; Ausloos, P. J. Am. Chem. Soc. 1978, 100, 6027.

Lias, S. G.; Bartmess, J. E.; Liebman, J. F.; Holmes, J. L.; Levin, R. D.; Mallard, W. G. J. Chem. Ref. Data 1988, 17(1).

Marshall, A. G. and Grosshans, P. B. Anal. Chem. 1991, 63, 215A.

Marshall, A. G. and Roe, D. C. J. Chem. Phys. 1980, 79, 1581.

Marshall, A. G. and Verdun, F. R. "Fourier Transforms in NWR, Optical, and Mass Spectrometry"; Elsevier: New York, 1990.

Mauclaire, G.; Derai, R.; Fenistein, S.; Marx, R. J. Chem. Phys. 1979, 70, 4023.

McDaniel, E. W.; Martin, D. W.; Barnes, W. S. Rev. Sci. Instrum. 1962, 33, 2.

McDaniel, E. W." Collision Phenomena in Ionized Gases"; Wiley: New York, 1964; Appendix II.

McElvany, S. W.; Dunlap, B. I.; O'Keefe, A. J. Chem. Phys. 1987a, 86, 715.

McElvany, S.; Nelson, H.; Baronavski, A.; Watson, C. H.; Eyler, J. R. Chem. Phys. Lett. 1987b, 134, 214.

McFarland, M.; Albritton, D. L.; Fehsenfeld, F. C.; Ferguson, E. E.; Schmeltekopf, A. L. J. Chem. Phys. 1973, 59, 6620.

McIver, R. T. Rev. Sci. Instrum. 1970, 41, 555.

McIver, R. T.; Baykut, G.; Hunter, R. L. Int. J. Mass Spectrom. Ion Processes 1989, 89, 343-358.

McMahon, T.B.; Willett, G. D. Int. J. Mass Spectrom. Ion Processes 1990, 101, 225-231.

Meot-ner, M. in "Gas Phase Ion Chemistry Vol. 2" Bowers, M. T. Ed.; Academic Press: New York, San Francisco, London, 1979; p 198-268.

Miller, K. J. and Savchik, J. A. J. Am. Chem. Soc. 1979, 101, 7206.

Moini, M. and Eyler, J. R. Chem. Phys. Lett. 1987, 137, 311.

Moini, M. and Eyler, J. R. J. Chem. Phys. 1988, 88, 5512.

Nelsen, S. F.; Rumack, D. T.; Meot-ner, M. J. Am. Chem. Soc. 1987, 109, 1373.

Nimlos, M. R.; Harding, G. B.; Ellison, G. B. J Chem. Phys. 1987, 87, 5116.

Raghavachari, K. and Rohlfing, C. M. J. Chem. Phys. 1991, 94, 3670.

Rempel, D. I.; Huang, S. K.; Gross, M. L. Int. J. Mass Spectrom. Ion Proc. 1986, 70, 163-184.

Richardson, D. E.; Christ, C. S.; Sharpe, P.; Eyler, J. R. J. Am. Chem. Soc. 1987, 109, 3894.

Rincon, M. E.; Pearson, J.; Bowers, M. T. J. Phys. Chem. 1988, 92, 4290-4292.

Rohlfing, E. A.; Cox D.M.; Kaldor, A. J. Chem. Phys. 1984, 81, 3322.

Sen, A. D.; Huntress, W. T.; Anicich, V. G.; McEwan, M. J.; Denison, A. B. J. Chem. Phys. 1991, 94, 5462.

Sharpe, P.; Eyler, J. R.; Richardson, D. E. Inorg. Chem. 1990, 29, 2779.

Taft, R. W. in "Kinetics of Ion-Molecule Reactions" Ausloos, P., Ed.; Plenum: New York, 1979 p 271.

van der Hart, W. J.; van de Guchte, W. J. Int. J. Mass Spectrom. Ion Proc. 1988, 17-31.

Viggiano, A. A.; Van Doren, J. M.; Morris, R. A.; Paulson, J. F. J. Chem. Phys. 1990, 93, 4761.

Wanczek, K. P. Int. J. Mass Spectrom. Ion Proc. 1989, 95, 1.

Weltner, W., Jr. and van Zee, R. J. Chem. Rev. 1989, 89, 1713.

Wilkins, C. L.; Chowdhury, A. K.; Nuwaysir, L. M.; Caotes, M. L. Mass Spec. Reviews 1989, 8, 67.

Yang, S. H.; Pettiette, C. L.; Conceicao, J.; Cheshnovsky, O.; Smalley, R. E.; Chem. Phys. Lett. 1987, 139, 233.

Yang, S; Taylor, K. J.; Craycraft, M. J.;Conceicao, J; Pettiette, C. L.; Cheshnovsky, O.; Smalley, R. E. Chem. Phys. Lett. 1988, 144, 431.

Zhang, Q. L.; O'Brien, S. C.; Heath, J. R.; Liu, Y.; Curl, R. F.; Kroto, H. W.; Smalley, R. E. J. Phys. Chem. 1986, 90, 525.

Zimmerman, J. A.; Bach, S. B. H.; Watson, C. H.; Eyler, J. R. J. Phys. Chem. 1991a, 95, 98.

Zimmerman, J. A.; Eyler,J. R.; Bach, S. B. H.; McElvany, S. J. Chem. Phys. 1991b, 94, 3556.

BIOGRAPHICAL SKETCH

James E. Bruce was born and spent most of his youth in Wellsboro, Pennsylvania. He moved to Avon Park, Florida, with his family in January, 1982 and graduated from high school there in 1983. He then attended Troy State University, in Troy, Alabama, where he received the degree of Bachelor of Science in 1987. Later that same year he enrolled in the chemistry graduate program at the University of Florida, in Gainesville, Florida. Shortly thereafter, he joined the research group of Professor John R. Eyler involved in the field of FTICR mass spectrometry.

He has accepted a postdoctoral position with Dr. Richard D. Smith, Chemical Science Group, Battelle, Pacific Northwest Laboratory, where he will continue research on trapped ions in Fourier transform ion cyclotron resonance mass spectrometers.

I certify that I have read this study and that in my opinion it conforms to acceptable standards of scholarly presentation and is fully adequate, in scope and quality, as a dissertation for the degree of Doctor of Philosophy.

John R. Eyler, Chair
Professor of Chemistry

I certify that I have read this study and that in my opinion it conforms to acceptable standards of scholarly presentation and is fully adequate, in scope and quality, as a dissertation for the degree of Doctor of Philosophy.

Martin T. Vala
Professor of Chemistry

I certify that I have read this study and that in my opinion it conforms to acceptable standards of scholarly presentation and is fully adequate, in scope and quality, as a dissertation for the degree of Doctor of Philosophy.

Willis B. Person
Professor of Chemistry

I certify that I have read this study and that in my opinion it conforms to acceptable standards of scholarly presentation and is fully adequate, in scope and quality, as a dissertation for the degree of Doctor of Philosophy.

Kirk S. Schanze
Assistant Professor of Chemistry

I certify that I have read this study and that in my opinion it conforms to acceptable standards of scholarly presentation and is fully adequate, in scope and quality, as a dissertation for the degree of Doctor of Philosophy.

David C. Wilson
Professor of Mathematics

This dissertation was submitted to the Graduate Faculty of the Department of Chemistry in the College of Liberal Arts and Sciences and to the Graduate School and was accepted as partial fulfillment of the requirements for the degree of Doctor of Philosophy.

August, 1992

_____

Dean, Graduate School